PERFORMANCE OF RECTANGULAR FINS ON A VERTICAL BASE IN FREE CONVECTION HEAT TRANSFER

A THESIS SUBMITTED TO
THE GRADUATE SCHOOL OF NATURAL AND APPLIED SCIENCES
OF
MIDDLE EAST TECHNICAL UNIVERSITY

BY

BURAK YAZICIOĞLU

IN PARTIAL FULFILLMENT OF THE REQUIREMENTS
FOR
THE DEGREE OF MASTER OF SCIENCE
IN
MECHANICAL ENGINEERING

JANUARY 2005

Approval of the Graduate School of Natural and Applied Sciences

Prof. Dr. Canan Özgen
Director

I certify that this thesis satisfies all the requirements as a thesis for the degree of Master of Science.

Prof. Dr. Kemal İder
Head of Department

This is to certify that we have read this thesis and that in our opinion it is fully adequate, in scope and quality, as a thesis for the degree of Master of Science.

Prof. Dr. HafitYüncü
Supervisor

Examining Committee Members

Prof. Dr. Zafer Dursunkaya	(METU,ME)	
Prof. Dr. Hafit Yüncü	(METU,ME)	
Assoc. Prof. Dr. Ahmet N. Eraslan	(METU,ES)	
Asst. Prof. Dr. A. Tahsin Çetinkaya	(METU,ME)	
Asst. Prof. Dr. İlker Tarı	(METU,ME)	

I hereby declare that all information in this document has been obtained and presented in accordance with academic rules and ethical conduct. I also declare that, as required by these rules and conduct, I have fully cited and referenced all material and results that are not original to this work.

Name, Last name : Burak Yazıcıoğlu

Signature :

ABSTRACT

PERFORMANCE OF RECTANGULAR FINS ON A VERTICAL BASE IN FREE CONVECTION HEAT TRANSFER

Yazıcıoğlu, Burak
M.S., Department of Mechanical Engineering
Supervisor: Prof. Dr. Hafit Yüncü

January 2005, 116 pages

The steady-state natural convection heat transfer from vertical rectangular fins extending perpendicularly from vertical rectangular base was investigated experimentally. The effects of geometric parameters and base-to-ambient temperature difference on the heat transfer performance of fin arrays were observed and the optimum fin separation values were determined.

Two similar experimental set-ups were employed during experiments in order to take measurements from 30 different fin configurations having fin lengths of 250 mm and 340 mm. Fin thickness was maintained fixed at 3 mm. Fin height and fin spacing were varied from 5 mm to 25 mm and 5.75 mm to 85.5 mm, respectively. 5 heat inputs ranging from 25 W to 125 W were supplied for all fin configurations, and hence, the base and the ambient temperatures were measured in order to evaluate the heat transfer rate from fin arrays.

The results of experiments have shown that the convection heat transfer rate from fin arrays depends on all geometric parameters and base-to-ambient temperature difference. The effect of these parameters on optimum fin spacing was also examined, and it was realized that for a given base-to-ambient temperature difference, an optimum fin spacing value which maximizes the convective heat transfer rate from the fin array is available for every fin height. The results indicated that the optimum fin spacings are between 8.8 mm and 14.7 mm, for the fin arrays employed in this work.

Using the experimental results of present study and experimental results in available literature [2,3,9,10,11,12,14], a correlation for optimum fin spacing at a given fin length and base-to-ambient temperature difference was obtained as a result of scale analysis.

Keywords: Natural convection, rectangular fins, optimum fin spacing

ÖZ

DÜŞEY PLAKA ÜZERİNDE BULUNAN DİKDÖRTGEN KANATÇIKLARIN DOĞAL TAŞINIM İLE ISI TRANSFERİ PERFORMANSI

Yazıcıoğlu, Burak
Yüksek Lisans, Makina Mühendisliği Bölümü
Tez Yöneticisi: Prof. Dr. Hafit Yüncü

Ocak 2005, 116 Sayfa

Düşey dikdörtgen plaka üzerinden dik olarak yükselen düşey dikdörtgen kanatçıklardan kararlı halde doğal taşınım ile ısı transferi deneysel olarak incelenmiştir. Geometrik parametrelerin ve taban plakası sıcaklığı ile ortam sıcaklığı farkının kanatçık dizisi ısı transfer performansı üzerine etkileri araştırılmış ve optimum kanatçık aralığı değerleri belirlenmiştir.

Deneyler esnasında, 250 mm ve 340 mm uzunluğundaki kanatçıklara sahip 30 farklı kanatçık dizisinden ölçüm almak için iki benzer deney düzeneği kullanılmıştır. Kanatçık kalınlığı 3 mm'de sabit tutulmuş, kanatçık yüksekliği ve kanatçık aralığı sırasıyla 5 mm ile 25 mm ve 5.75 mm ile 85.5 mm arasında değiştirilmiştir. 25 W ile 125 W arasında değişen 5 değişik ısı akımı ile ısıtılan tüm kanatçıklı yüzeylerden ısı transferini hesaplamak için taban plakası sıcaklığı ile ortam sıcaklığı ölçülmüştür.

Deneysel sonuçlar kanatçıklardan doğal taşınım ile ısı transferinin tüm geometrik parametrelere ve taban plakası sıcaklığı ile ortam sıcaklığı farkına bağlı olduğunu göstermektedir. Bu parametrelerin optimum kanatçık aralığına etkileri de incelenmiştir. Deneysel sonuçlardan, her kanatçık yüksekliğinde verilen bir taban plakası sıcaklığı ile ortam sıcaklığı farkı için taşınım ile ısı transferini maksimum yapan bir optimum kanatçık aralığı değerinin mevcut olduğu anlaşılmıştır. Optimum kanatçık aralığı 8.8 mm ile 14.7 mm arasında değişmektedir.

Mevcut çalışmanın deneysel sonuçları ile literatürde [2,3,9,10,11,12,14] bulunan deneysel sonuçlar kullanılarak verilen bir kanatçık yüksekliği ve taban plakası ile ortam sıcaklığı farkı için optimum kanatçık aralığını hesaplayan bir eş-ilişki mertebe analizi sonucunda elde edilmiştir.

Anahtar kelimeler: Doğal taşınım, dikdörtgen kanatçıklar, optimum kanatçık aralığı

To My Family

ACKNOWLEDGEMENTS

The author wishes to express his appreciation to his thesis supervisor Prof. Dr. Hafit Yüncü for his guidance, suggestions and constructive criticisms throughout the study.

The technical aid of Heat Transfer Lab technician Mustafa Yalçın in the construction and maintenance of the experimental set-ups is gratefully acknowledged.

The assistance of Mechanical Engineering Machine Shop technicians in the production of the fin configurations is thankfully acknowledged.

The author would like to thank to his family for their endless support, love and faith.

The help and encouragement of all friends throughout the research are particularly appreciated.

TABLE OF CONTENTS

PLAGIARISM iii

ABSTRACT iv

ÖZ vi

DEDICATION viii

ACKNOWLEDGEMENTS ix

TABLE OF CONTENTS x

LIST OF TABLES xii

LIST OF FIGURES xiv

LIST OF SYMBOLS xix

CHAPTER

1. INTRODUCTION 1
2. REVIEW OF PREVIOUS WORK 3
3. EXPERIMENTAL EQUIPMENT AND INSTRUMENTATION 11
    - 3.1 The Set-ups 11
    - 3.2 The Instrumentation 15
        - 3.2.1 Electrical Measurements 16
        - 3.2.1 Temperature Measurements 17
4. EXPERIMENTAL PROCEDURE 20
    - 4.1 Calibration of Set-ups 20
    - 4.2 Verification of Calibration Method 25
    - 4.3 Testing Procedure of the Fin Arrays 28

5. EXPERIMENTAL RESULTS AND DISCUSSION 29

6. SCALE ANALYSIS 44

6.1 The Small-s Limit 45

6.2 The Large-s Limit 47

7. CONCLUSIONS 55

REFERENCES 59

APPENDICES

A. SOLUTION PROCEDURE OF HEAT CONDUCTION EQUATION 61

B. A SAMPLE CALCULATION FOR CALIBRATION EXPERIMENTS 66

C. A SAMPLE CALCULATION FOR VERIFICATION PROCEDURE 70

D. RADIATION ANALYSIS 76

E. TABULATED DATA AND RESULTS 84

F. UNCERTAINTY ANALYSIS 94

G. A SAMPLE CALCULATION FOR FIN ARRAYS 98

H. METHOD OF SCALE ANALYSIS 103

I. EXPERIMENTAL DATA OBTAINED FROM AVAILABLE LITERATURE 108

LIST OF TABLES

TABLES

Table 3.1 Component Dimensions of Set-up 1 and Set-up 2 13

Table 3.2 Dimensions of Fin Configurations 14

Table 5.1 Optimum Fin Spacings 43

Table B.1 Data Recorded for Calibration of Set-up 1 66

Table B.2 Data Recorded for Calibration of Set-up 2 67

Table B.3 Results of Calibration Experiments for Set-up 1 ……………………. 68

Table B.4 Results of Calibration Experiments for Set-up 2 ……………………. 69

Table C.1 Data Recorded for Verification of Set-up 1 …………………………. 70

Table C.2 Data Recorded for Verification of Set-up 2 …………………………. 71

Table C.3 Average Relative Errors of the Correlations ……………………….... 74

Table C.4 Comparison of Experimental and Theoretical Calculations ………… 74

Table D.1 View Factors ………………………………………………………… 83

Table E.1 Experimental Data for L=250 mm ……………………….................. 85

Table E.2 Experimental Data for L=340 mm ……………………….................. 86

Table E.3 Convection Heat Transfer Rates from Vertical Plate and

Fin-Arrays for L=250 mm ……………………………………………………… 88

Table E.4 Convection Heat Transfer Rates from Vertical Plate and

Fin-Arrays for L=340 mm ……………………………………………………… 89

Table E.5 Scale Analysis Data for L=250 mm ………………………………… 91

Table E.6 Scale Analysis Data for L=340 mm …………………………………… 92

Table G.1 View Factors for Sample Calculation ………………………………. 101

Table I.1 Summary of the Values of Experimental and Geometric
Parameters Used in Available Literature ………………………………………. 109

LIST OF FIGURES

FIGURES

Figure 3.1 Schematic View of the Experimental Set-up 12

Figure 3.2 A Photograph of Experimental Set-ups and Instrumentations 12

Figure 3.3 Fin Configuration Geometry 15

Figure 3.4 Power and Thermocouple Circuits 16

Figure 3.5 Locations of the Thermocouples on Fin Arrays 17

Figure 3.6 Thermocouple Calibration Curve 18

Figure 4.1 Calibration Plates 22

Figure 4.2 Calibration Curve for Set-up 1 23

Figure 4.3 Calibration Curve for Set-up 2 24

Figure 4.4 Comparison of Experimental and Theoretical Nusselt Numbers 27

Figure 5.1 Variation of Convection Heat Transfer Rate with Fin Height at a Fin Spacing of s=5.85 mm and at a Fin Length of L=250 mm 30

Figure 5.2 Variation of Convection Heat Transfer Rate with Fin Height at a Fin Spacing of s=8.8 mm and at a Fin Length of L=250 mm 30

Figure 5.3 Variation of Convection Heat Transfer Rate with Fin Height at a Fin Spacing of s=14.7 mm and at a Fin Length of L=250 mm 31

Figure 5.4 Variation of Convection Heat Transfer Rate with Fin Height at a Fin Spacing of s=32.4 mm and at a Fin Length of L=250 mm 31

Figure 5.5 Variation of Convection Heat Transfer Rate with Fin Height at a Fin Spacing of s=85.5 mm and at a Fin Length of L=250 mm 32

Figure 5.6 Variation of Convection Heat Transfer Rate with Fin Height at
a Fin Spacing of s=5.85 mm and at a Fin Length of L=340 mm 32
Figure 5.7 Variation of Convection Heat Transfer Rate with Fin Height at
a Fin Spacing of s=8.8 mm and at a Fin Length of L=340 mm 33
Figure 5.8 Variation of Convection Heat Transfer Rate with Fin Height at
a Fin Spacing of s=14.7 mm and at a Fin Length of L=340 mm 33
Figure 5.9 Variation of Convection Heat Transfer Rate with Fin Height at
a Fin Spacing of s=32.4 mm and at a Fin Length of L=340 mm 34
Figure 5.10 Variation of Convection Heat Transfer Rate with Fin Height at
a Fin Spacing of s=85.5 mm and at a Fin Length of L=340 mm 34
Figure 5.11 Variation of Convection Heat Transfer Rate with Fin Spacing
at a Fin Height of H=5 mm and at a Fin Length of L=250 mm 36
Figure 5.12 Variation of Convection Heat Transfer Rate with Fin Spacing
at a Fin Height of H=15 mm and at a Fin Length of L=250 mm 36
Figure 5.13 Variation of Convection Heat Transfer Rate with Fin Spacing
at a Fin Height of H=25 mm and at a Fin Length of L=250 mm 37
Figure 5.14 Variation of Convection Heat Transfer Rate with Fin Spacing
at a Fin Height of H=5 mm and at a Fin Length of L=340 mm 37
Figure 5.15 Variation of Convection Heat Transfer Rate with Fin Spacing
at a Fin Height of H=15 mm and at a Fin Length of L=340 mm 38
Figure 5.16 Variation of Convection Heat Transfer Rate with Fin Spacing
at a Fin Height of H=25 mm and at a Fin Length of L=340 mm 38

Figure 5.17 Variation of Convection Heat Transfer Rate with Base-to-Ambient Temperature Difference at a Fin Height of H=5 mm and a Fin Length of L=250 mm 39

Figure 5.18 Variation of Convection Heat Transfer Rate with Base-to-Ambient Temperature Difference at a Fin Height of H=15 mm and a Fin Length of L=250 mm 40

Figure 5.19 Variation of Convection Heat Transfer Rate with Base-to-Ambient Temperature Difference at a Fin Height of H=25 mm and a Fin Length of L=250 mm 40

Figure 5.20 Variation of Convection Heat Transfer Rate with Base-to-Ambient Temperature Difference at a Fin Height of H=5 mm and a Fin Length of L=340 mm 41

Figure 5.21 Variation of Convection Heat Transfer Rate with Base-to-Ambient Temperature Difference at a Fin Height of H=15 mm and a Fin Length of L=340 mm 41

Figure 5.22 Variation of Convection Heat Transfer Rate with Base-to-Ambient Temperature Difference at a Fin Height of H=25 mm and a Fin Length of L=340 mm 42

Figure 6.1 Asymptotic Plot for Extreme Limits 47

Figure 6.2 Plot of Dimensionless Eq. (6.7) 48

Figure 6.3 Plot of Dimensionless Eq. (6.15) 50

Figure 6.4 Comparison of Eq. (6.18c) with Rayleigh Numbers Obtained By Using Estimated Optimum Fin spacings 52

Figure 6.5 Comparison of Eq. (6.19c) with Experimentally Estimated
Optimum Fin Spacings 53
Figure 6.6 Comparison of Eq. (6.20) with Experimentally Estimated
Maximum Convection Heat Transfer Rates 54
Figure A.1 Schematic of the Experimental Set-up 61
Figure D.1 Basic Fin Model for Radiation Analysis 76
Figure D.2 Network Representation of the Radiative Exchange
between Surface 1 and the Remaining Surfaces 78
Figure D.3 Network Representation of the Radiative Exchange
between Surface 5 and the Remaining Surfaces 79
Figure D.4 Geometry for Perpendicular Rectangles with a Common Edge 80
Figure D.5 Geometry for Aligned Parallel Rectangles 81
Figure I.1 Variation of Total Heat Transfer Rate with Base-to-
Ambient Temperature Difference for Fin Heights of H=10 mm
and H=17 mm Presented in Ref. [2] 110
Figure I.2 Variation of Total Heat Transfer Rate with Base-to-
Ambient Temperature Difference Presented in Ref. [3] 110
Figure I.3 Variation of Total Heat Transfer Rate with Fin Height
at a Base-to-Ambient Temperature Difference of ΔT=40 ºC
Presented in Ref. [9] 111
Figure I.4 Variation of Total Heat Transfer Rate with Base-to-
Ambient Temperature Difference Presented in Ref. [9] 111

Figure I.5 Variation of Total Heat Transfer Rate with Fin Length

at a Base-to-Ambient Temperature Difference of ΔT=40 ºC

Presented in Ref. [10] 112

Figure I.6 Variation of Total Heat Transfer Rate with Fin Thickness

at a Base-to-Ambient Temperature Difference of ΔT=20 ºC

Presented in Ref. [11] 112

Figure I.7 Variation of Total Heat Transfer Rate with Fin Thickness

at a Base-to-Ambient Temperature Difference of ΔT=40 ºC

Presented in Ref. [11] 113

Figure I.8 Variation of Total Heat Transfer Rate with Base-to-

Ambient Temperature Difference Presented in Ref. [12] 113

Figure I.9 Variation of Convection Heat Transfer Rate with Base-to-

Ambient Temperature Difference for Fin Heights of H=25 mm

Presented in Ref. [14] 114

Figure I.10 Variation of Convection Heat Transfer Rate with Base-to-

Ambient Temperature Difference for Fin Heights of H=15 mm

Presented in Ref. [14] 114

Figure I.11 Variation of Convection Heat Transfer Rate with Base-to-

Ambient Temperature Difference for Fin Heights of H=5 mm

Presented in Ref. [14] 115

LIST OF SYMBOLS

A	Area, m^2
C_p	Specific heat at constant pressure, kJ/(kg·K)
d	Distance between opposing plates, m
E_b	Blackbody radiosity, W/ m^2
F_{ji}	View factor
g	Gravitational acceleration, m/s^2
h	Convection heat transfer coefficient, W/(m^2·K)
h_{exp}	Experimental convection heat transfer coefficient of vertical plate, W/(m^2·K)
H	Fin height
I	Input current to heater, A
J	Radiosity, W/m^2
k	Thermal conductivity, W/(m·K)
L	Fin length, m
$\dot{m}$	Mass flow rate, kg/s
n	Number of fins
Nu	Nusselt number
Pr	Prandtl number
$\dot{Q}$	Power input to the heater, W
$\dot{Q}_{out}$	Total heat transfer rate, W
$\dot{Q}_c$	Convection heat transfer rate, W
$\dot{Q}_c^{(1)}$	Convection heat transfer rate from fins in small-s limit, W
$\dot{Q}_c^{(2)}$	Convection heat transfer rate from fins in large-s limit, W
$\dot{Q}_r$	Radiation heat transfer rate, W
$\dot{Q}_o$	Total heat transfer rate from vertical plate, W
$\left(\dot{Q}_o\right)_c$	Convection heat transfer rate from vertical plate, W

$\left(\dot{Q}_o\right)_r$	Radiation heat transfer rate from vertical plate, W
Ra	Rayleigh number
s	Fin spacing, m
t	Fin thickness, m
T_a	Ambient temperature, K
T_f	Film temperature, K
T_w	Base-plate temperature, K
T_1	Temperature of heated plate, K
T_2	Temperature of opposite plate, K
V	Input voltage to heater, V
W	Fin width, m
α	Thermal diffusivity, m^2/s
β	Volumetric thermal expansion coefficient, 1/K
ε	Emissivity
ν	Kinematic viscosity, m^2/s
σ	Stefan-Boltzmann constant, $W/(m^2 \cdot K^4)$
ΔT	Base-to-ambient temperature difference, K

CHAPTER 1

INTRODUCTION

The operation of many engineering systems results in the generation of heat. This unwanted by-product can cause serious overheating problems and sometimes leads to failure of the system. The heat generated within a system must be dissipated to its surrounding in order to maintain the system at its recommended working temperatures and functioning effectively and reliably. This is especially important in modern electronic systems, in which the packaging density of circuits can be high. In order to overcome this problem, thermal systems with effective emitters as fins are desirable [1].

In order to achieve the desired rate of heat dissipation, with the least amount of material, the optimal combination of geometry and orientation of the finned surface is required. Among the geometrical variations, rectangular fins are the most commonly encountered fin geometry because of their simple construction, cheap cost and effective cooling capability. Two common orientations of rectangular fin configurations, horizontally based vertical fins and vertically based vertical fins, have been widely used in the applications. However, the horizontal orientation is not preferable because of its relatively poorer ability to dissipate heat [2].

The heat dissipation from the finned systems to the external ambient atmosphere can be obtained by using the mechanisms of the convection and radiation heat transfer. The effect of radiation contribution in total heat transfer rate is quite low due to low emmisivity values of used fin materials, such as duralumin and aluminum alloys. The basic equation describing such heat losses is given by:

$$\dot{Q}_c = h \cdot A \cdot \Delta T \tag{1.1}$$

As seen from Eq. (1.1), the rate of heat dissipation from the surface can be increased either by increasing the heat transfer coefficient, h or by increasing the surface area, A. An enhanced value of h can usually be achieved by creating appropriate conditions of forced flow over the surface. Although such forced convection is effective, extra space will be needed to accommodate a fan which causes additional initial and operational costs. Therefore, forced convection is not always preferable. Since the use of extended surfaces is often more economical, convenient and trouble free, most proposed application of increasing surface area is adding fins to the surface in order to achieve required rate of heat transfer. However, the designer should optimize the spacing or the number of fins on base carefully; otherwise fin additions may cause the deterioration of the rate of heat transfer. Although adding numerous fins increases the surface area, they may resist the air flow and cause boundary layer interferences which affect the heat transfer adversely [3].

The experimental investigations related to the thermal performances of rectangular fins were reported extensively in literature [1-6,9-14,16]. However, except for a few of them, studies were performed for limited ranges of fin configurations. In this study, the steady-state natural convection heat transfer from a wide range of vertical rectangular fin configurations protruding from a vertical base is investigated experimentally. The main objective of this experimental work is to determine the effects of geometric parameters and base-to-ambient temperature difference on the heat transfer performance of the fin arrays and obtain a correlation which estimates the optimum fin spacing values for maximum convection heat transfer rates from the fin arrays considered in this study. In Chapter 2, previous experimental studies on various fin configurations are summarized. In Chapter 3, the experimental set-up and the instrumentation is explained in detail. In Chapter 4, the experimental procedure consisting of the calibration and verification methods is given. The experimental results are presented and discussed in Chapter 5. In Chapter 6, a scale analysis of convection heat transfer from fins is given in order to obtain a correlation for optimum fin spacing. The conclusions are given in Chapter 7.

CHAPTER 2

REVIEW OF PREVIOUS WORK

Natural convection heat transfer rate from fin arrays has been investigated for several geometries in literature. The theoretical and experimental investigations were performed in order to find the optimum geometric parameters for achieving maximum heat transfer rates from the finned surfaces.

Starner and McManus [1] conducted one of the earliest studies about the heat transfer performance of rectangular fin arrays. In their experiments, four sets of fin arrays were tested to investigate free convection heat transfer performances. The fin arrays were positioned with three base types, vertical, 45 degrees and horizontal. Besides the main heater, guard heaters were employed to reduce side heat losses. The average heat transfer coefficients were obtained from all fin configurations for all test positions. From experimental data, it was found that heat transfer rates obtained from the tests with vertical arrays fell 10 to 30 percent below those of similarly spaced parallel plates. For the 45-degree base position, heat transfer rates were 5 to 20 percent below from the values taken at vertical position. With the use of smoke filaments, the flow patterns were observed for each base position. The effect of fin height was also discussed and it was realized that fin height, fin spacing and base orientation affected the heat transfer performance significantly.

Leung and Probert [2] performed another experimental study to investigate steady-state rates of heat dissipation under natural convective conditions from either vertically based or horizontally based vertical rectangular fins. They tried to figure out the effect of fin height on optimum fin spacing, and hence, two fin lengths were employed, namely 10 mm and 17 mm. The tests were carried out with the base of the fin array at either 20 °C or 40 °C above the mean temperature of the environmental air in the laboratory. As a result of limited number of experiments, it was concluded that for 150 mm length of fins, the optimum fin spacing values were 9.0 ± 0.5 mm to 9.5 ± 0.5 mm for the vertical fins protruding outwards from the vertical base and upwards from the horizontal base, respectively. It was also deduced that the change of fin height and base-to-ambient temperature difference did not affect optimum fin spacing values for the orientations considered in the study.

An experimental investigation of the heat transfer rate from an array of vertical rectangular fins on vertical rectangular base has been reported by Leung, Probert and Shilston [3]. The fins were manufactured from light aluminum alloy. The spacer bars made of the same material was produced to adjust the separation between adjacent fins by predetermined amounts. The wooden case was located at the rear of the test section to cover thermal insulation and heater plate. For various fin configurations, the experiments were conducted at base temperatures 20 °C, 40 °C, 60 °C and 80 °C above the mean temperature of ambient air. It was determined that the optimum fin spacing, corresponding to the maximum rate of heat transfer, was 10 ± 1 mm.

Welling and Wooldridge [4] performed another experimental study to compare actual rectangular fin experiments with those of vertical plate, enclosed duct and parallel plate data from previous studies. During the tests, guard heater plate was utilized to minimize the heat losses from the sides and rear of the set-up. Data obtained from experiments showed that with closely spaced fins, the heat transfer coefficients were smaller compared to wider fin spacings because of boundary layer interference, which prevents air inflow. It was observed that the heat transfer coefficients of finned arrays were smaller than those of vertical plate and greater than either those of enclosed ducts or those of parallel plates. For a given base-to-ambient temperature difference, an optimum H/s (fin height to fin spacing) ratio at which heat transfer coefficient is maximum was determined from the considered fin configurations.

Harahap and McManus [5] observed the flow field of horizontally based rectangular fin arrays for natural convection heat transfer to determine average heat transfer coefficients. In the experimental unit, guard heaters and guard fins were located near the end fins to eliminate the end effects. To visualize the flow field, schlieren-shadowgraph techniques and smoke injection were used. Several types of chimney flow were observed. For equal fin spacing and fin height, two series of rectangular fin arrays differing in length was compared. The result of comparison indicated that the array having shorter fin length (by half) had higher average heat transfer coefficient because of its effective utilization caused by single chimney flow. This result revealed that single chimney flow pattern was favorable to high rates of heat transfer. Using the average heat transfer coefficient data, the following correlations were proposed in terms of Gr_L, Pr, s, n, h.

$$\mathrm{Nu_L} = 5.22 \cdot 10^{-3} \cdot \left(\mathrm{Gr_L} \cdot \mathrm{Pr} \cdot \frac{s \cdot n}{h} \right)^{0.570} \cdot \left(\frac{h}{L} \right)^{0.656} \cdot \left(\frac{s}{L} \right)^{0.412} \tag{2.1}$$

for $10^6 < \mathrm{Gr_L} \cdot \mathrm{Pr} \cdot \frac{s \cdot n}{h} \leq 2.5 \cdot 10^7$

$$\mathrm{Nu_L} = 2.787 \cdot 10^{-3} \cdot \left(\mathrm{Gr_L} \cdot \mathrm{Pr} \cdot \frac{s \cdot n}{h} \right)^{0.745} \cdot \left(\frac{h}{L} \right)^{0.656} \cdot \left(\frac{s}{L} \right)^{0.412} \tag{2.2}$$

for $2.5 \cdot 10^7 < \mathrm{Gr_L} \cdot \mathrm{Pr} \cdot \frac{s \cdot n}{h} < 1.5 \cdot 10^8$

where Nu_L is the average Nusselt number based on the half fin length L, Gr_L is the Grashof number based on the half fin length L, n is the number of spacing in the array, s is the fin spacing and h is the fin height. All the thermophysical properties of air are evaluated at the wall temperature.

An experimental study to predict optimum fin spacing in terms of fin height and base-to-ambient temperature difference for natural convection heat transfer from rectangular fins on horizontal surfaces has been reported by Jones and Smith [6]. Determination of local heat transfer coefficients were achieved by measuring local temperature gradients with interferometer. Integrating the measured local heat transfer coefficients, the average heat transfer coefficient for the array was determined. Since the determined heat transfer coefficients were for convection only and were independent of the radiation, the interferometric technique was used directly. The results have shown that fin spacing, s is primary geometric parameter that affects the heat transfer coefficient. They also compared the measured values with the limited comparable data in literature, and it was concluded that the agreement between them was satisfactory. The experimental results were correlated with the following relation:

$$\mathrm{Nu_s} = 6.7\cdot 10^{-4}\cdot \mathrm{Gr_s}\cdot \mathrm{Pr}\cdot\left[1-\exp\left(\frac{0.746\cdot 10^{4}}{\mathrm{Gr_s}\cdot \mathrm{Pr}}\right)^{0.44}\right]^{1.7} \quad \text{for } s < 2 \text{ in} \tag{2.3}$$

$$\mathrm{Nu_s} = 0.54\cdot\left(\mathrm{Gr_s}\cdot \mathrm{Pr}\right)^{0.25} \quad \text{for } s > 2 \text{ in} \tag{2.4}$$

where Nu_s and Gr_s are the Grashof number and average Nusselt number based on fin spacing. All the thermophysical properties are evaluated at film temperature.

Filtzroy [7] performed a study to determine the optimum spacing of a set of parallel vertical fins cooled by free convection heat transfer in the laminar flow regime. The experimental results obtained from channels and parallel plates in available literature were correlated and the following equation that relates the ratio of average heat transfer coefficient based on fin spacing, h_s, to the vertical heat transfer coefficient, h_b was proposed:

$$\frac{h_s}{h_b} = \frac{1.68}{24}\cdot F^3\cdot\left[1-\exp\left(\frac{-24}{1.68\cdot F^3}\right)\right] \tag{2.5}$$

where $F = \frac{s}{H}\cdot\left(\mathrm{Gr_s}\cdot \mathrm{Pr}\right)^{0.25}$ is a factor. All the required thermophyical properties of air are evaluated at the film temperature. Gr_s is the Grashof number based on fin spacing, Pr is the Prandtl number.

Bar-Cohen [8] analytically investigated the effect of fin thickness on free convection heat transfer performances of rectangular fin arrays. The results of analysis have shown that for each distinct combination of environmental, geometric and material constraints, an optimum fin thickness that maximizes the thermal performance of an array exists. It was suggested that in air, the optimum fin thickness value of an array can be taken approximately equal to optimum fin spacing value for the best thermal performance. Based on his analysis, the following equation which gives the fin height associated with the optimum fin spacing was proposed:

$$H_{opt} = 1.7 \cdot \left(\frac{k}{k_{air}} \cdot \frac{s}{Ra_s^{0.25}} \right)^{0.5} \cdot t^{0.5} \tag{2.6}$$

where Ra_s is the Rayleigh number based on fin spacing, k is the thermal conductivity of the fin material and t is the fin thickness.

Leung, Probert and Shilston [9] studied the thermal performances of rectangular fins on vertical and horizontal rectangular bases, experimentally. Experiments were performed for three different cases; horizontally based vertical fins, vertically based vertical fins and vertically based horizontal fins. Optimum fin spacing values were predicted for each case. For constant base temperatures of 40°C, 60°C and 80°C, the experiments were conducted to reveal the effect of base position on heat transfer performances of fin arrays. For three different fin heights, namely 32 mm, 60 mm and 90 mm, and for a base temperature of 60°C, the experiments were also performed. The results have shown that for vertical fins on a vertical base, fin spacing is the most effective parameter influencing the heat transfer rate. It was also determined that unlike fin spacing, the variation in fin height did not cause an effective change in heat transfer rate for vertical fins on both vertical base and horizontal base. It was concluded that among the all considered base positions vertical fins on a vertical base was the best solution for better heat transfer performance.

The effects of changing fin length from 250 to 375 mm on the rate of heat transfer and the optimum fin spacing of vertical rectangular fins protruding from a horizontal or a vertical rectangular base have been investigated by Leung, Probert and Shilston [10], experimentally. Except fin length, other geometric parameters of several fin configurations were kept fixed for considered orientations. Experiments were conducted at a constant base temperature, 40°C above that of the ambient environment. The experimental measurements for vertical base showed that the increase in fin length caused reduction in the rate of heat dissipation per unit base area from the fin array. In addition, the optimal fin spacing rose from 10 ± 1 mm to 11 ± 1 mm as a result of fin length increase. On the other hand, with horizontal base, large reduction in the rate of heat transfer per unit area occurred when the fin length was increased. The optimal fin spacing of horizontally based fin array increased from 11 ± 1 mm to 14 ± 1 mm as the fin length was increased from 250 mm to 375 mm. All these consequences revealed that the effect of fin length on heat transfer performance of fin arrays is significant.

Leung and Probert [11] investigated effects of varying fin thickness on the rate of heat transfer from vertical duralumin fins protruding perpendicularly outwards from a vertical rectangular base, experimentally for free convection conditions. The experiments were performed with five different fin thicknesses, namely 1, 3, 6, 9 and 19 mm, for base temperatures of 20°C and 40°C above that of the ambient environment, which was maintained at 20°C. It was observed that the average optimal uniform fin thickness was 3 ± 0.5 mm, for maximum rates of heat transfer, when the uniform separations between the adjacent fins exceeded 20 mm and for 20 mm $\leq s \leq$ 50 mm, the optimal fin thickness decreased slightly as either the fin separation or the base temperature was reduced.

Yüncü and Anbar [13] performed an experimental study of free convection heat transfer from rectangular fin arrays on a horizontal base. 15 different fin arrays and a base plate were tested. The effects of fin height, fin spacing and base-to-ambient temperature difference on heat transfer performance were investigated. It was found that the rate of convective heat transfer from the fin array mainly depends on these parameters. The experimental results indicated that optimum fin spacing, for maximum heat transfer rate from fin array, decreased as the fin height increased. The effect of base-to-ambient temperature on the optimum fin spacing was also discussed and it was concluded that this effect is not significant. A correlation relating the ratio of convective heat transfer rate from a fin array to that of a base plate as a function of number of fins n, fin height H and fin spacing s was estimated and proposed as:

$$\frac{\dot{Q}_{fc}}{\dot{Q}_{pc}} = 0.923 \cdot \exp\left[1.336 \cdot \left(n^{-0.013n}\right) \cdot \frac{H}{s}\right] \tag{2.7}$$

Yüncü and Güvenc [14] investigated the performance of rectangular fins on a vertical base in free convection heat transfer, experimentally. During experiments, the length, width and thickness of fins on arrays were kept fixed, but other parameters such as fin spacing and fin height were varied. The effects of fin height, fin spacing and base-to-ambient temperature difference on the heat transfer performance of fin arrays was observed for several heat inputs. According to the experimental results, it was deduced that fin spacing is the most important parameter in the thermal performance of fin arrays and an optimum fin spacing can be found for every fin height, for a given base-to-ambient temperature difference. This result revealed that optimum fin spacing depends on two main parameters, fin height and base-to-ambient temperature difference. The experimental results were compared with those of obtained from horizontally based fin arrays in Ref. [13]. It was concluded that for vertically based fin arrays, higher heat transfer enhancement can be achieved.

Yüncü and Mobedi [15] performed a three dimensional numerical study on natural convection heat transfer from longitudinally short horizontal rectangular fin arrays. The governing equations, momentum and energy, were solved by using a finite difference code based on vorticity-vector potential approach. For various geometric parameters, fin length, fin height and fin spacing, flow configurations occurring in the channel of the fin arrays were analyzed. Two types of flows were defined as a result of observations. In first type flow configurations; with small fin spacing, air enters from the ends of the channel moves along the fin length and flows out at the center of the channel. On the other hand, in the second case, with large fin spacing, fresh air can also enter into the channel from the middle part since the space between two fins is sufficiently large. Then, it turns 180 degree at the base and flows up along the fin height while it moves to the central part of the channel. The effects of fin length and fin height on the heat transfer rate of horizontal fin array were also examined and it was concluded that an increase in these geometric parameters causes reduction in the rate of heat transfer from array. This is due to more boundary layer interference along the channels which lowers the amount of intake cold air in the channel.

Natural convective heat transfer from annular fins has been investigated by Yüncü and Yildiz [16] experimentally. 18 sets of annular fin arrays were tested to observe their heat transfer performances. The fin arrays were heated with several heat inputs and corresponding base and ambient temperature differences were recorded. Using the measured data, total heat transfer rates from fin configurations were evaluated. A radiation analysis was applied to estimate the rates of radiation heat transfer. Then, radiation contributions were subtracted from total heat dissipations to obtain essential convection heat transfer rates. It was concluded that the convection heat transfer rate from the fin arrays depends on fin diameter, fin spacing and base-to-ambient temperature difference. A scale analysis was also performed in order to estimate a correlation which evaluates order-of-magnitude of optimum fin spacing at a given fin diameter and base-to-ambient temperature difference. The correlation is:

$$\frac{S_{opt}}{D} = 3.38 \cdot Ra_D^{-0.25} \tag{2.8}$$

CHAPTER 3

EXPERIMENTAL EQUIPMENT AND INSTRUMENTATION

Two similar experimental set-ups, named as Set-up 1 and Set-up 2, were constructed to test vertically based rectangular fin arrays. The experimental set-ups are similar to those used in Refs. [13, 14]. Each of the experimental set-ups primarily consists of an aerated concrete case and supporting frame on which the concrete is mounted, and various instruments for measuring the ambient temperature, base-plate temperature and the power input for the heater. A schematic view of the experimental set-up and a photograph of the experimental equipment and the instrumentation are presented in Figures 3.1 and 3.2, respectively.

3.1 The Set-ups

The essential dimensions of the components of Set-up 1 and Set-up 2 are given in Table 3.1. The frames of set-ups are filled with styrofoam in order to maintain the insulation of the aerated concrete cases. The front surfaces of the frames are covered with metal plates, which have rectangular holes at the center, so that fin arrays are placed into the cases through these holes. The heaters are placed into the cases. 3 mm thick aluminum plates are located between the heaters and base-plates in order to distribute the power input evenly. Thus, a more uniform temperature distribution at the base of the fin array can be achieved. Each heater covered by cases fully consists of a nichrome wire wound around a thin mica plate and mica sheets on both sides of mica plate for insulation. They are rated for 600 W and 220 V, AC

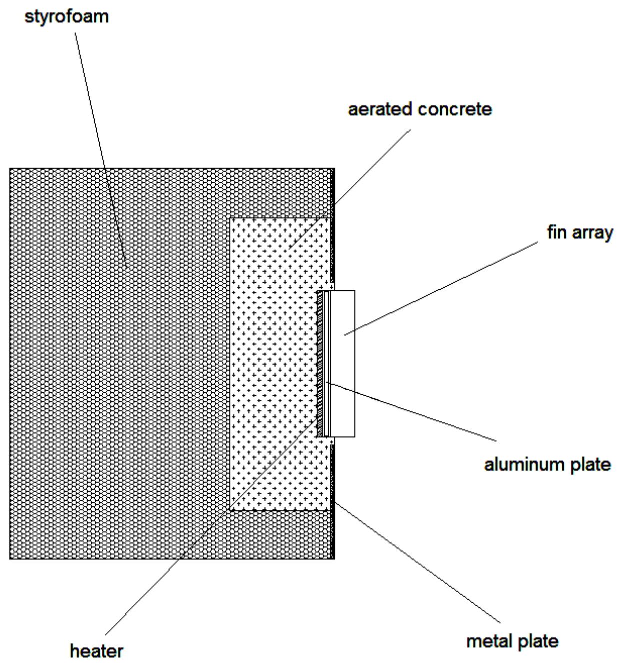

Figure 3.1 Schematic View of the Experimental Set-up

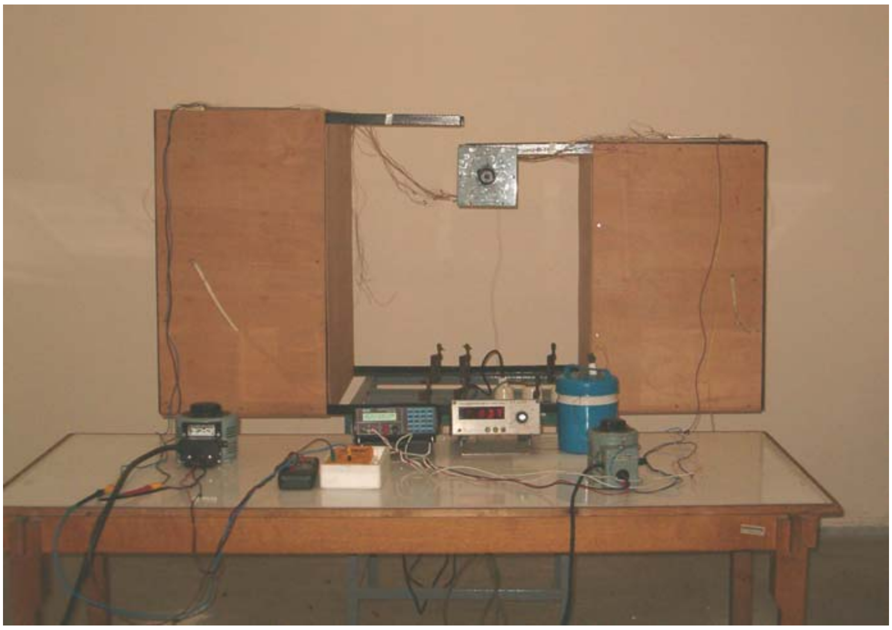

Figure 3.2 A Photograph of Experimental Set-ups and Instrumentations

Table 3.1 Component Dimensions of Set-up 1 and Set-up 2

Dimensions (mm)		
Components	Set-up 1	Set-up 2
Frame	750x700x500	850x700x500
Case	255x185x20	345x185x20
Hole	275x215	375x215
Heater	250x180x5	340x180x5

The test sections were insulated carefully. The aerated concrete case insulating the rear surface of the heater and the four lateral surfaces of the fin base-plate was used as the primary insulation material. The remaining part between set-up boundaries and concrete was filled with styrofoam serving as the secondary insulation. Therefore, the boundaries of the set-ups were maintained approximately at the ambient air temperature. The case material was chosen as aerated concrete due to its high insulation quality (thermal conductivity, $k \sim 0.15$ W/m·K) and high temperature resistance. In addition, it can be shaped easily so that all necessary processes, digging, drilling etc., can be performed on these materials. The experiments were conducted in a windowless large room. Precautions were taken to maintain almost constant room temperature, free of air currents.

The fin configurations were produced by milling longitudinal grooves in one of the faces of a rectangular bar. The fin arrays were produced from rectangular bars with dimensions 250x180x30 mm and 340x180x30 mm, respectively. The fins were integral with the base-plate. The fin configurations, having fin length of 250 mm, were tested at Set-up 1 and those having fin length of 340 mm were tested at Set-up 2. For all fin configurations, the base-plate thickness, the fin thickness and the width of the fin array were kept fixed at 5 mm, 3 mm and 180 mm, respectively. The dimensions of the fin configurations are listed in Table 3.2. The geometry of the fin arrays and the symbols used to denote the dimensions are illustrated in Figure 3.3.

Table 3.2 Dimensions of Fin Configurations

Fin Length L(mm)	Fin Width W(mm)	Fin Thickness t(mm)	Base Thickness d(mm)
250, 340	180	3	5
Set No.	Fin Height H(mm)	Fin Spacing s(mm)	Number of Fins n
1	25	85.5	3
2	25	32.4	6
3	25	14.7	11
4	25	8.8	16
5	25	5.85	21
6	15	85.5	3
7	15	32.4	6
8	15	14.7	11
9	15	8.8	16
10	15	5.85	21
11	5	85.5	3
12	5	32.4	6
13	5	14.7	11
14	5	8.8	16
15	5	5.85	21

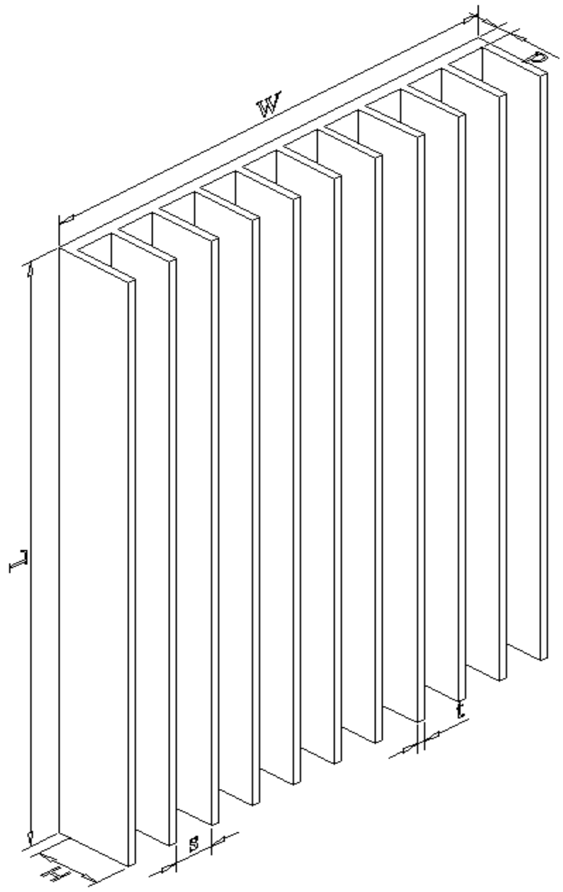

Figure 3.3 Fin Configuration Geometry

The fin material was selected as aluminum because of its high thermal conductivity (~130 W/mK at 20 ºC), low emissivity (~ 0.2 at 20 ºC), structural strength and durability.

3.2 The Instrumentation

During the experiments, both electrical power measurements and temperature measurements were performed in order to supply desired power inputs to the heaters and read the ambient temperature and the temperature values at various locations on the fin base-plates.

3.2.1 Electrical Measurements

The electrical power was supplied through a regulated a-c supply. The output of supply was fed to two variable transformers so that for each of the set-ups, the power inputs could be selected independently. The voltage drops, the current flows and the power inputs of each set-up were monitored simultaneously by TRMS power analyzers. The thermocouple and power circuits are shown in Figure 3.4.

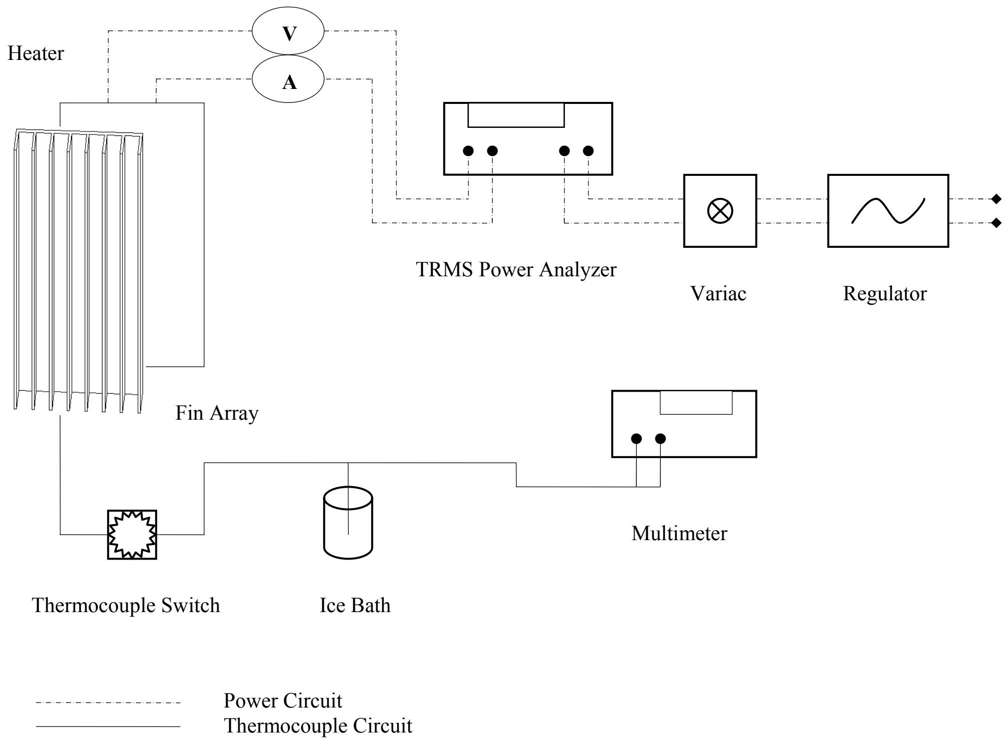

Figure 3.4 Power and Thermocouple Circuits

3.2.2 Temperature Measurements

The ambient temperature was measured by using mercury in glass thermometer with 1/20 of degree Celsius accuracy. The base-plate temperatures of fin arrays were measured at six points by 25 gage copper-constantan thermocouples, whose positions are shown in Figure 3.5. The measurements were done at six points in order to see if large variations exist along the base-plate. The average of these six readings was taken as the plate temperature. To avoid disturbing the flow past the front surface, temperature measurements were not made at the fin tips. Since fin material (aluminum) has high thermal conductivity and fin heights are short (maximum fin height is 25mm), it was assumed that the temperatures along the fin and at the fin tip did not vary significantly from the base-plate.

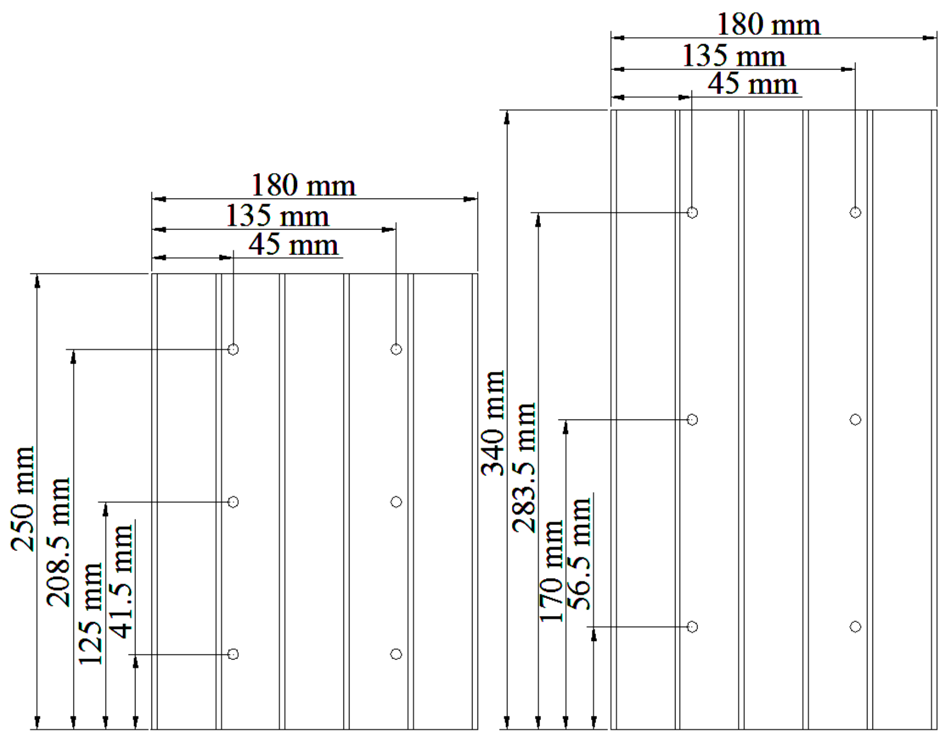

Figure 3.5 Locations of the Thermocouples on Fin Arrays

To measure temperature of the base-plate, six holes were drilled through each base-plate first, and then the hot junctions of the thermocouples were inserted into these holes from the front surface to the rear surface. The cold junctions of the thermocouples were immersed into an ice-water mixture bath. In order to measure the thermocouple voltages, a one hundredth of a microvolt resolution digital multimeter and a selector switch were used.

A sample thermocouple was calibrated to be used during experiments. For this purpose, an oil bath was utilized. The hot junction of the thermocouple was immersed into the oil bath together with a one tenth of degree precision mercury in glass thermometer. While the hot oil cooled from 260 ºC to ambient temperature, its temperature was measured both with the thermocouple via the multimeter and the thermometer, at certain time intervals. Figure 3.6 shows the obtained calibration curve.

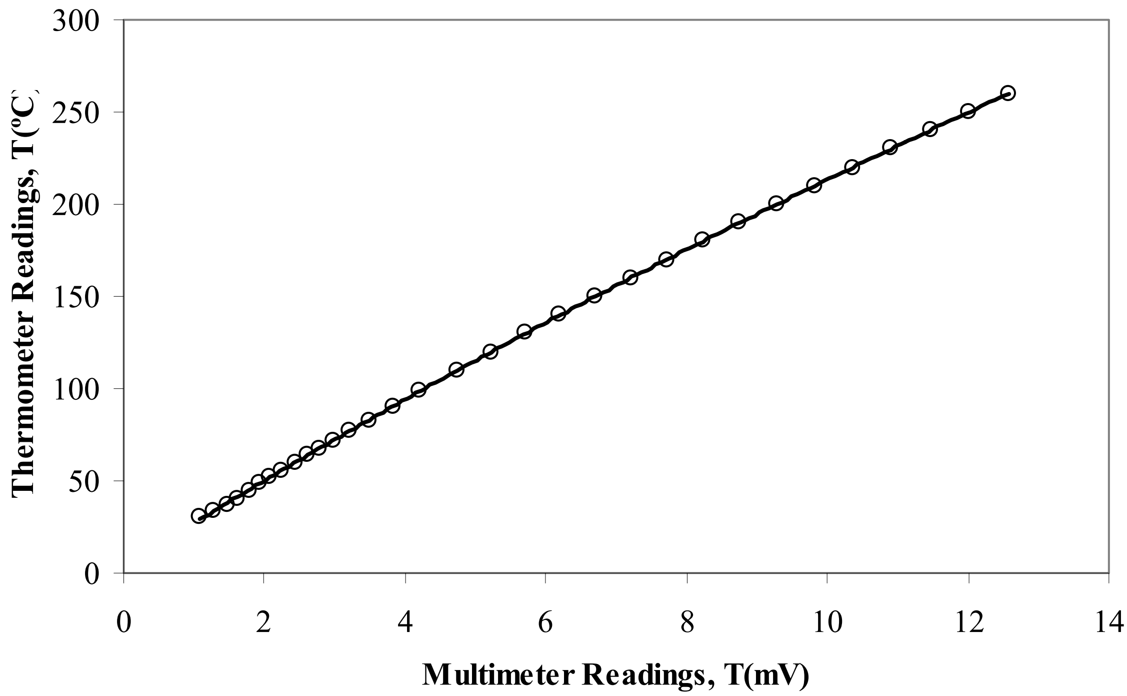

Figure 3.6 Thermocouple Calibration Curve

Thermometer readings in Celsius scale versus multimeter readings in the milivolt scale were plotted in Figure 3.6. A third order polynomial was used to fit the data set. Therefore, the thermocouple calibration curve was determined as:

$$T(°C)=0.0067.(T(mV))^3 - 0.383.(T(mV))^2 + 24.186.T(mV) + 3.0861 \quad (3.1)$$

CHAPTER 4

EXPERIMENTAL PROCEDURE

In order to be able to determine the convective heat transfer performances of the fin arrays under steady-state conditions, total heat losses from the set-ups should be calculated first. Hence, the experimental set-ups were calibrated and the calibration method was verified before starting experiments. The total heat, which occurs as a result of the power inputs to the heaters, is dissipated in modes of natural convection, radiation from the fin arrays and conduction from the remaining parts of the set-ups. Since the heat transfer coefficients can not be determined by the current experimental method, direct estimation of the convection heat transfer rates from the fin arrays is not possible. Thus, after calculating total heat transfer rate, the radiation contribution should be subtracted from it to determine the convection heat transfer rate. The calculation procedure of the radiation heat transfer rate is given in Appendix D.

4.1 Calibration of Set-ups

For the calibration of the set-ups, the heat transfer rate from the heated base-plate should be determined. Since the experimental set-ups had similar properties except dimensions, the solution procedures of heat conduction equations were same. Using a procedure similar to that proposed in Ref. [13,14], the heat conduction equation was solved with the method of integral transform technique. The solution procedure is given in Appendix A. For the heat transfer rate from heated base-plate, the following equation was obtained:

$$\frac{\dot{Q}_{out}}{\dot{Q}} = \zeta - \tau \cdot \frac{(T_w - T_a)}{\dot{Q}} \tag{4.1}$$

where $\dot{Q}$ is the power input to the heater, T_a is the ambient temperature, T_w is the average surface temperature of the heated plate, $\dot{Q}_{out}$ is the total heat transfer rate from the heated plate and, ζ and τ (W/K) are constants that depend on the geometry and the average thermal conductivity of the system.

The constants (ζ, τ) of the calibration equation can be found if and only if the total heat transfer rates are known. Since the parameters ($\dot{Q}$, T_a and T_w) in Eq. (4.1) can be measured, the rate of heat transfer through the heated plate should be calculated with these data set. Moreover, the total heat transfer rate should not involve the convective component since the heat transfer coefficients cannot be estimated directly. For this reason, two parallel plates were attached opposite to each other and were mounted onto the each set-up as shown in Figure 4.2. The plates were of the same size and same material as the base-plates of fin arrays. The calibration plate dimensions of set-up 1 and set-up 2 are 250x180 mm and 340x180 mm, respectively. For each of the set-ups, the distance between the plates was kept fixed at 2 mm by means of four fiber supports at the corners of the plate to create conditions to prevent the convection heat transfer.

In order to have pure conduction through the air between the plates, either the Rayleigh number based on plate length (250 mm and 340 mm) had to be less than 1000, or the aspect ratio (ratio of the plate length to the distance between the plates) had to be greater than or equal to 100 [17]. Since the Rayleigh number based on plate width was at the order of 10^6, the first criterion could not be achieved with air. However, the second criterion was satisfied for calibration plates since the ratios were greater than 100. Therefore, the heat transfer between the plates was by conduction and radiation. At steady state, the heat transfer between the plates was in the following form:

$$\dot{Q}_{out} = \frac{k}{d} \cdot A \cdot (T_1 - T_2) + \sigma \cdot \frac{\varepsilon}{\varepsilon - 2} \cdot A \cdot (T_1^4 - T_2^4) \qquad (4.2)$$

In Eq. (4.2), k is the thermal conductivity of air between the plates, evaluated at the average of plate temperatures, T_1 is the temperature of heated plate, T_2 is the temperature of opposite plate, d is the distance between the plates, σ is the Stefan-Boltzmann constant and ε is the emissivity of the plates, measured as 0.20 using an emissivitymeter. This value agreed well with those given in literature [18].

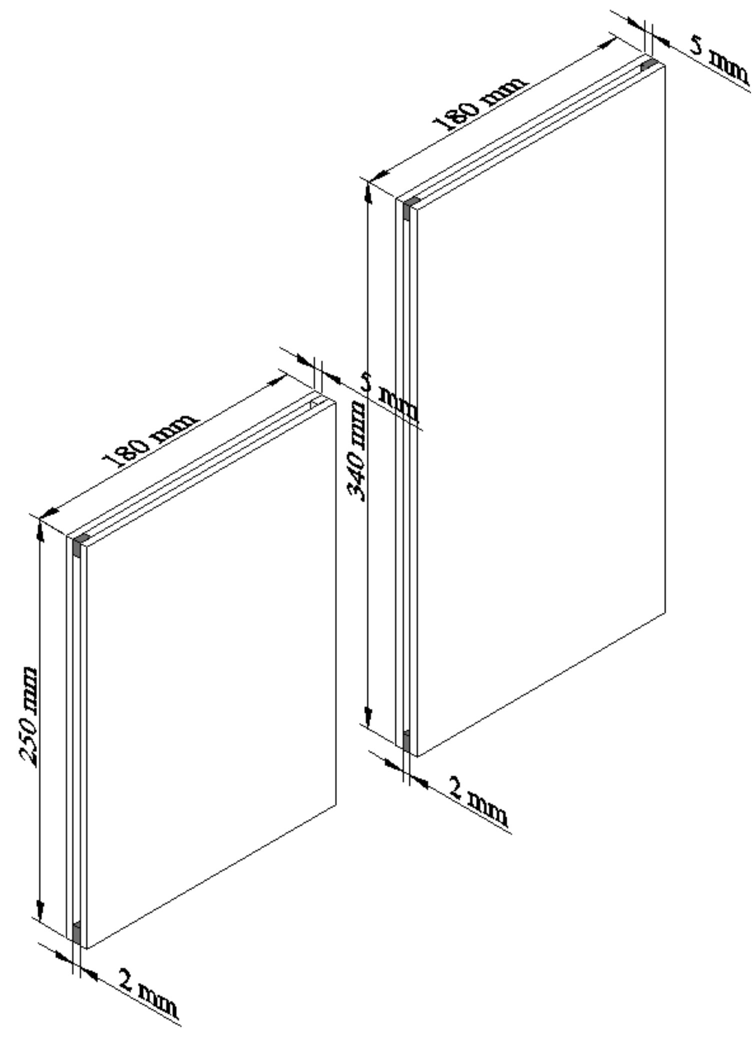

Figure 4.1 Calibration Plates

The heated plates mounted onto each of the set-ups were heated with 13 power inputs. For each input, the ambient temperatures, T_a, and the plate temperatures, T_1 and T_2 were measured at each of the set-ups when steady state condition was satisfied. During measurements, six thermocouples were placed on each plate at identical points as shown in Figure 3.5 and the ambient temperatures were also measured and recorded simultaneously. The steady state assumption was valid when readings taken at thirty-minute intervals did not vary more than 0.5 °C. The measured quantities were presented in Appendix A.

Using the supplied power inputs and the measured temperature values, corresponding total heat transfer rates from heated base-plates were found by using Eq. (4.2). Then, the variation of $\dot{Q}_{out}/\dot{Q}$ with $(T_1\text{-}T_a)/\dot{Q}$ for Set-up 1 and Set-up 2 were plotted as shown in Figures 4.2 and Figure 4.3, respectively.

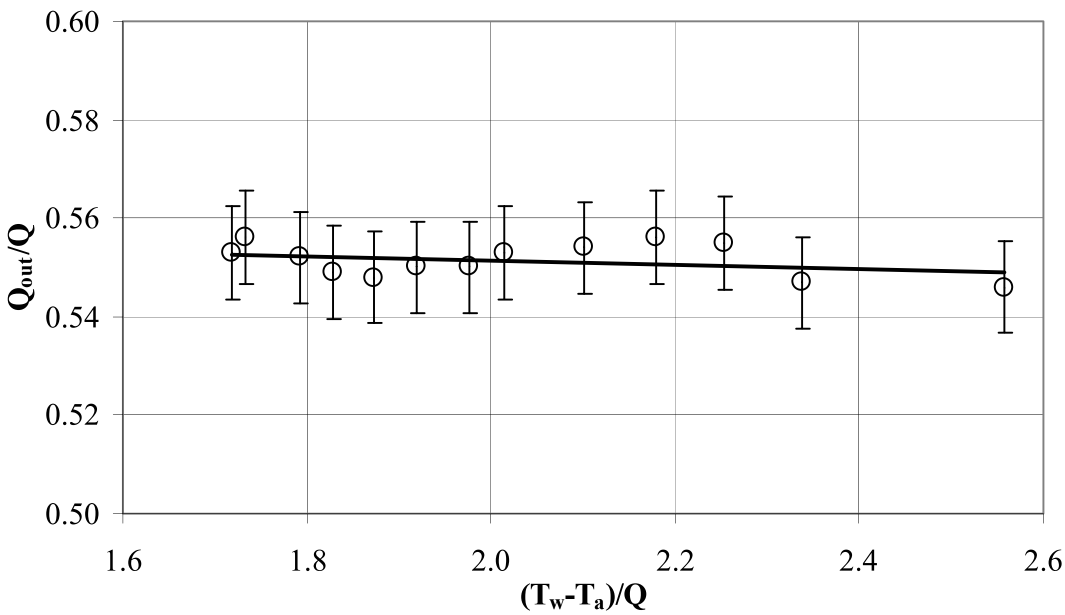

Figure 4.2 Calibration Curve for Set-up 1

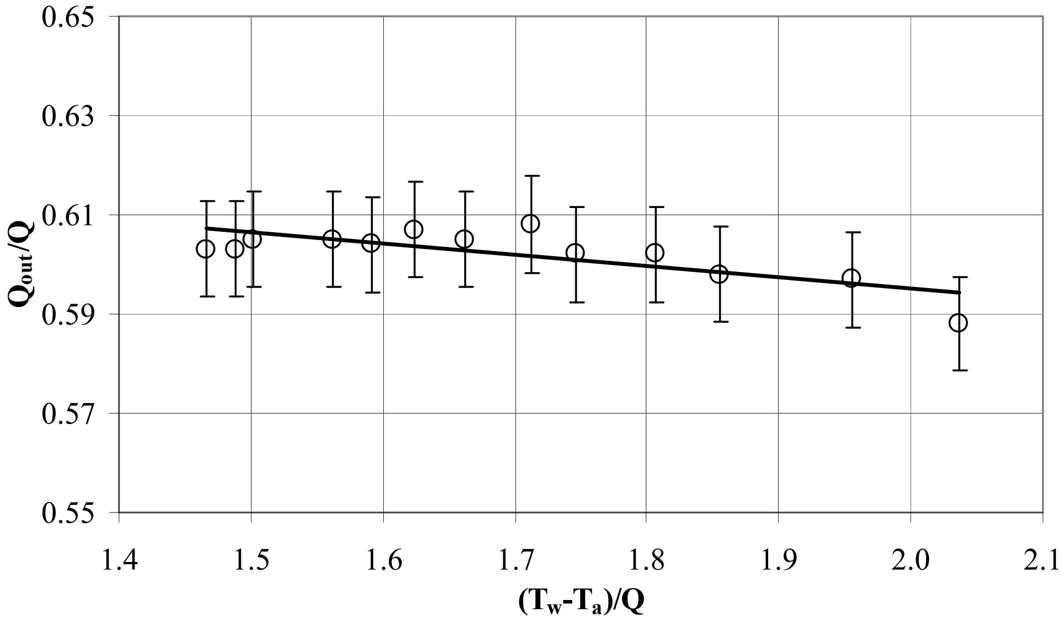

Figure 4.3 Calibration Curve for Set-up 2

Using these plots, ζ and τ (W/K) values were determined and calibration equations were obtained as:

$$\frac{\dot{Q}_{out}}{\dot{Q}} = 0.5601 - 0.0043 \cdot \frac{(T_w - T_a)}{\dot{Q}} \qquad \text{for Set-up 1} \qquad (4.3)$$

$$\frac{\dot{Q}_{out}}{\dot{Q}} = 0.6396 - 0.0222 \cdot \frac{(T_w - T_a)}{\dot{Q}} \qquad \text{for Set-up 2} \qquad (4.4)$$

The values of ζ, 0.5601 and 0.6396 are dimensionless, but the coefficients of $(T_w\text{-}T_a)/\dot{Q}$ term, 0.0043 and 0.0222, have the dimension of (W/K). Since the dimensions of the set-ups are not equal, the calibration equations, Eq. (4.3) and (4.4) are also different as expected.

4.2 Verification of Calibration Method

In order to determine the validity of the used calibration equations and method, a set of experiments were conducted on a vertical plate for each set-up. Using the experimental results, experimentally and theoretically estimated Nusselt numbers were compared for verification.

For each of the set-ups, 13 predetermined power inputs were supplied to heat the vertical plates. Under steady-state conditions, the vertical plate temperatures, T_w, the ambient temperatures, T_a and the power inputs, $\dot{Q}$ were measured. The measurement results are presented in Appendix C.

For each power input, the total heat transfer rate from vertical plate was calculated by substituting the measured data into Eqs. (4.3) or (4.4). Then, the radiation heat transfer rate from vertical plate was estimated by assuming the environment as a blackbody at ambient temperature T_a as:

$$\left(\dot{Q}_o\right)_r = \sigma \cdot \varepsilon \cdot A \cdot (T_w^{\,4} - T_a^{\,4}) \tag{4.5}$$

The convection heat transfer was evaluated as:

$$\left(\dot{Q}_o\right)_c = \dot{Q}_o - \left(\dot{Q}_o\right)_r \tag{4.6}$$

Therefore, the heat transfer coefficient based on the surface area of the vertical plate was determined as:

$$h_{exp} = \frac{\left(\dot{Q}_o\right)_c}{A \cdot (T_w - T_a)} \tag{4.7}$$

Rayleigh and Nusselt numbers were also evaluated from the definitions as:

$$Ra = \frac{g \cdot \beta \cdot L^3 \cdot (T_w - T_a)}{\nu \cdot \alpha} \tag{4.8}$$

$$Nu_{exp} = \frac{h_{exp} \cdot L}{k} \tag{4.9}$$

where L, the length of the vertical plate is the characteristic length. The thermophysical properties necessary to evaluate Rayleigh and Nusselt numbers were taken at the film temperature, $T_f = (T_w+T_a)/2$.

After determining experimental Nusselt numbers for both of the set-ups, they were compared with the Nusselt numbers evaluated by using available vertical plate correlations from literature.

The correlations utilized for the comparison are:

1. Churchill and Chu's first relation (for laminar and turbulent flows) [19]:

$$Nu_{th1} = \left[0.825 + \frac{0.387 \cdot (Ra)^{1/6}}{\left[1 + \left(\frac{0.492}{Pr} \right)^{9/16} \right]^{8/27}} \right]^2 \qquad \text{for} \quad 10^{-1} < Ra < 10^{12} \tag{4.10}$$

2. Churchill and Chu's second relation (for laminar flows only) [19]:

$$Nu_{th2} = 0.68 + \frac{0.67 \cdot (Ra)^{1/4}}{\left[1 + \left(\frac{0.492}{Pr} \right)^{9/16} \right]^{4/9}} \qquad \text{for} \quad 10^{-1} < Ra < 10^{9} \tag{4.11}$$

3. McAdams' relation [19]:

$$\mathrm{Nu}_{\mathrm{th3}} = 0.59 \cdot (\mathrm{Ra})^{1/4} \qquad \text{for} \quad 10^4 < \mathrm{Ra} < 10^9 \tag{4.12}$$

4. Churchill and Usagi's relation [19]:

$$\mathrm{Nu}_{\mathrm{th4}} = \frac{0.67 \cdot (\mathrm{Ra})^{1/4}}{\left[1 + \left(\frac{0.492}{\mathrm{Pr}}\right)^{9/16}\right]^{4/9}} \qquad \text{for} \quad 10^5 < \mathrm{Ra} < 10^9 \tag{4.13}$$

The theoretical and experimental Nusselt numbers were plotted in the same graph as shown in Figure 4.4 in order to display the agreement between them. Table C.3 in Appendix C summarizes the percent relative errors of these correlations with respect to the Nusselt numbers evaluated from the experimental data.

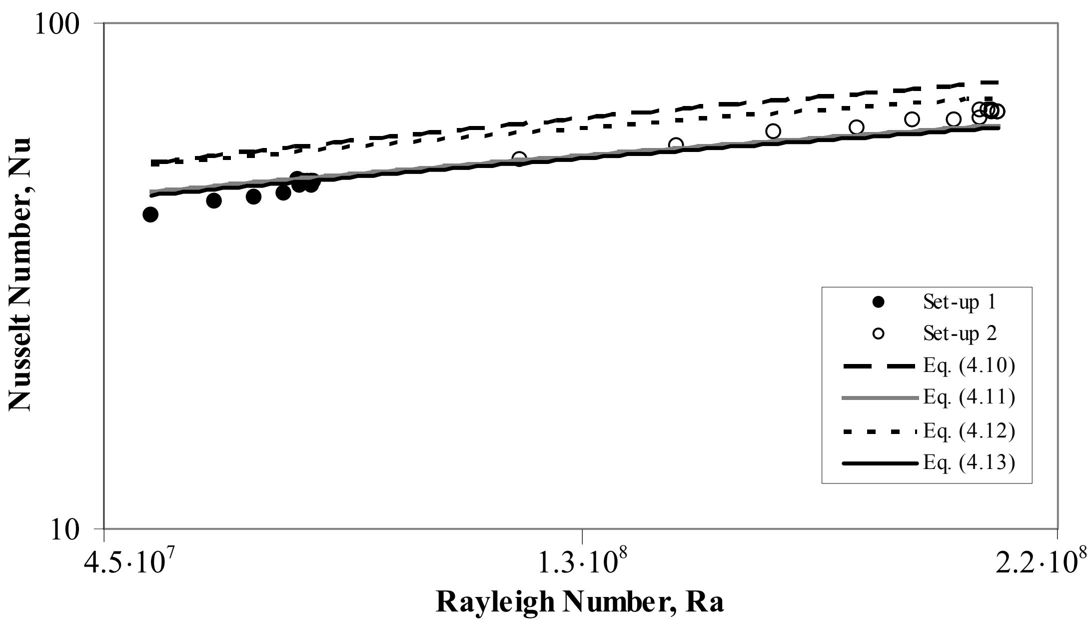

Figure 4.4 Comparison of Experimental and Theoretical Nusselt Numbers

Examination of Figure 4.4 reveals that the experimental data are in a good agreement with the correlations. The average relative errors are less than 20 % for Churchill and Chu's and McAdams' correlations. The average relative errors of the remaining correlations do not exceed 5 %. These results indicate the validity of the experimental set-ups, the experimental procedure and the calibration method. A sample calculation for the verification procedure is given in Appendix C.

4.3 Testing Procedure of the Fin Arrays

After calibrating the experimental set-ups and verifying the calibration method, 30 fin arrays were mounted into the cases of Set-up 1 or Set-up 2. For each of the 30 fin arrays, the power input was adjusted to 25 W initially and the base-plate was heated about 10 hours. Then, the base temperature was measured by means of six thermocouples located on the outer surface of base plate. In order to decide whether the fin array was at steady-state or not, the thermocouple readings were taken at thirty minute intervals and this condition was assumed to be reached when the difference between two successive readings of each thermocouple was less than 0.5ºC. The base-plate temperature T_w, the ambient temperature T_a and the power input to the heater $\dot{Q}$ were recorded at steady-state. The testing procedure mentioned above was repeated for the power inputs 50 W, 75 W, 100 W and 125 W for all the fin arrays. The measured data were given in Table E.1 in Appendix E.

The calibration equations, Eq. (4.3) and (4.4) were employed to evaluate the total heat transfer rates from the fin arrays. Then, using the procedure presented in Appendix D, the radiation contributions were determined. The convection heat transfer rates were calculated as:

$$\dot{Q}_c = \dot{Q}_{out} - \dot{Q}_r \tag{4.14}$$

A sample calculation for the fin arrays is given in Appendix F.

CHAPTER 5

EXPERIMENTAL RESULTS AND DISCUSSION

The experimental data obtained from 30 different fin configurations are presented in this chapter. These results are utilized to reveal the effects of geometric parameters, fin spacing, fin height and fin length, and the effects of base-to-ambient temperature difference on the steady-state heat transfer rates from finned surfaces. The experimental data are presented in 22 figures to examine the effect of each parameter separately.

The convection heat transfer rates from fin arrays and the vertical flat plate are plotted as a function of base-to-ambient temperature difference for fin spacings, s = 5.85 mm, s = 8.8 mm, s = 14.7 mm, s = 32.4 mm and s = 85.5 mm and for fin lengths, L = 250 mm and L = 340 mm in Figures 5.1 to 5.10, respectively. Each figure involves the results plotted for three fin heights H = 5 mm, H =15 mm and H = 25 mm, and for a vertical flat plate.

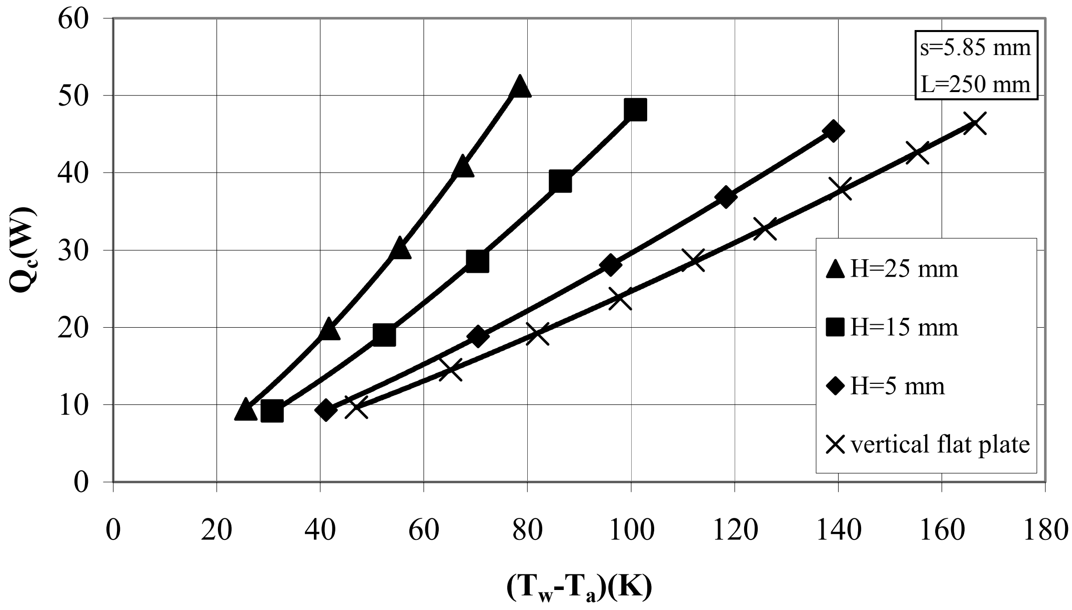

Figure 5.1 Variation of Convection Heat Transfer Rate with Fin Height at a Fin Spacing of s=5.85 mm and at a Fin Length of L=250 mm

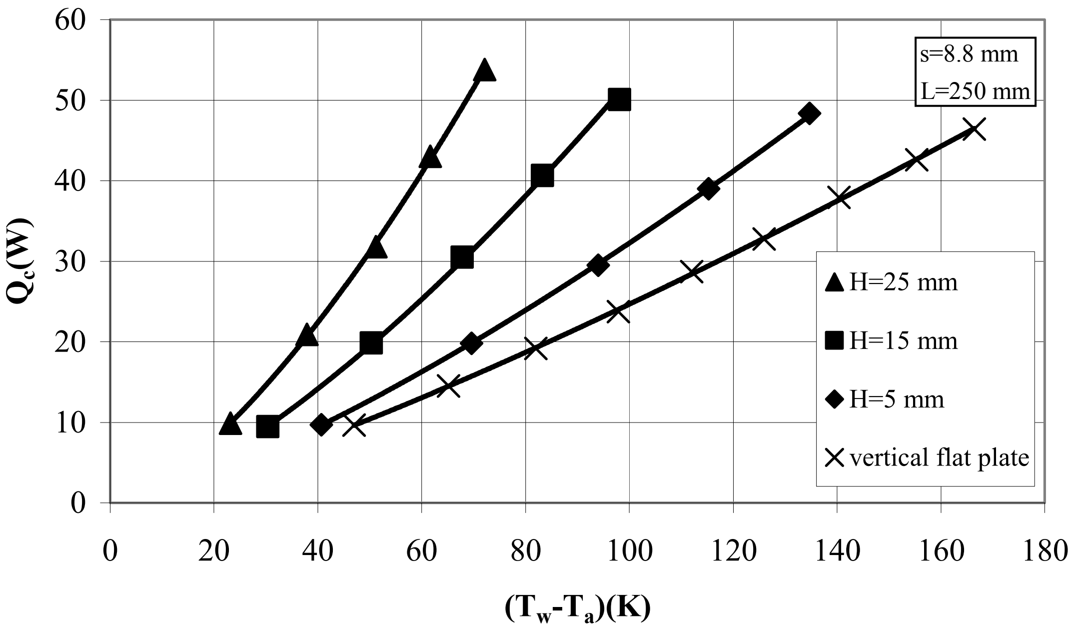

Figure 5.2 Variation of Convection Heat Transfer Rate with Fin Height at a Fin Spacing of s=8.8 mm and at a Fin Length of L=250 mm

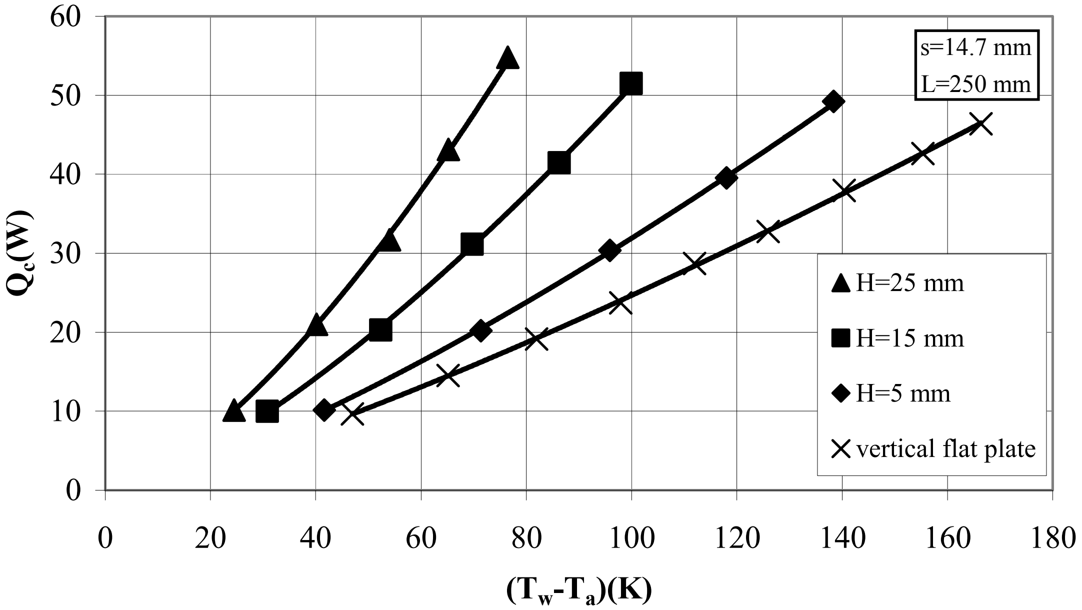

Figure 5.3 Variation of Convection Heat Transfer Rate with Fin Height at a Fin Spacing of s=14.7 mm and at a Fin Length of L=250 mm

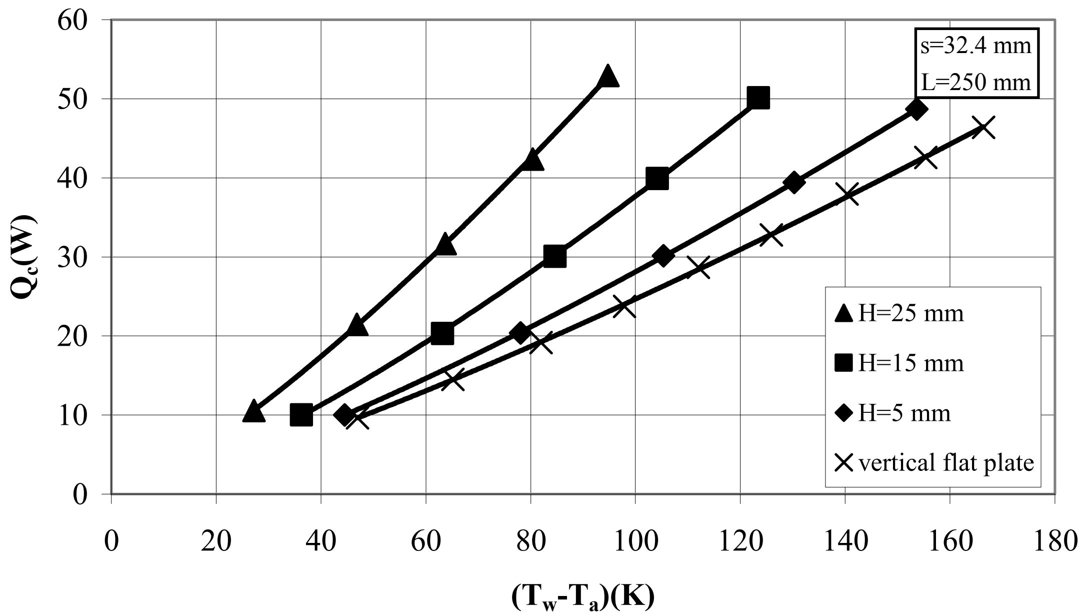

Figure 5.4 Variation of Convection Heat Transfer Rate with Fin Height at a Fin Spacing of s=32.4 mm and at a Fin Length of L=250 mm

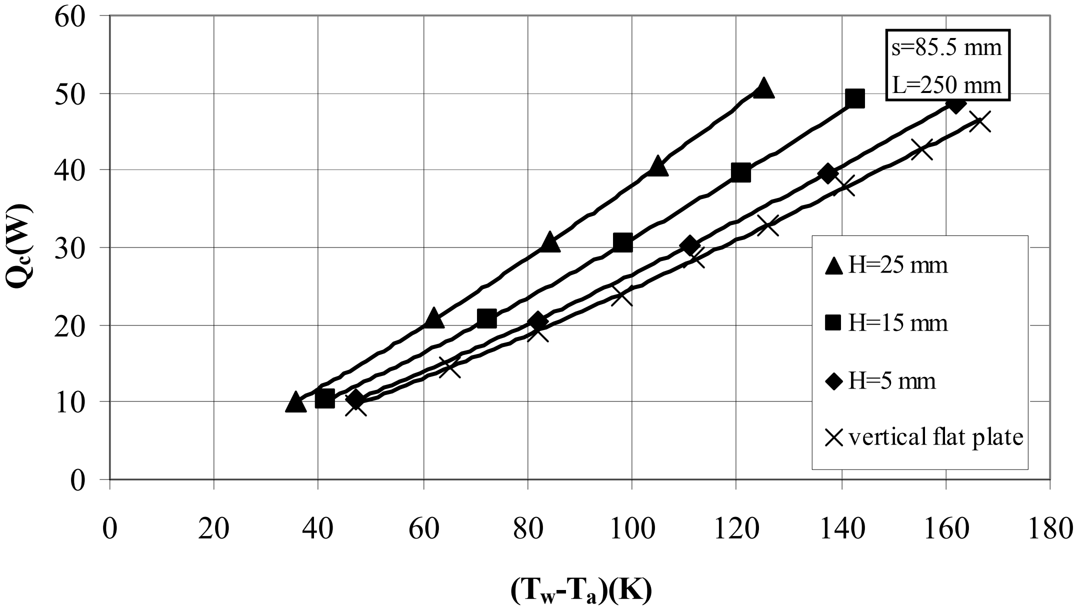

Figure 5.5 Variation of Convection Heat Transfer Rate with Fin Height at a Fin Spacing of s=85.5 mm and at a Fin Length of L=250 mm

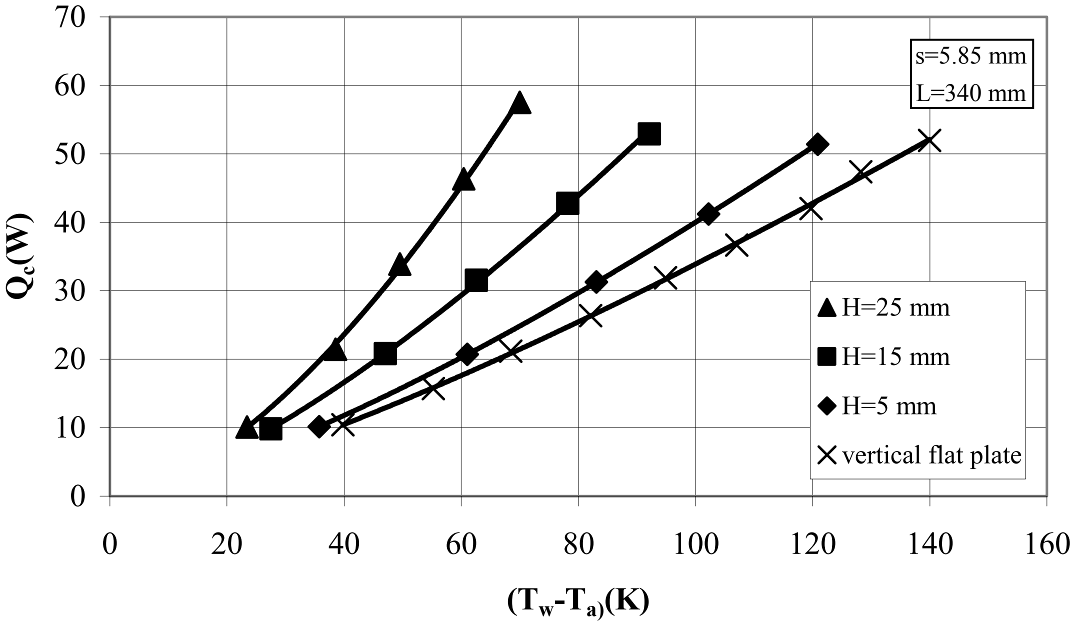

Figure 5.6 Variation of Convection Heat Transfer Rate with Fin Height at a Fin Spacing of s=5.85 mm and at a Fin Length of L=340 mm

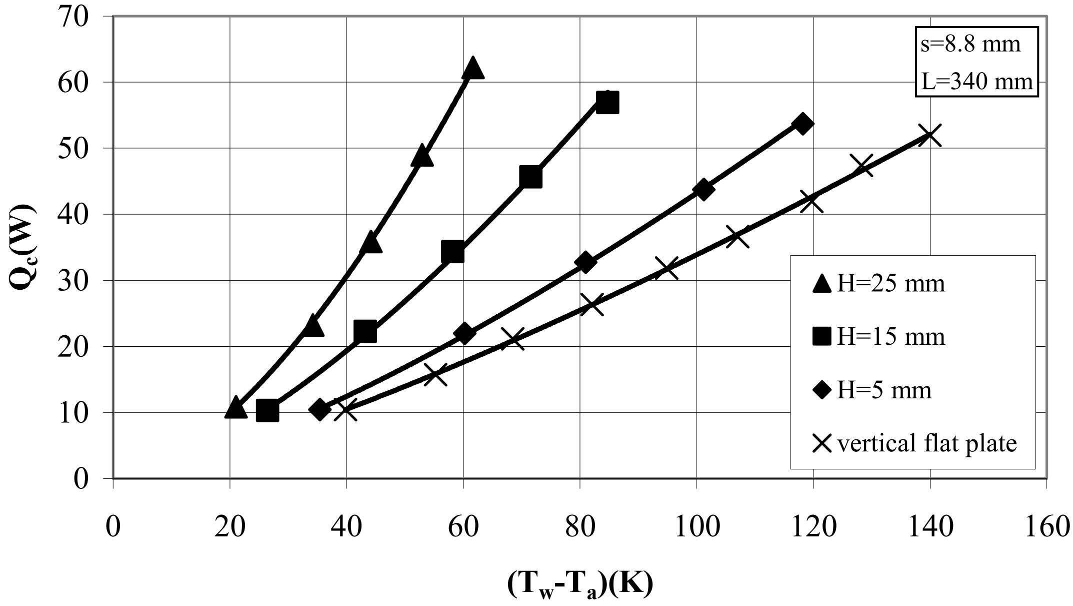

Figure 5.7 Variation of Convection Heat Transfer Rate with Fin Height at a Fin Spacing of s=8.8 mm and at a Fin Length of L=340 mm

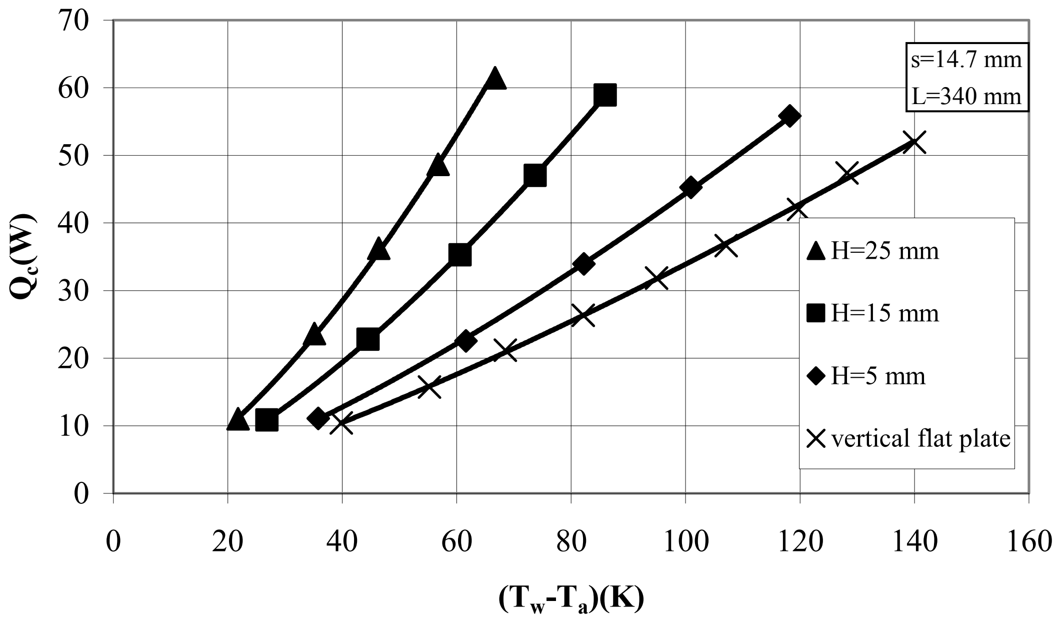

Figure 5.8 Variation of Convection Heat Transfer Rate with Fin Height at a Fin Spacing of s=14.7 mm and at a Fin Length of L=340 mm

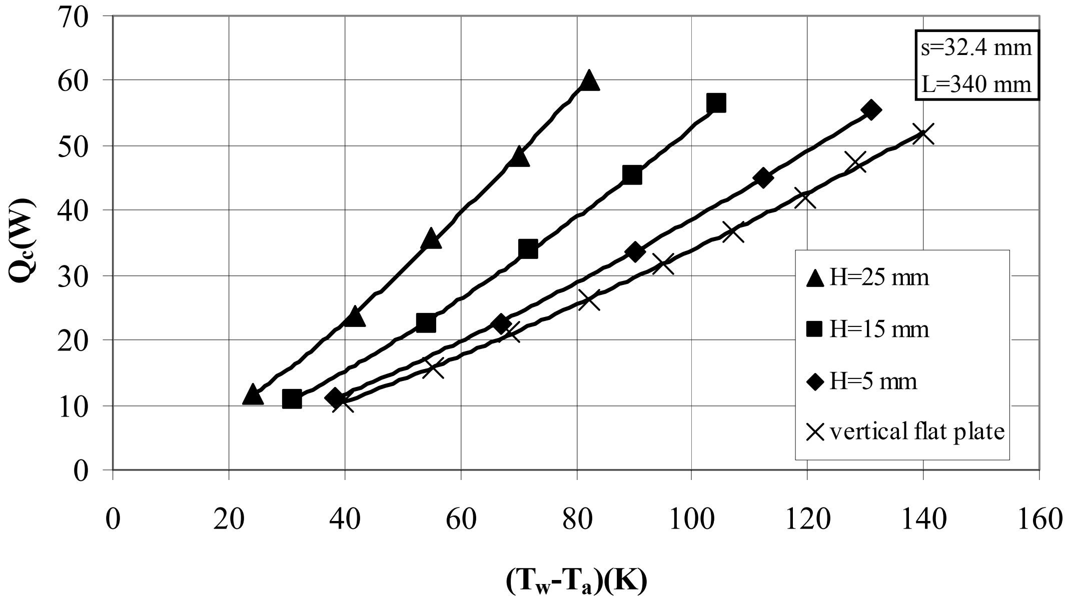

Figure 5.9 Variation of Convection Heat Transfer Rate with Fin Height at a Fin Spacing of s=32.4 mm and at a Fin Length of L=340 mm

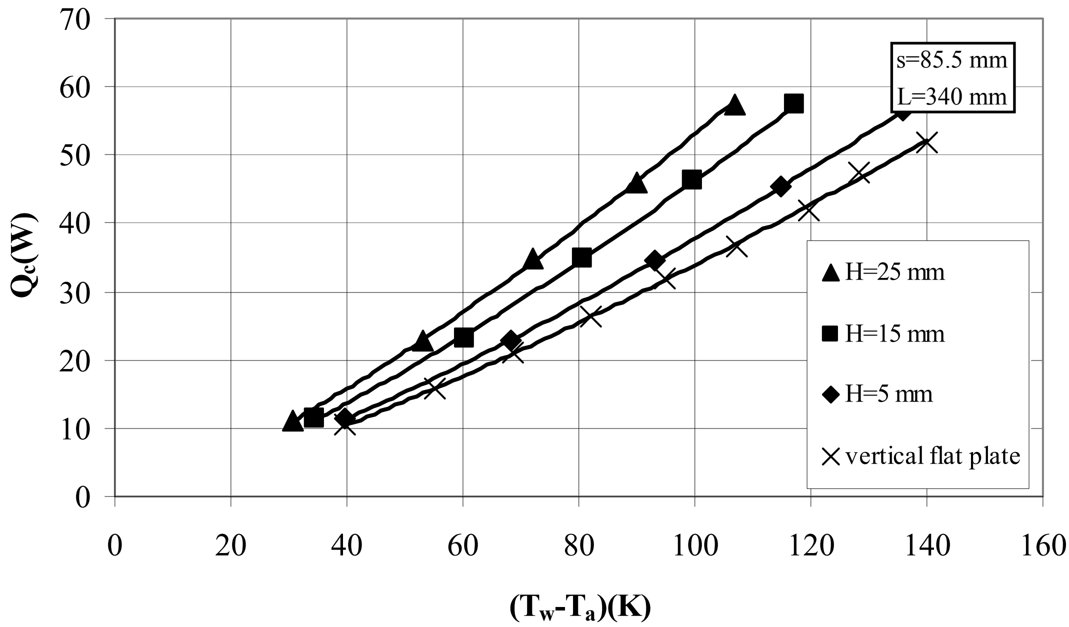

Figure 5.10 Variation of Convection Heat Transfer Rate with Fin Height at a Fin Spacing of s=85.5 mm and at a Fin Length of L=340 mm

As observed in Figures 5.1 through 5.10, the convection heat transfer rate from fin arrays depends on fin height, fin length, fin spacing and base-to-ambient temperature difference. It is seen that the convective heat transfer rates from the fin arrays increases with fin height and base-to-ambient temperature difference. The effect of extending the fin length from 250 mm to 340 mm results in higher steady-state convective heat dissipation from the fin arrays. However, the curves demonstrating the behaviors of fin heights show similar trends for similarly spaced and longitudinally different fin arrays. The heat transfer rates measured from three fin heights are close to each other at low base-to-ambient temperature differences whereas at high base-to-ambient temperature differences, the heat transfer rates tend to diverge with the variation in fin height.

With increasing fin spacing, the convection heat transfer rates from fin arrays approach the values measured from vertical flat plates, regardless of the presence of fin height parameter. However, the effect of fin height can be realized more clearly for the fin arrays having relatively smaller fin spacings. The change of fin length from 250 mm to 340 mm causes an increase in convection heat transfer rates for each fin configuration. The average relative improvements in the rates of convection heat transfer from identically spaced fin arrays for fin heights of 5 mm, 15 mm and 25 mm are 37.44 %, 39.01 % and 41.28 %, respectively.

The effect of fin spacing on convection heat transfer rate can be observed in Figures 5.11 through 5.16. These figures are classified for fin lengths L = 250 mm and L = 340 mm, for fin heights H = 5 mm, H = 15 mm and H = 25 mm, respectively. In each figure the data groups are separated for 5 different fin separations and the vertical plate.

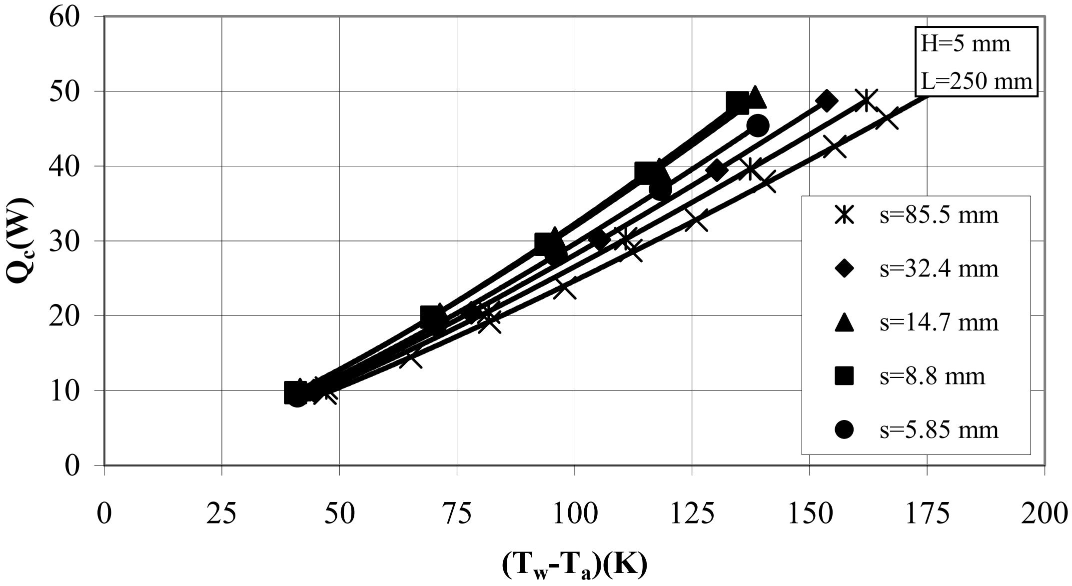

Figure 5.11 Variation of Convection Heat Transfer Rate with Fin Spacing at a Fin Height of H=5 mm and at a Fin Length of L=250 mm

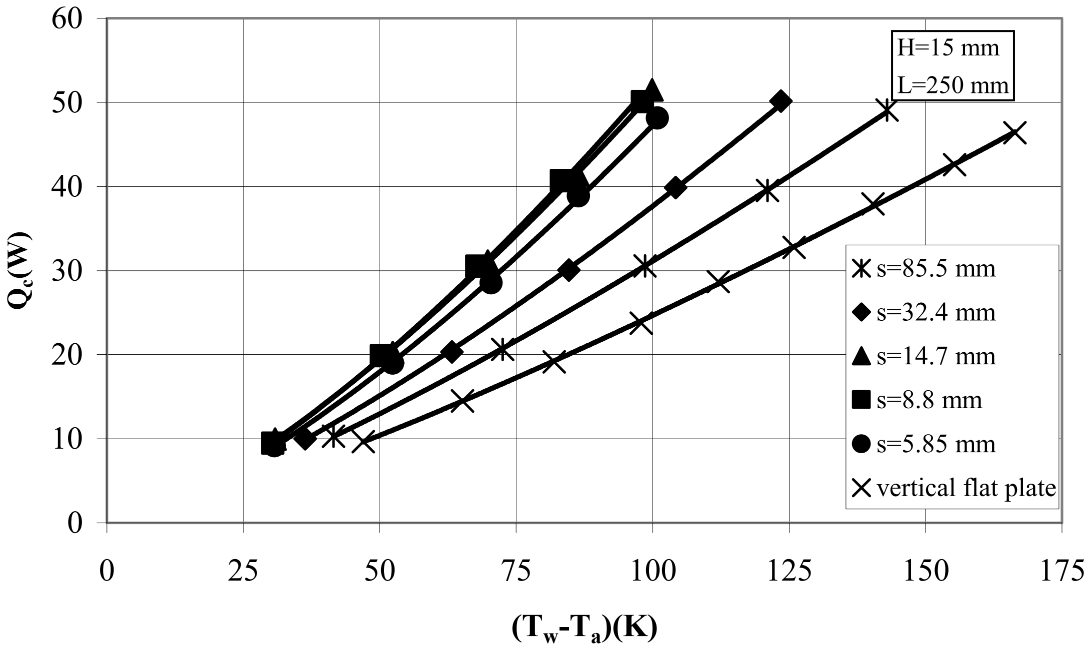

Figure 5.12 Variation of Convection Heat Transfer Rate with Fin Spacing at a Fin Height of H=15 mm and at a Fin Length of L=250 mm

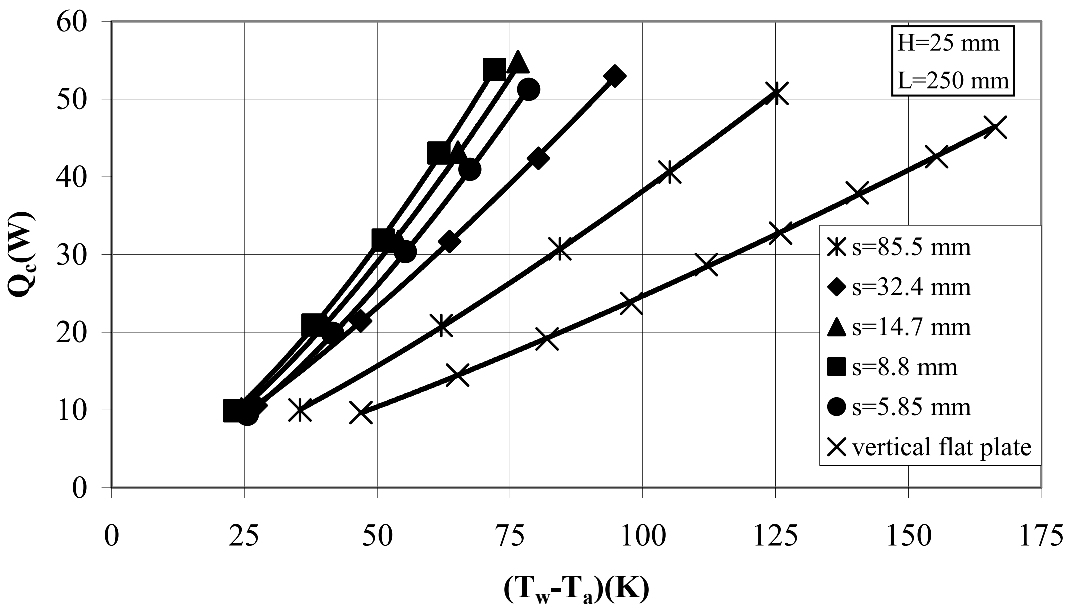

Figure 5.13 Variation of Convection Heat Transfer Rate with Fin Spacing at a Fin Height of H=25 mm and at a Fin Length of L=250 mm

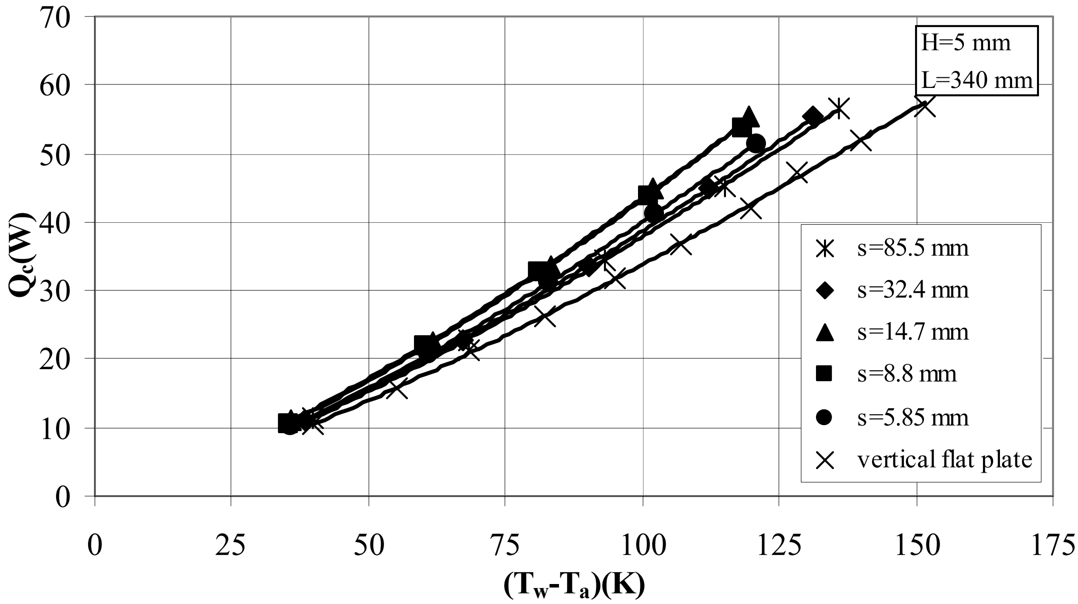

Figure 5.14 Variation of Convection Heat Transfer Rate with Fin Spacing at a Fin Height of H=5 mm and at a Fin Length of L=340 mm

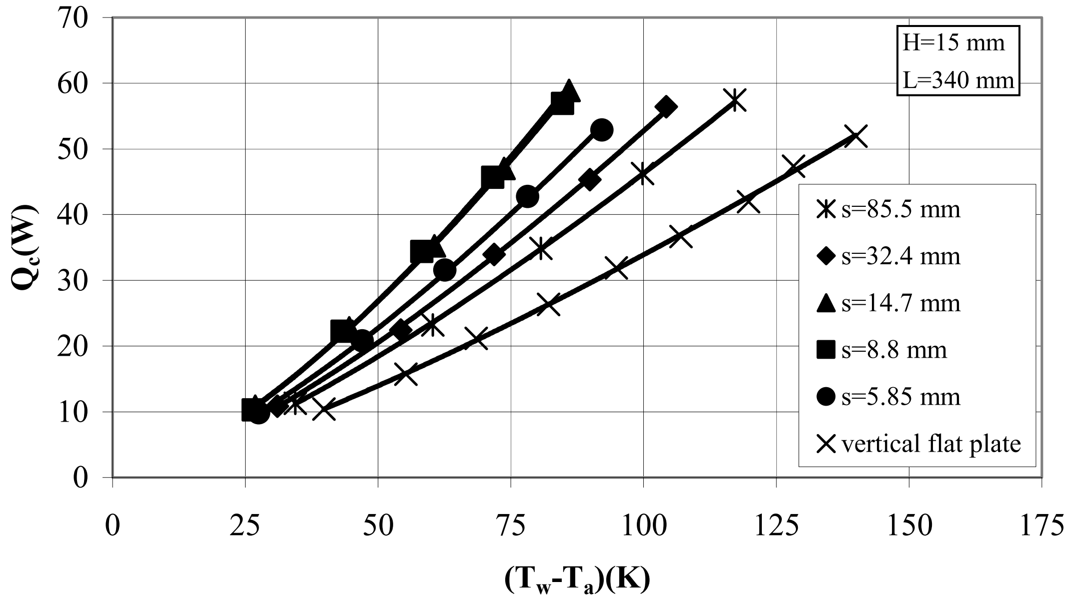

Figure 5.15 Variation of Convection Heat Transfer Rate with Fin Spacing at a Fin Height of H=15 mm and at a Fin Length of L=340 mm

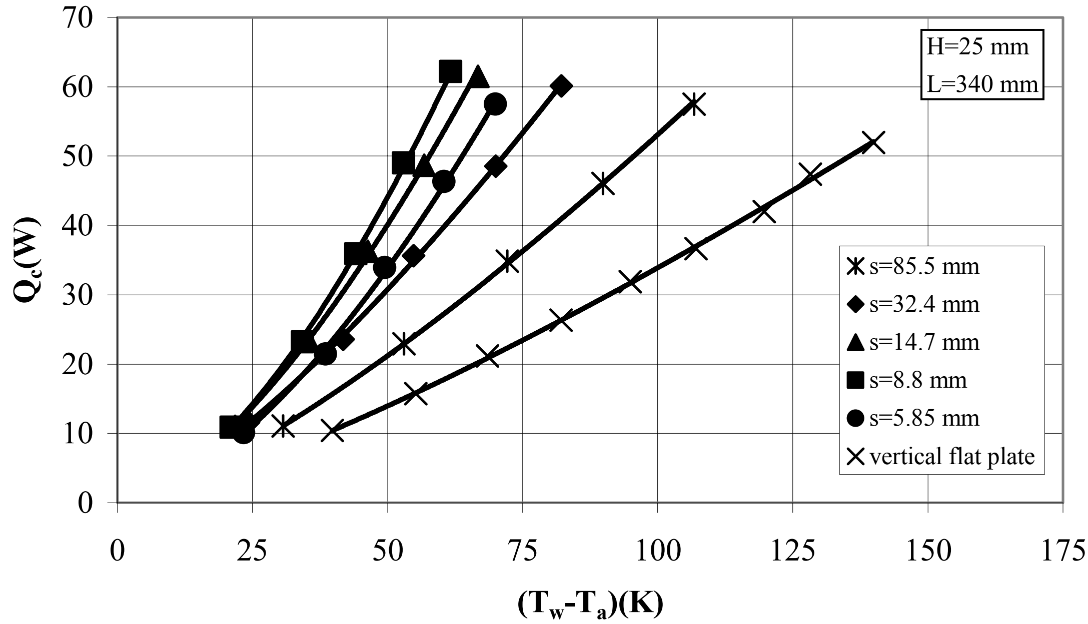

Figure 5.16 Variation of Convection Heat Transfer Rate with Fin Spacing at a Fin Height of H=25 mm and at a Fin Length of L=340 mm

When the curves in Figures 5.11 through 5.16 are considered together, it can be concluded that at low heat inputs, the convection heat transfer rate from fins are closer than those at high heat inputs, regardless of variation in fin spacing and fin height. In all of these six figures, the convection heat transfer rates from fin arrays for fin spacing values, s = 8.8 mm or s = 14.7 mm are greater than those of remaining fin separations, for a given base-to-ambient temperature difference and fin height. This observation is valid for both fin lengths since the trend of curves showing the heat transfer performances for the identically spaced fin arrays are quite similar.

The effect of base-to-ambient temperature difference on convection heat transfer rate can be seen more clearly in Figures 5.17 through 5.22. In these figures, convection heat transfer rates are plotted as a function of fin spacing. The figures were prepared for fin lengths L = 250 mm and L = 340 mm, and for fin heights H = 5 mm, H = 15 mm and H = 25 mm, respectively.

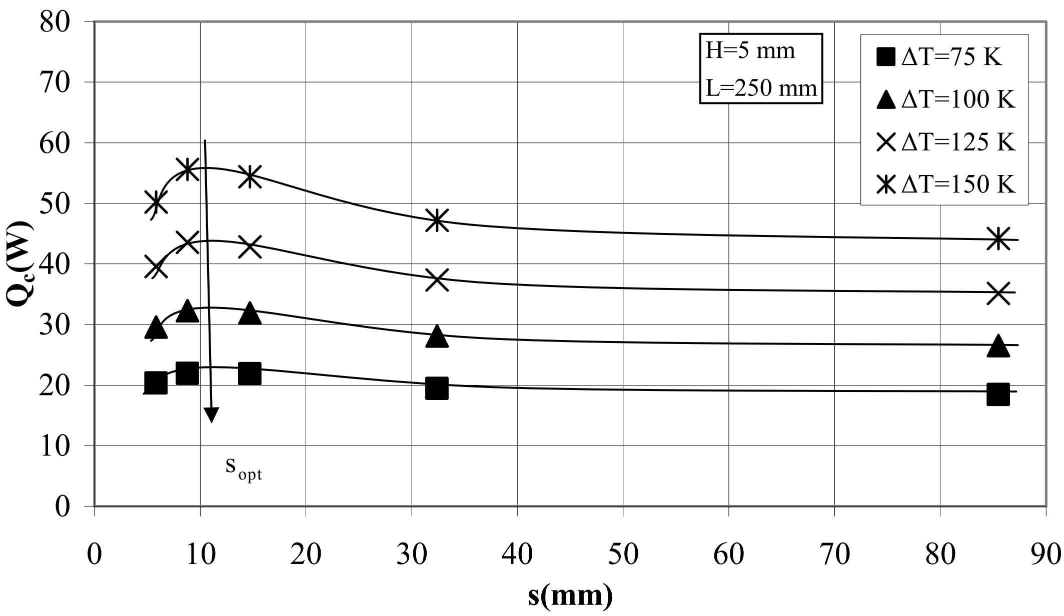

Figure 5.17 Variation of Convection Heat Transfer Rate with Base-to-Ambient Temperature Difference at a Fin Height of H=5 mm and a Fin Length of L=250 mm

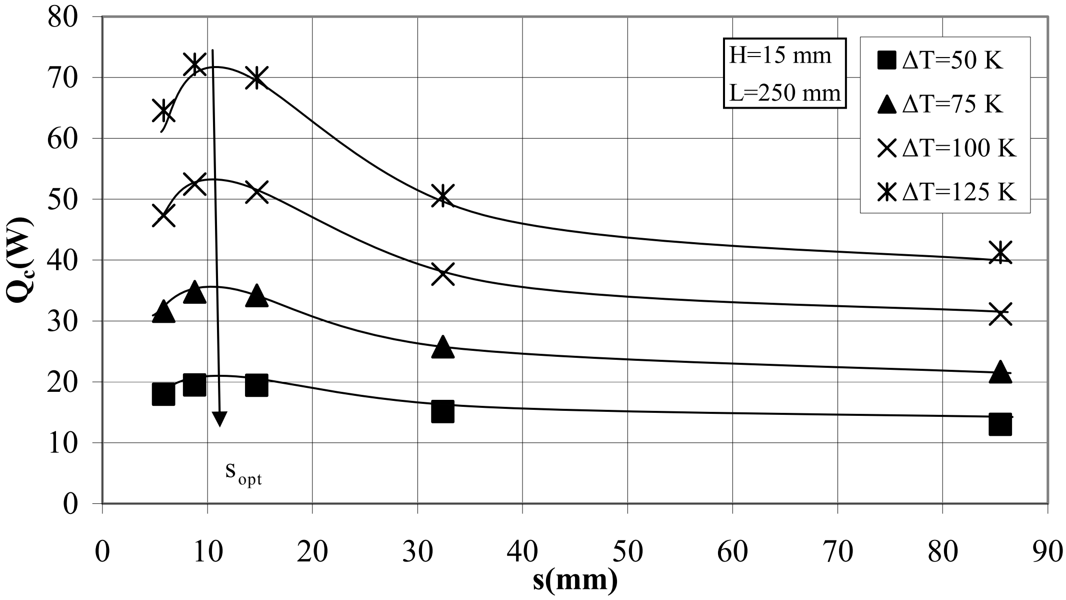

Figure 5.18 Variation of Convection Heat Transfer Rate with Base-to-Ambient Temperature Difference at a Fin Height of H=15 mm and a Fin Length of L=250 mm

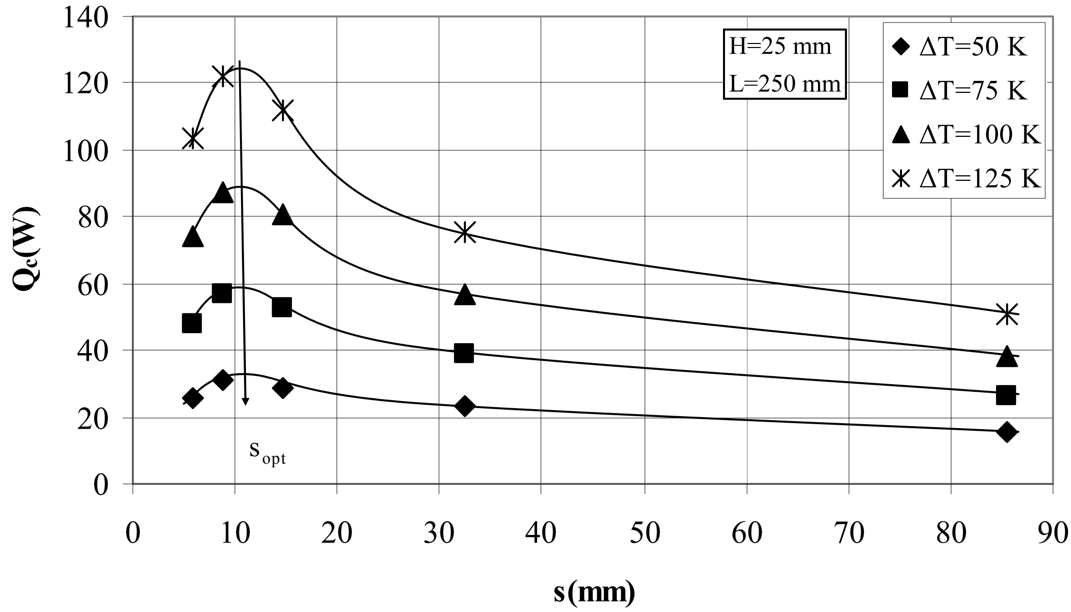

Figure 5.19 Variation of Convection Heat Transfer Rate with Base-to-Ambient Temperature Difference at a Fin Height of H=25 mm and a Fin Length of L=250 mm

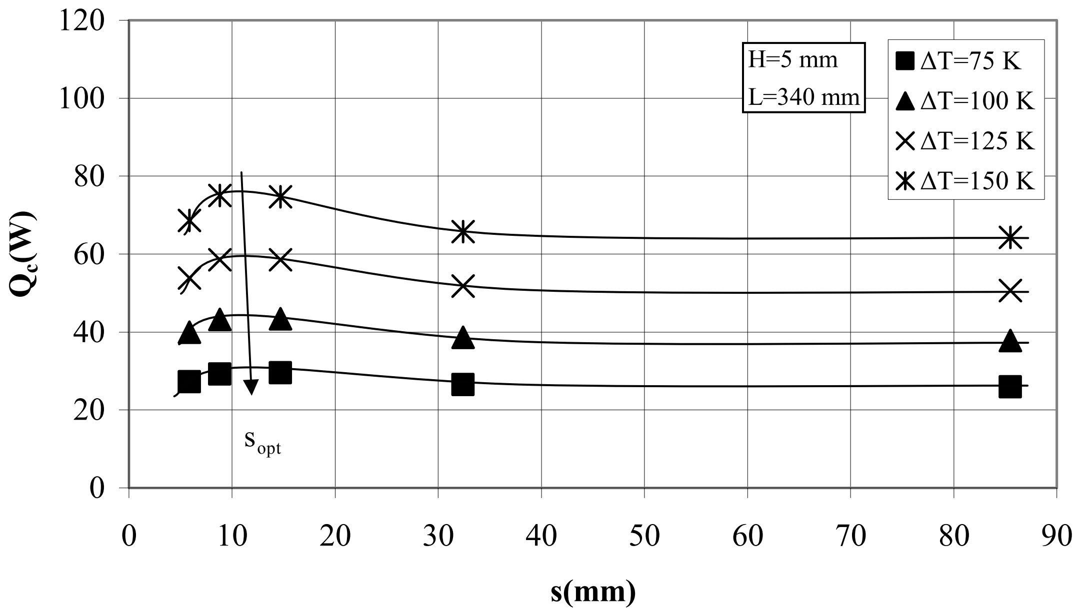

Figure 5.20 Variation of Convection Heat Transfer Rate with Base-to-Ambient Temperature Difference at a Fin Height of H=5 mm and a Fin Length of L=340 mm

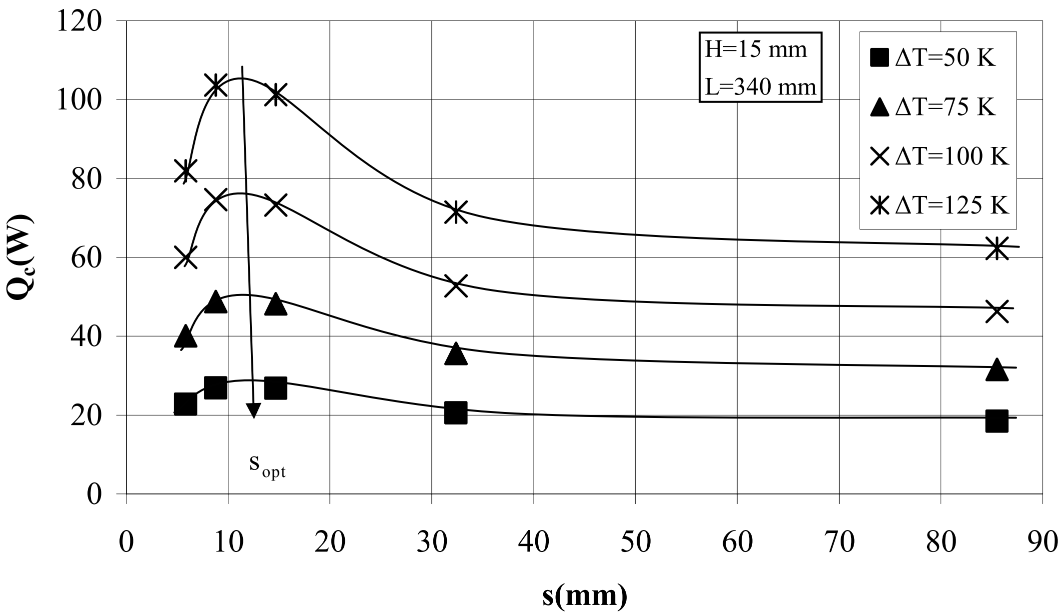

Figure 5.21 Variation of Convection Heat Transfer Rate with Base-to-Ambient Temperature Difference at a Fin Height of H=15 mm and a Fin Length of L=340 mm

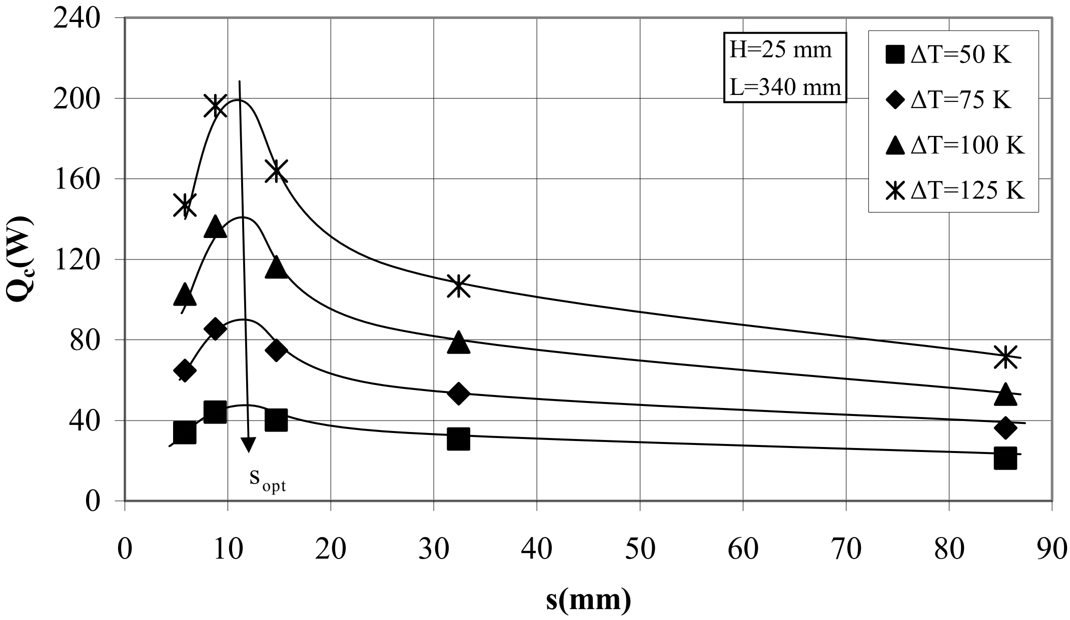

Figure 5.22 Variation of Convection Heat Transfer Rate with Base-to-Ambient Temperature Difference at a Fin Height of H=25 mm and a Fin Length of L=340 mm

From examination of Figures 5.17 through 5.22, it can be deduced that the convection heat transfer rate from an array increases with fin spacing, and after reaching its maximum point, it starts decreasing at a given fin height, fin length and base-to-ambient temperature difference. The corresponding fin spacing value of the maximum convection heat transfer rate point is called optimum fin spacing, s_{opt}.

It is observed that the optimum fin spacing varies between 8.8 mm and 14.7 mm. This conclusion reveals that the optimum fin spacing is sensitive to the variations in fin height, fin length and base-to-ambient temperature difference parameters. The variation of optimum fin spacings with fin length, fin height and base-to-ambient temperature difference are given in Table 5.1.

Table 5.1 Optimum Fin Spacings

s_{opt}(mm)						
	H=5 mm		H=15 mm		H=25 mm	
	L(mm)		L(mm)		L(mm)	
ΔT(K)	250	340	250	340	250	340
50	-	-	10.9	11.8	11	11.9
75	10.7	11.6	10.8	11.7	10.9	11.8
100	10.6	11.5	10.7	11.6	10.8	11.7
125	10.5	11.4	10.6	11.4	10.7	11.6
150	10.4	11.3	-	-	-	-

CHAPTER 6

SCALE ANALYSIS

The main purpose of this chapter is to obtain a relation for the optimum fin spacing that maximizes the heat transfer rate from vertical rectangular fins extending perpendicularly out of a vertical rectangular base. The scale analysis, which uses the basic principles of free convection heat transfer in order to produce order-of-magnitude estimates for optimum fin spacing, is performed for the relation.

To develop a general relationship, the experimental results of this study and the experimental results in available literature [2,3,9,10,11,12,14] are correlated. Experimental data obtained from literature are presented in Appendix I. Summary of the values of experimental and geometric parameters used in available literature are also given in Table I.1.

For the scale analysis, the procedure applied for annular fins on horizontal cylinder in Ref. [15] was adapted for the current geometry. With the following assumptions:

- The vertical base plate of length L is modeled as isothermal at temperature T_w, and the temperature of ambient air is taken as constant at T_a
- To maximize the total convection heat transfer rate from the fin array to the ambient, the two parameters, fin height L and fin spacing s, are utilized
- The thickness of the fins is considered negligible
- The flow is accepted as laminar
- The fin surfaces are assumed to be sufficiently smooth to justify the use of heat transfer results for natural convection over vertical smooth wall

- The base-to-ambient temperature difference, $\Delta T = T_w - T_a$, in the order of magnitude sense, is assumed to be representative of the temperature difference in the flow field.

In order to determine an optimum fin spacing for which the convection heat transfer rate from the fins is maximum, the following two extreme conditions are considered:

1. In the limiting cases of very small value of s (small-s limit), the flow is fully developed channel flow.
2. When fin spacing s, is much greater than the boundary layer thickness (large-s limit), the flow is boundary layer flow.

6.1 The Small-s Limit

In small-s limit, the boundary layer interferences occur immediately after air enters to the channels of the fin array, and therefore, the flow through each channel of the array can be assumed as fully developed channel flow. The total heat transfer rate from a single channel is given by:

$$\dot{Q}^{(1)}_{c_{\substack{\text{single}\\\text{channel}}}} = \dot{m} \cdot C_p \cdot \Delta T \tag{6.1}$$

where $\dot{m}$ is the mass flow rate through a single channel, C_p is the specific heat of air at constant pressure and ΔT is order-of-magnitude of the temperature difference.

From the scale analysis of continuity and momentum equations, mass flow rate can be written as:

$$\dot{m} \approx \frac{\rho \cdot g \cdot \beta \cdot s^3 \cdot \Delta T}{\nu} \cdot H \tag{6.2}$$

If the number of channels (or the fins) is defined as n = W/s ($W/s \gg 1$), then the total heat transfer rate from the fins may be expressed as:

$$\dot{Q}_c^{(1)} \approx \frac{\rho \cdot g \cdot \beta \cdot s^3 \cdot \Delta T}{\nu} \cdot H \cdot C_p \cdot \Delta T \cdot \frac{W}{s} \tag{6.3}$$

where $\dot{Q}_c^{(1)}$ is the difference between total convection heat transfer rate, $\dot{Q}_c$, and the convection heat transfer from the base-plate, $\left(\dot{Q}_o\right)_c$, as:

$$\dot{Q}_c^{(1)} = \dot{Q}_c - \left(\dot{Q}_o\right)_c \tag{6.4}$$

In Eq. (6.4), both $\dot{Q}_c$ and $\left(\dot{Q}_o\right)_c$ are evaluated at the same base-to-ambient temperature difference. Introducing the thermal diffusivity, α into Eq. (6.3), the following equation is obtained as:

$$\dot{Q}_c^{(1)} \approx \frac{g \cdot \beta \cdot s^3 \cdot \Delta T}{\nu \cdot \alpha} \cdot H \cdot k \cdot \Delta T \cdot \frac{W}{s} \tag{6.5}$$

As seen from Eq. (6.5), in the small-s limit, the total heat convection heat transfer rate is directly proportional with s^2. Figure 6.1 shows the trend indicated by small-s asymptote.

A dimensionless form of Eq. (6.5) may be obtained as:

$$\frac{\dot{Q}_c^{(1)} \cdot \frac{s}{W}}{H \cdot k \cdot \Delta T} \approx \frac{g \cdot \beta \cdot s^3 \cdot \Delta T}{\nu \cdot \alpha} \tag{6.6}$$

The right hand side of Eq. (6.6) can be written in terms of Rayleigh number based on fin spacing as:

$$\frac{\dot{Q}_c^{(1)}}{n \cdot k \cdot H \cdot \Delta T} \approx Ra_s \tag{6.7}$$

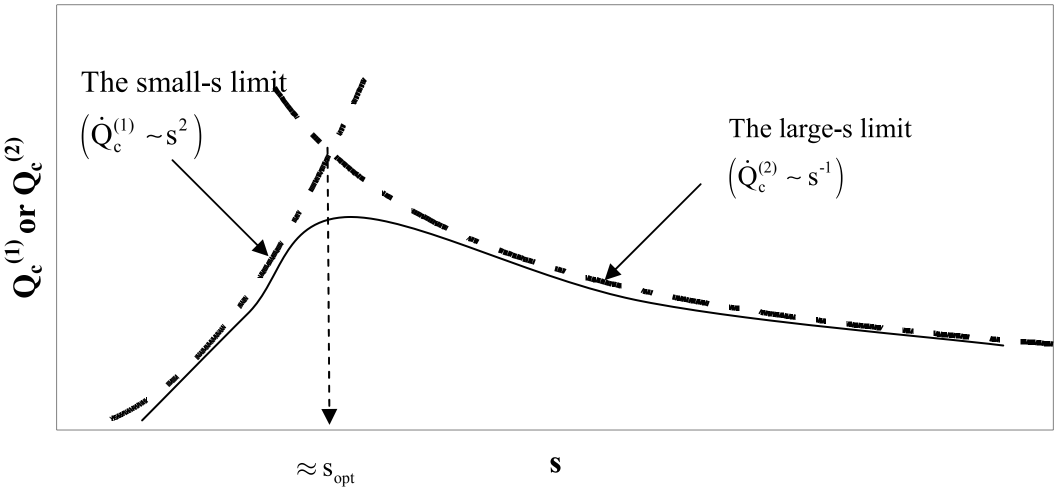

Figure 6.1 Asymptotic Plot for Extreme Limits

The experimental results valid for the small-s limit ($s<s_{opt}$) were substituted into Eq. (6.7) and the variation of $\frac{\dot{Q}_c^{(1)}}{n \cdot k \cdot H \cdot \Delta T}$ is plotted as a function of Ra_s. The trends of the data points are demonstrated with three curves in Figure 6.2. The equations of these curves are obtained by least square regression as:

$$\frac{\dot{Q}_c^{(1)}}{n \cdot k \cdot H \cdot \Delta T} = 0.010 \cdot Ra_s \qquad (6.8a)$$

$$\frac{\dot{Q}_c^{(1)}}{n \cdot k \cdot H \cdot \Delta T} = 0.026 \cdot Ra_s \qquad (6.8b)$$

$$\frac{\dot{Q}_c^{(1)}}{n \cdot k \cdot H \cdot \Delta T} = 0.018 \cdot Ra_s \qquad (6.8c)$$

Eqs. (6.8a), (6.8b) and (6.8c) are obtained from the data points of present study, those of Refs. [2,3,9,10,11,12,14] and those of all studies, respectively.

6.2 The Large-s Limit

In the large-s limit, the fin spacing s is sufficiently greater than the boundary layer thickness, and hence, the boundary layers develop without any interference in the channel. Under boundary layer flow conditions, the total convection heat transfer rate from a single fin can be expressed as:

$$\dot{Q}^{(2)}_{c_{\substack{\text{single}\\\text{fin}}}} = 2 \cdot h \cdot A \cdot \Delta T \tag{6.9}$$

where h is the heat transfer coefficient over single fin, A is the area of single fin and ΔT is order-of-magnitude of the temperature difference.

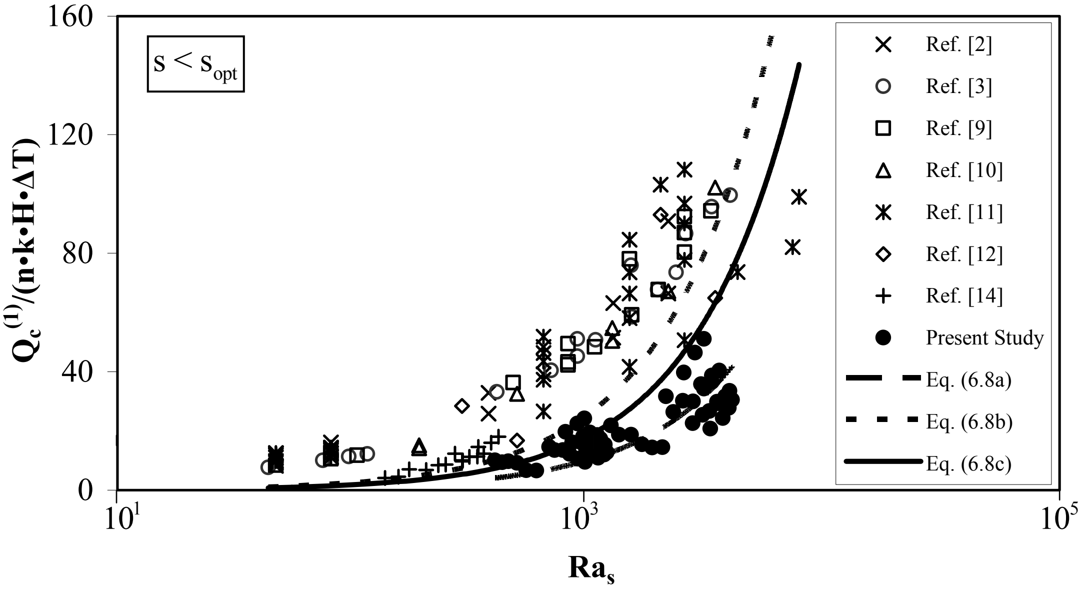

Figure 6.2 Plot of Dimensionless Eq. (6.7)

Applying the scale analysis to Navier-Stokes equations and energy equation as presented in Appendix G, heat transfer coefficient can be written as:

$$h \approx \left(\frac{\rho \cdot g \cdot \beta \cdot L^3 \cdot \Delta T}{\nu \cdot \alpha} \right)^{0.25} \cdot \frac{k}{L} \tag{6.10}$$

If the area of the single fin, A = H·L and the number of fins, n = W/s are introduced into Eq. (6.9), the total heat transfer rate from the fins can be expressed as:

$$\dot{Q}_c^{(2)} \approx 2 \cdot \left(\frac{g \cdot \beta \cdot L^3 \cdot \Delta T}{\nu \cdot \alpha} \right)^{0.25} \cdot \frac{k}{L} \cdot H \cdot L \cdot \Delta T \cdot \frac{W}{s} \tag{6.11}$$

where $\dot{Q}_c^{(2)}$ is the difference between total convection heat transfer rate, $\dot{Q}_c$, and the convection heat transfer from the base-plate, $\left(\dot{Q}_o\right)_c$, as:

$$\dot{Q}_c^{(2)} = \dot{Q}_c - \left(\dot{Q}_o\right)_c \tag{6.12}$$

Eq. (6.11) can be written in the following form as:

$$\dot{Q}_c^{(2)} \approx 2 \cdot \left(\frac{g \cdot \beta \cdot L^3 \cdot \Delta T}{\nu \cdot \alpha} \right)^{0.25} \cdot k \cdot H \cdot \Delta T \cdot \frac{W}{s} \tag{6.13}$$

As seen from Eq. (6.13), in the large-s limit, the convection heat transfer rate from the fins is inversely proportional with s. Figure 6.1 shows the trend indicated by large-s asymptote.

A dimensionless form of Eq. (6.13) may be obtained as:

$$\frac{\dot{Q}_c^{(2)} \cdot \frac{s}{W}}{H \cdot k \cdot \Delta T} \approx 2 \cdot \left(\frac{g \cdot \beta \cdot L^3 \cdot \Delta T}{\nu \cdot \alpha} \right)^{0.25} \tag{6.14}$$

The right hand side of Eq. (6.14) can be written in terms of Rayleigh number based on fin length as:

$$\frac{\dot{Q}_c^{(2)}}{n \cdot k \cdot H \cdot \Delta T} \approx 2 \cdot Ra_L^{0.25} \tag{6.15}$$

Substituting the experimental results valid for the large-s limit ($s>s_{opt}$) into Eq. (6.15), the variation of $\frac{\dot{Q}_c^{(2)}}{n\cdot k\cdot H\cdot \Delta T}$ is plotted as a function of $Ra_L^{0.25}$ as shown in Figure 6.3. The data points obtained from experimental results for the case of large-s limit, $s>s_{opt}$ are fitted with curves whose equations are evaluated by least square regression as:

$$\frac{\dot{Q}_c^{(2)}}{n\cdot k\cdot H\cdot \Delta T} = 0.671\cdot Ra_L^{0.25} \tag{6.16a}$$

$$\frac{\dot{Q}_c^{(2)}}{n\cdot k\cdot H\cdot \Delta T} = 1.517\cdot Ra_L^{0.25} \tag{6.16b}$$

$$\frac{\dot{Q}_c^{(2)}}{n\cdot k\cdot H\cdot \Delta T} = 1.204\cdot Ra_L^{0.25} \tag{6.16c}$$

Eqs. (6.16a), (6.16b) and (6.16c) are obtained from the data points of present study, those of Refs. [2,3,9,10,11,12,14] and those of all studies, respectively.

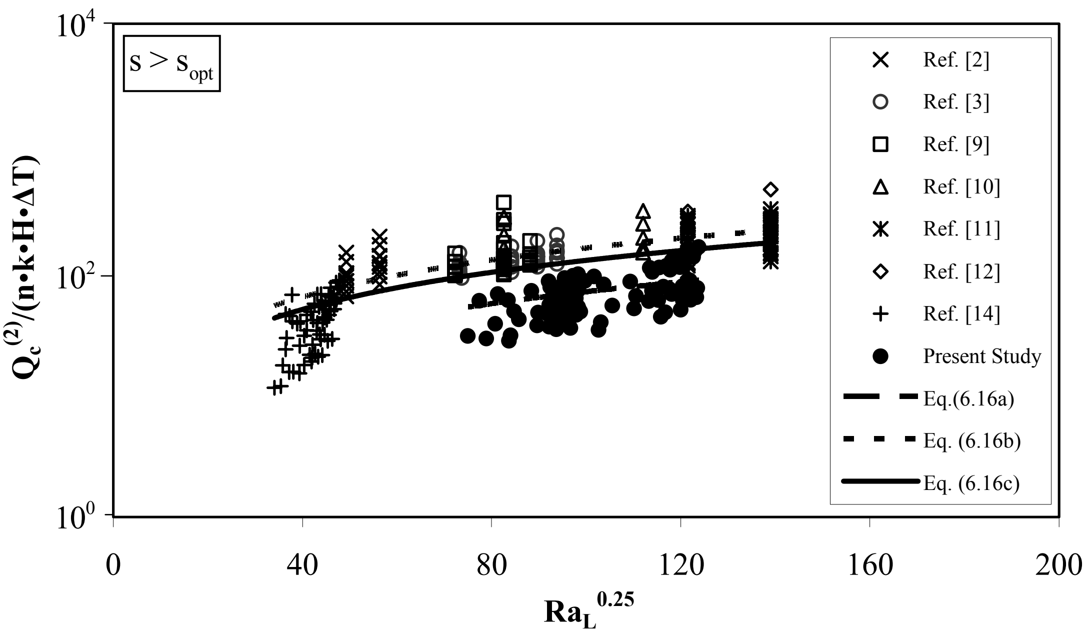

Figure 6.3 Plot of Dimensionless Eq. (6.15)

It is seen from Figures 6.2 and 6.3 that the data of dimensionless heat transfer from fins, obtained from the experimental results of present study and Ref. [14] are smaller than those of Refs. [2,3,9,10,11,12] for the same Rayleigh numbers. This is presumably due to the differences in the experimental set-ups and experimental procedures used in these studies.

The relations obtained from two extreme conditions are two asymptotes of convective heat transfer versus fin spacing. It is estimated from the scale analysis that the total convection heat transfer rate is proportional with s^2 for the case of small-s limit. On the other hand, for large-s limit, the total heat transfer rate is inversely proportional with fin spacing, s. The trends of two curves reveal that the intersection of curves must give the maximum rate of total convection heat transfer which indicates the optimum fin spacing. As shown in Figure 6.1, the maximum occurs in the vicinity of the intersection [20]:

$$\dot{Q}_c^{(1)} = \dot{Q}_c^{(2)} \tag{6.17}$$

Substituting the expressions for total convection heat transfer rates into Eq. (6.17), the intersections of Eqs. (6.8) and (6.16) may be obtained in terms of Rayleigh numbers as:

$$Ra_s = 67.1 \cdot Ra_L^{0.25} \tag{6.18a}$$

$$Ra_s = 59.3 \cdot Ra_L^{0.25} \tag{6.18b}$$

$$Ra_s = 65.8 \cdot Ra_L^{0.25} \tag{6.18c}$$

The Rayleigh numbers based on fin spacing estimated by experimentally obtained values of optimum fin spacings versus Rayleigh numbers, based on fin lengths estimated for that optimum fin spacing is given in Figure 6.4. Eq. (6.18c) is also plotted in Figure 6.4 in order to compare the curve with the values that are obtained experimentally. Since Eqs. (6.18a), (6.18b) and (6.18c) are similar, Eq. (6.18c), obtained from the curves fitting all data points, can be used for comparison.

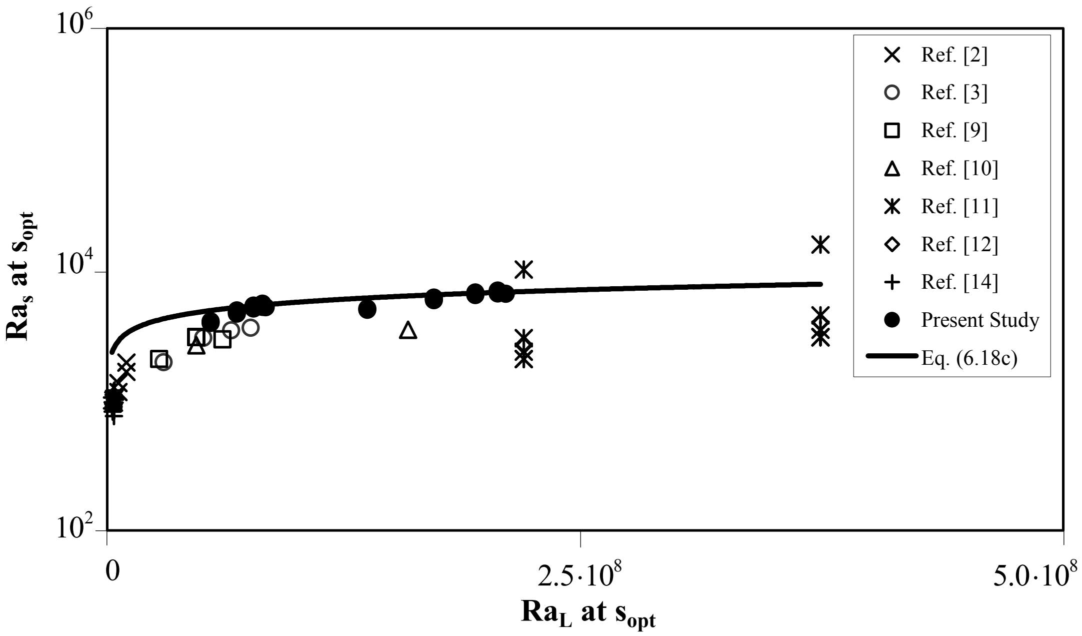

Figure 6.4 Comparison of Eq. (6.18c) with Rayleigh Numbers Obtained by Using Estimated Optimum Fin Spacings

As seen from Figure 6.4, Eq. (6.18c) does not fit all the estimated experimental values. Since this analysis gives only an order-of-magnitude estimation, a perfect agreement between the experimental data and the equation should not be expected.

If the definitions of Ra_s and Ra_L are introduced into Eqs. (6.18a), (6.18b) and (6.18c), the optimum fin spacing s_{opt} for maximum heat transfer rate can be approximated as:

$$\frac{s_{opt}}{L} = 4.064 \cdot Ra_L^{-0.25} \tag{6.19a}$$

$$\frac{s_{opt}}{L} = 3.899 \cdot Ra_L^{-0.25} \tag{6.19b}$$

$$\frac{s_{opt}}{L} = 4.037 \cdot Ra_L^{-0.25} \tag{6.19c}$$

As seen from Eqs. (6.18a), (6.18b) and (6.18c), the correlations obtained from three data groups are roughly equal to each other. Therefore, Eq. (6.19c), estimated from Eq. (6.18c), can be used as a general correlation for optimum fin spacing. The experimentally estimated optimum fin spacing values are utilized to demonstrate the variation of s_{opt}/L with Ra_L evaluated at each optimum fin spacing values in Figure 6.5. These experimental data were compared with Eq. (6.19c) by plotting the results in the same graph.

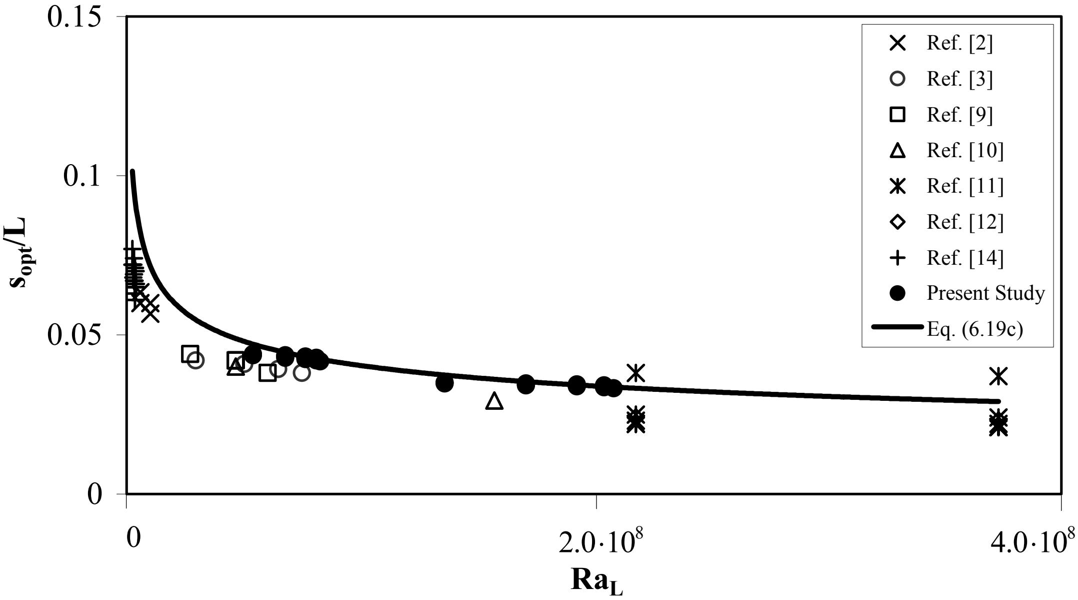

Figure 6.5 Comparison of Eq. (6.19c) with Experimentally Estimated Optimum Fin Spacings

As observed from Figure 6.5, the experimental results follow similar trend with the curve of Eq. (6.19c). The deviations between the experimental data and the curve may be due to the uncertainty of the experimental data and the errors of optimum fin spacing readings obtained from figures in Chapter 5 and Appendix I.

Substituting s_{opt} into Eq. (6.16c), an order-of-magnitude estimate for the maximum convection heat transfer rate from fins can also be obtained as:

$$\dot{Q}_{c_{max}} - \left(\dot{Q}_o\right)_c \leq 0.298 \cdot k \cdot H \cdot \Delta T \cdot Ra_L^{0.5} \cdot \frac{W}{L} \tag{6.20}$$

Eq. (6.20) shows that the maximum heat transfer rate from fins is roughly proportional to $\Delta T^{1.5}$. The inequality in Eq. (6.20) reveals that the peak of convection heat transfer rate curve falls under the intersection of the two asymptotes in Figure 6.1. The comparison of Eq. (6.20) with the experimental results is given in Figure 6.6.

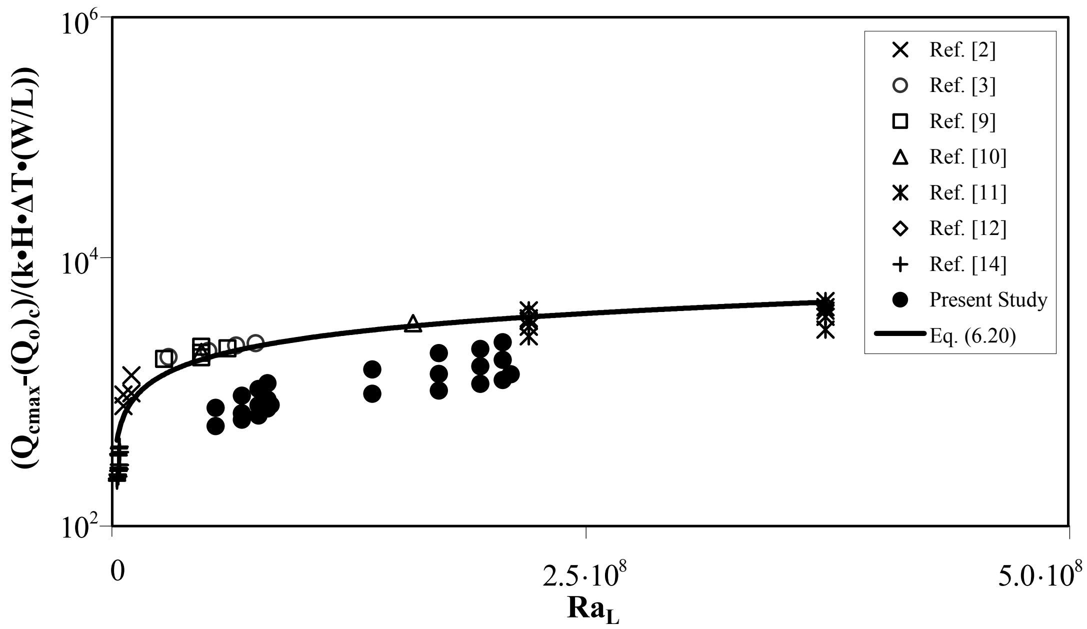

Figure 6.6 Comparison of Eq. (6.20) with Experimentally Estimated Maximum Convection Heat Transfer Rates

In Figure 6.6, it is seen that some experimental data points are slightly above the curve of Eq. (6.20). This is presumably due to the maximum heat transfer rate readings taken from figures presented in Chapter 5 and Appendix I. In general, values estimated from experimental results are below the curve which shows the validity of the inequality in Eq. (6.20) for the set of the experiments.

CHAPTER 7

CONCLUSIONS

In this study, the steady-state natural convection heat transfer from vertical rectangular fins protruding from a vertical base was investigated experimentally. The effects of geometric parameters, fin height, fin length and fin spacing, and base-to-ambient temperature difference on the heat transfer performance of fin arrays was discussed. A relation for the optimum fin spacing value that maximizes the heat transfer rate was obtained.

Two similar experimental set-ups were constructed and calibrated to perform the experiments with longitudinally different two fin array groups each of which has 15 sets of fin configurations. After the calibration of experimental set-ups had been verified, experiments were conducted on 30 different fin configurations in order to determine the heat transfer performances of the fin arrays.

The results of the experiments were presented graphically in Chapter 5 and tabulated in Appendix E. The results of the experimental work were reported in such a way that the effect of each parameter on the convection heat transfer rate from the fin arrays can be seen separately.

Experimental results showed that the larger fin height results in higher convection heat transfer rates from the fin arrays. As the temperature differences between fins and ambient decrease, the effect of fin height becomes insignificant. On the other hand, the variation in fin height influence the rate of convection heat transfer more effectively for smaller fin spacings with respect to larger fin separations. Since the array with smaller fin spacing has higher fin number, the increase in fin height causes larger surface area and higher convection heat transfer rate.

The effect of fin length on convection heat transfer performance of fin arrays was also observed. As a result of experimental data, the change of fin length from 250 mm to 340 mm causes an increase in convection heat transfer rates for each fin configuration. The average relative improvements in convection heat transfer rates from identically spaced fin arrays for fin heights of 5 mm, 15 mm and 25 mm are 37.44 %, 39.01 % and 41.28 %, respectively.

Another important parameter that influences the convection heat transfer rate is the fin spacing. As observed in Figures 5.17 through 5.22, the convection heat transfer rate from fin arrays increases as fin spacing decreases, and after a certain value of fin spacing, it starts to decrease with the further decrease in the fin spacing. The point which gives the maximum value of convection heat transfer is called the optimum fin spacing. At the optimum fin spacing, the air entering between the adjacent fins is not resisted, and hence, the boundary layer flow occurs without any interference. Therefore, the convection heat transfer from the fin array is maximized.

It is concluded from the tested 30 fin configurations that the optimum fin spacings are between 8.8 mm and 14.7 mm. In order to determine the optimum fin spacings for two longitudinally different fin array groups, Figures 5.17 through 5.22 were inspected carefully and for the given fin length, fin height and base-to-ambient temperature difference, the optimum fin spacing results are presented in Table 5.1. As seen from Table 5.1, optimum fin spacing depends on fin height, fin length and base-to-ambient temperature difference. However, neither of these parameters changes the value of the optimum fin spacing more than an amount of 1.5 mm.

This result can be supported with the study performed in Ref. [10]. The effects of changing fin length from 250 mm to 375 mm on the rate of heat transfer and on the optimum fin spacing of rectangular fins protruding from vertical base was investigated, experimentally. The experimental measurements showed that the optimum fin spacing rose from 10 ± 1 mm to 11 ± 1 mm as a result of the increase in fin length. The dimensions of the fin configurations employed in their study were similar to those of tested currently. Therefore, optimum fin spacing values determined in Ref. [10] are close to the values presented in Table 5.1, as expected.

A scale analysis is applied in order to produce order-of-magnitude estimates for the optimum fin spacing values. The problem was defined by two extreme conditions which indicate the type of flow through fin array. To develop general relations from the scale analysis, the experimental results of present study were combined with those of available literature and rearranged to be presented in dimensionless parameters as proposed in Chapter 6.

As a result of scale analysis, Eqs. (6.8) and (6.16) were obtained for the two different flow conditions. Eqs. (6.8) and (6.16) represent the curves shown in Figure 6.1. It is realized from these equations that in the small-s limit, where the channel flow is valid, the convection heat transfer rate is directly proportional with square of fin spacing, s^2. However, in the second case, for boundary layer flow, it is inversely proportional with s. Since the intersection of two equations gives the optimum fin spacing, Eqs. (6.8) and (6.16) were equated and Eq. (6.18) was obtained. Then, rearranging dimensionless terms in Eq. (6.18), Eqs. (6.19) and (6.20) were derived. Among these correlations, the most convenient one is the correlation numbered as Eq. (6.19) since it evaluates order-of-magnitude of the optimum fin spacing at a given fin length and base-to-ambient temperature difference.

The data points obtained from the experimental results of each study were classified with different marker styles in Figures 6.2 through 6.6 to display the consistency among each other. It was observed from Figures 6.2 and 6.3 that the dimensionless convective heat transfer rate from fins data of present study and Ref. [14] did not show similar behavior with those of Refs. [2,3,9,10,11,12] for the same Rayleigh numbers. This result reveals that the differences in the experimental set-ups and the experimental procedures used in these studies affect the values of dimensionless data.

In Figures 6.4, 6.5 and 6.6, Eqs. (6.18), (6.19) and (6.20) were compared with the experimentally estimated Rayleigh numbers based on fin spacing, the ratio of optimum fin spacing to fin length and the dimensionless maximum convection heat transfer from fins data, respectively. It is seen that the experimental results are in a good agreement with the correlations estimated by scale analysis. Since the scale analysis gives only an order-of-magnitude estimation, a perfect agreement between the experimental data and the equations should not be expected. These correlations are obtained from the experimental results of different studies. The experimental systems and procedures used in these studies may cause the deviations between the dimensionless data and the curves representing Eqs. (6.18), (6.19) and (6.20). In addition, the uncertainty of experiments and reading errors during the collection of maximum heat transfer rate and optimum fin spacing data from figures, presented in Chapter 5 and Appendix I, should be taken into account while examining the consequences.

REFERENCES

[1] Starner K.E. and McManus H.N., "An Experimental Investigation of Free Convection Heat Transfer from Rectangular Fin Arrays", Journal of Heat Transfer, 273-278, (1963)

[2] Leung C.W. and Probert S.D., "Thermal Effectiveness of Short-Protrusion Rectangular, Heat-Exchanger Fins", Applied Energy, 1-8, (1989)

[3] Leung C.W., et al., "Heat Exchanger: Optimal Separation for Vertical Rectangular Fins Protruding from a Vertical Rectangular Base", Applied Energy, 77-85, (1985)

[4] Welling J.R. and Wooldridge C.N., "Free Convection Heat Transfer Coefficients from Vertical Fins", Journal of Heat Transfer, 439-444, (1965)

[5] Harahap F. and McManus H.N., "Natural Convection Heat Transfer from Horizontal Rectangular Fin Arrays", Journal of Heat Transfer, 32-38, (1967)

[6] Jones C.D. and Smith L.F., "Optimum Arrangement of Rectangular Fins on Horizontal Surfaces for Free Convection Heat Transfer", Journal of Heat Transfer, 6-10, (1970)

[7] Fitzroy N.D., "Optimum Spacing of Fins Cooled by Free Convection", Journal of Heat Transfer, 462-463, (1971)

[8] Bar-Cohen A., "Fin Thickness for an Optimized Natural Convection Array of Rectangular Fins", Journal of Heat Transfer, 564-566, (1979)

[9] Leung C.W., et al., "Heat Exchanger Design: Thermal Performances of Rectangular Fins Protruding from Vertical or Horizontal Rectangular Bases", Applied Energy, 123-140, (1985)

[10] Leung C.W., et al., "Heat Transfer Performances of Vertical Rectangular Fins Protruding from Rectangular Bases: Effect of Fin Length", Applied Energy, 313-318, (1986)

[11] Leung C.W. and Probert S.D., ”Heat-Exchanger Design: Optimal Uniform Thickness of Vertical Rectangular Fins Protruding Perpendicularly Outwards, at Uniform Separations, from a Vertical Rectangular ‘Base’”, Applied Energy, 111-118, (1987)

[12] Ko Y.M., et al., “Steady –State Free-Convective Cooling of Heat Exchangers with Vertical Rectangular Fins: Effect of Fin Material”, Applied Energy, 181-191, (1989)

[13] Yüncü H. and Anbar G., “An Experimental Investigation on Performance of Rectangular Fins on a Horizontal Base in Free Convection Heat Transfer”, Heat and Mass Transfer, 507-514, (1998)

[14] Yüncü H. and Güvenc A., “An Experimental Investigation on Performance of Rectangular Fins on a Vertical Base in Free Convection Heat Transfer”, Heat and Mass Transfer, 409-416, (2001)

[15] Yüncü H. and Mobedi M., “A Three Dimensional Numerical Study on Natural Convection Heat Transfer from Short Horizontal Rectangular Fin Array”, Heat and Mass Transfer, (2003)

[16] Yüncü H. and Yildiz Ş., “An Experimental Investigation on Performance of Annular Fins on a Horizontal Cylinder in Free Convection Heat Transfer”, Heat and Mass Transfer, 239-251, (2004)

[17] Kakaç S., Convective Heat Transfer, METU, Ankara, (1980)

[18] Incropera F.P. and DeWitt D.P., Fundamentals of Heat and Mass Transfer, John Wiley & Sons, New York, (1990)

[19] McAdams W. H., Heat Transmission, McGraw-Hill, New York, (1954)

[20] Bejan A., Convection Heat Transfer, John Wiley & Sons, New York, (1984)

[21] Siegel R. and Howell J.R., Thermal Radiation Heat Transfer, McGraw-Hill, Tokyo, (1972)

APPENDIX A

SOLUTION PROCEDURE OF HEAT CONDUCTION EQUATION

For the solution of the heat conduction equation, the steady-state temperature of the heated base-plate is denoted as T_w and the boundary temperatures of the set-up are assumed to be at the ambient temperature T_a. Figure A.1 illustrates the schematic of the experimental set-up to show the necessary dimensions required during the solution of the heat conduction equation.

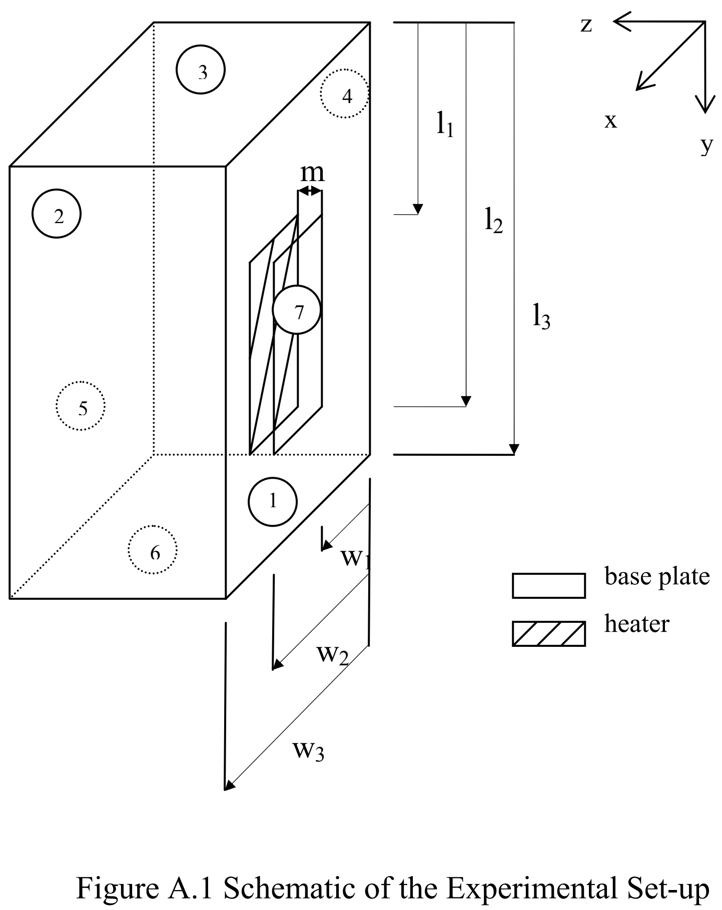

Figure A.1 Schematic of the Experimental Set-up

At steady state, the heat conduction equation and the boundary conditions of the problem are given by:

$$\nabla^2\theta(r_i)+\frac{\dot{q}'''(r_i)}{k}=0 \tag{A.1a}$$

$$\theta(r_i)=0 \qquad s_i \quad i=1,2,3,4,5,6 \tag{A.1b}$$

$$\theta(r_i)=\theta_w \qquad s_7 \tag{A.1c}$$

where θ=T-T_a,θ_w=T_w-T_a and $\dot{q}'''(r_i)$ is the volumetric energy source in (W/m^3)

The volumetric energy source, $\dot{q}'''$ may be converted to the strength of the plane-surface energy source, $\dot{q}_s''(x,y)$ by means of Dirac delta function as:

$$\dot{q}''' = \dot{q}_s''(x,y)\cdot\delta(z\text{-}m) \tag{A.2a}$$

$$\text{where} \int_{-\infty}^{\infty}\delta(z-m)\cdot dz=1 \tag{A.2b}$$

The distribution of the plane-surface energy source on the boundaries of the set-up may be given by:

$$\dot{q}_s''(x,y)=\begin{Bmatrix} 0 & \text{for} & 0<x<w_1 & \text{or} & 0<y<\ell_1 \\ \dot{q}''' & \text{for} & w_1<x<w_2 & \text{and} & \ell_1<y<\ell_2 \\ 0 & \text{for} & x>w_2 & \text{or} & y>\ell_2 \end{Bmatrix} \tag{A.3}$$

To solve the heat conduction equation given in Eq. (A.1), the following auxiliary homogeneous problem for the dependent variable $\psi(r)$ subject to homogeneous boundary conditions was considered:

$$\nabla^2\psi(r)+\lambda^2\psi(r)=0 \tag{A.4a}$$

$$\psi(r_i)=0 \qquad s_i \quad i=1,2,3,4,5,6,7 \tag{A.4b}$$

If $\psi_m(r)$ is the solution (eigenfunction) and λ_m are the eigenvalues of the system given in Eq. (A.4), the integral transform of the temperature may be defined as:

$$\overline{\theta}(\lambda_m)=\int_R \psi_m(\lambda_m,r)\cdot\theta(r)\cdot dr \tag{A.5a}$$

and the inversion formula is:

$$\theta(r)=\sum_{m=1}^{\infty}\frac{\overline{\theta}(\lambda_m)}{\int_R \psi_m{}^2(\lambda_m)\cdot dr}\cdot\psi_m(\lambda_m,r) \tag{A.5b}$$

Multiplying both sides of Eq. (A.1a) by eigenfunction, $\psi(r)$ and integrating over the region:

$$\int_R \psi_m(\lambda_m,r)\cdot\nabla^2\theta(r)\cdot dr+\frac{1}{k}\int_R \dot{q}'''(r)\cdot\psi_m(\lambda_m,r)\cdot dr=0 \tag{A.6}$$

The first integral in Eq. (A.6) can be evaluated by using Green's theorem as:

$$\int_R \psi_m\cdot\nabla^2\theta\cdot dr=\int_R \theta\cdot\nabla^2\psi_m\cdot dr+\sum_{i=1}^{s_i}\int_{s_i}\left[\psi_m\cdot\frac{\partial\theta}{\partial n_i}-\theta\cdot\frac{\partial\psi_m}{\partial n_i}\right]\cdot ds_i \tag{A.7}$$

where $\frac{\partial}{\partial n_i}$ represents differentiation along the outward normal to the boundary surface s_i.

The first term on the right hand side of Eq. (A.7) can be written in the following form as:

$$\int_R \theta \cdot \nabla^2 \psi_m \cdot dr = -\lambda_m^2 \int_R \psi_m \cdot \theta \cdot dr = -\lambda_m^2 \cdot \overline{\theta}(\lambda_m) \tag{A.8}$$

The remaining term on the right hand side of Eq. (A.7) may be evaluated using the boundary conditions:

$$\sum_{i=1}^{s_i} \int_{s_i} \left[\psi_m \cdot \frac{\partial \theta}{\partial n_i} - \theta \cdot \frac{\partial \psi_m}{\partial n_i} \right] \cdot ds_i = -\theta_w \int_{s_7} \frac{\partial \psi_m}{\partial n_7} \cdot ds_7 \tag{A.9}$$

The second integral term in Eq. (A.6) may be expressed as:

$$\frac{1}{k} \int_R \dot{q}'''(r) \cdot \psi_m(\lambda_m, r) \cdot dr = \frac{\dot{q}''}{k} \int_{s_{heater}} \psi(r) \cdot ds_{heater} \tag{A.10}$$

Substituting Eqs. (A.8), (A.9) and (A.10) into Eq. (A.6):

$$-\lambda_m^2 \cdot \overline{\theta}(\lambda_m) - \theta_w \cdot a(\lambda_m) + \dot{Q} \cdot b(\lambda_m) = 0 \tag{A.11}$$

where

$$a(\lambda_m) = \int_{s_7} \frac{\partial \psi_m}{\partial n_7} \cdot ds_7 \tag{A.11a}$$

and

$$b(\lambda_m) = \frac{1}{k \cdot (\ell_2 - \ell_1) \cdot (w_2 - w_1)} \int_{\ell_1}^{\ell_2} \int_{w_1}^{w_2} \psi_m(r)\Big|_{z=m} dx \cdot dy \tag{A.11b}$$

The solution of Eq. (A.11) is:

$$\overline{\theta}(\lambda_m) = -\theta_w \cdot \frac{a(\lambda_m)}{\lambda_m^2} + \dot{Q} \cdot \frac{b(\lambda_m)}{\lambda_m^2} \tag{A.12}$$

Substituting the integral transform of the temperature represented in Eq. (A.12) into the inversion formula, Eq. (A.5b):

$$\theta = -\theta_w \cdot \sum \frac{a(\lambda_m)}{\lambda_m^2} \cdot \frac{\psi_m(\lambda_m, r)}{\int_R \psi_m{}^2(\lambda_m) \cdot dr} + \dot{Q} \cdot \sum \frac{b(\lambda_m)}{\lambda_m^2} \cdot \frac{\psi_m(\lambda_m, r)}{\int_R \psi_m{}^2(\lambda_m) \cdot dr} \tag{A.13}$$

The heat transfer rate from surface s_7 is:

$$\dot{Q}_{out} = -k \int_{s_7} \left(\frac{\partial \psi_m}{\partial n_7} \right)_{s_7} \cdot ds_7 \tag{A.14}$$

Substituting Eq. (A.13) into Eq. (A.14), the heat conduction equation is:

$$\frac{\dot{Q}_{out}}{\dot{Q}} = \zeta - \tau \cdot \frac{(T_w - T_a)}{\dot{Q}} \tag{A.15}$$

APPENDIX B

A SAMPLE CALCULATION FOR CALIBRATION EXPERIMENTS

The total heat transfer rates from fin arrays were determined by using calibration equations. In order to obtain the calibration equations of set-ups, 13 experimental runs were conducted on two parallel vertical flat plates that were mounted on each set-up and were separated by a distance of 2 mm. Table B.1 and Table B.2 represent the data recorded during the calibration experiments for Set-up 1 and Set-up 2, respectively. T_1 and T_2 represent the temperatures of the heated plate and the temperatures of the opposite plate, respectively. The film temperature is denoted as T_f and it is calculated at the average temperatures of ambient temperature and heated plate temperature. $(T_1 + T_a)/2$. Using these data, the total heat transfer rate consisting of conduction and radiation, $\dot{Q}_{out}$, from the heated plate, was obtained for each power inputs, $\dot{Q}$. A sample calculation for the total heat transfer rate is given below. Table B.3 and Table B.4 give the calibration experiment results of Set-up 1 and Set-up 2, respectively.

Table B.1 Data Recorded for Calibration of Set-up 1

$\dot{Q}$ (W)	T_1(ºC)	T_2(ºC)	T_f(ºC)
20.10	71.09	53.95	45.40
30.20	88.82	63.80	53.51
39.96	108.20	75.30	63.10
49.40	125.20	85.65	71.55
59.90	143.70	80.80	80.75

Table B.1 (continued) Data Recorded for Calibration of Set-up 1

70.20	159.00	106.20	88.50
80.00	176.10	116.90	97.05
90.10	190.90	126.00	104.45
99.70	205.00	134.60	111.60
110.40	220.00	143.50	119.10
119.00	231.70	150.10	125.05
130.00	244.00	155.70	131.25
139.90	258.40	165.40	138.25

Table B.2 Data Recorded for Calibration of Set-up 2

$\dot{Q}$ (W)	T_1(ºC)	T_2(ºC)	T_f(ºC)
20.10	59.20	45.30	38.70
30.20	77.03	56.50	47.52
39.80	91.70	65.20	54.80
50.20	108.40	75.50	63.10
60.00	122.80	84.20	70.40
70.00	137.95	93.60	77.98
80.70	152.30	102.40	85.20
90.70	165.40	110.30	91.80
100.30	177.70	118.00	97.90
109.00	188.60	124.70	103.50
120.70	199.90	130.20	109.20
131.40	213.70	139.50	115.90
140.60	223.90	145.70	120.85

$d = 0.002$ m $\quad A = 0.045$ m^2 $\quad \varepsilon = 0.20 \quad \sigma = 5.67\text{x}10^{-8}$ W/(m$^2 \cdot$K^4)

$\dot{Q} = 40.03$ W $\quad T_1 = 108.2$ °C $\quad T_2 = 75.3$ °C $\quad T_a = 18$ °C $\quad T_f = 63.5$ °C

$k = 0.0290$ W/(m·K)

$$\dot{Q}_{out} = \frac{k}{d} \cdot A \cdot (T_1 - T_2) + \sigma \cdot \frac{\varepsilon}{2-\varepsilon} \cdot A \cdot ((T_1 + 273)^4 - (T_2 + 273)^4)$$

$$\dot{Q}_{out} = 22.22 \text{ W}$$

Table B.3 Results of Calibration Experiments for Set-up 1

$\dot{Q}$ (W)	$\dot{Q}_{out}/\dot{Q}$	$(T_1 - T_a)/\dot{Q}$ (K/W)
20.10	0.567	2.557
30.20	0.570	2.337
39.96	0.581	2.254
49.40	0.583	2.174
59.90	0.585	2.101
70.20	0.586	2.014
80.00	0.586	1.977
90.10	0.588	1.920
99.70	0.588	1.873
110.40	0.592	1.828
119.00	0.597	1.792
130.00	0.603	1.734
139.90	0.604	1.718

Table B.4 Results of Calibration Experiments for Set-up 2

$\dot{Q}$ (W)	$\dot{Q}_{out}/\dot{Q}$	$(T_1 - T_a)/\dot{Q}$ (K/W)
20.10	0.609	2.037
30.20	0.621	1.955
39.80	0.624	1.855
50.20	0.630	1.806
60.00	0.633	1.746
70.00	0.641	1.713
80.70	0.641	1.663
90.70	0.645	1.624
100.30	0.644	1.591
109.00	0.646	1.562
120.70	0.648	1.502
131.40	0.649	1.489
140.60	0.651	1.466

Using the results given in Table B.3 and B.4, the variations of $\dot{Q}_{out}/\dot{Q}$ with $(T_1 - T_a)/\dot{Q}$ were plotted in Figures 4.2 and 4.3 for each set-up and, the calibration curves were obtained. The equations representing the curves were determined and the calculation of total heat transfer rates from the fin arrays were employed by using these calibration equations.

APPENDIX C

A SAMPLE CALCULATION FOR VERIFICATION PROCEDURE

The validity of the applied calibration method was examined for each set-up by a set of experiments conducted on a vertical flat plate. The results of the calculations were compared with available correlations from literature. The data obtained from Set-up 1 and Set-up 2 is given in Table C.1 and Table C.2, respectively. Using these data, Nusselt numbers were calculated both experimentally and theoretically.

Table C.1 Data Recorded for Verification of Set-up 1

$\dot{Q}$ (W)	T_1(ºC)	T_f(ºC)
20.01	64.58	41.09
30.04	82.64	50.07
39.82	99.97	58.98
49.57	115.90	66.95
60.00	130.29	74.29
68.93	144.31	81.36
80.16	159.28	89.09
90.78	175.33	97.66
99.3	186.16	102.95
109.86	199.71	109.73
120.64	212.48	116.24
129.18	222.78	121.52
139.76	234.25	127.32

Table C.2 Data Recorded for Verification of Set-up 2

$\dot{Q}$ (W)	T_1(ºC)	T_f(ºC)
20.00	57.41	37.50
30.00	72.75	45.12
40.12	86.48	52.24
50.02	100.11	59.06
60.46	113.19	65.74
69.80	125.47	71.93
80.25	138.63	78.77
90.28	147.98	83.87
99.62	159.73	89.74
109.83	171.25	95.50
120.52	182.64	101.32
130.14	192.09	106.17
140.59	202.75	111.57

For a sample calculation, the required measured parameters are:

$T_w = 100.11\ °C \quad T_a = 18\ °C$

$\dot{Q} = V \cdot I = 66.6V \cdot 0.751A = 50.017\ W$

The constant parameters are:

$A = 0.0612\ m^2 \quad L = 0.34\ m \quad \varepsilon = 0.20$

$g = 9.81\ m/s^2 \qquad \sigma = 5.67 \cdot 10^{-8}\ W/(m^2 \cdot K^4)$

where L is the characteristic length of vertical plate used for verification of Set-up 2.

Using the above parameters, thermopyhsical properties of air and Rayleigh number may be obtained:

$$T_f = \frac{T_w + T_a}{2} = 59.06\ °C \qquad \beta = \frac{1}{T_f + 273} = 3.01 \cdot 10^{-3}\ (1/K) \quad Pr = 0.703$$

$$k = 0.0287\ W/(m \cdot K) \qquad \alpha = 2.72 \cdot 10^{-5}\ m^2/s \qquad \nu = 1.91 \cdot 10^{-5}\ m^2/s$$

$$Ra = \frac{g \cdot \beta \cdot L^3 \cdot (T_w - T_a)}{\nu \cdot \alpha} = 1.83 \cdot 10^8$$

Since $Ra<10^9$, the flow is laminar.

From the calibration equation of Set-up 2, Eq. (4.4), the total heat transfer rate from the vertical plate is:

$$\dot{Q}_o = 0.6396 \cdot \dot{Q} \ - \ 0.0222 \cdot (T_w - T_a) = 30.17\ W$$

The radiation heat transfer from the plate is:

$$(\dot{Q}_o)_r = A \cdot \varepsilon \cdot \sigma \cdot [(T_w + 273)^4 - (T_a + 273)^4] = 3.813\ W$$

The convection heat transfer is:

$$(\dot{Q}_o)_c = \dot{Q}_o - (\dot{Q}_o)_r = 26.35\ W$$

The experimental heat transfer coefficient and Nusselt number are:

$$h_{exp} = \frac{(\dot{Q}_o)_c}{A \cdot (T_w - T_a)} = 5.245\ W/(m^2 \cdot K)$$

$$Nu_{exp} = \frac{h_{exp} \cdot L}{k} = 62.19$$

The theoretical Nusselt numbers may be calculated using the following correlations as:

1. Churchill and Chu's first relation (for laminar and turbulent flows)

$$\mathrm{Nu}_{\mathrm{th1}} = \left[0.825 + \frac{0.387 \cdot (\mathrm{Ra})^{1/6}}{\left[1 + \left(\frac{0.492}{\mathrm{Pr}} \right)^{9/16} \right]^{8/27}} \right]^2 = 73.09$$

2. Churchill and Chu's second relation (for laminar flows only)

$$\mathrm{Nu}_{\mathrm{th2}} = 0.68 + \frac{0.67 \cdot (\mathrm{Ra})^{1/4}}{\left[1 + \left(\frac{0.492}{\mathrm{Pr}} \right)^{9/16} \right]^{4/9}} = 60.43$$

3. McAdams' relation

$$\mathrm{Nu}_{\mathrm{th3}} = 0.59 \cdot (\mathrm{Ra})^{1/4} = 68.63$$

4. Churchill and Usagi's relation

$$\mathrm{Nu}_{\mathrm{th4}} = \frac{0.67 \cdot (\mathrm{Ra})^{1/4}}{\left[1 + \left(\frac{0.492}{\mathrm{Pr}} \right)^{9/16} \right]^{4/9}} = 59.75$$

The average relative errors of the theoretical Nusselt numbers with respect to those of experimental Nusselt numbers are given in Table C.3. The results of the experimental and theoretical calculations are given in Table C.4. Using these results, Figure 4.4 was plotted.

Table C.3 Average Relative Errors of the Correlations

	Nu_{th1}	Nu_{th2}	Nu_{th3}	Nu_{th4}
% error	17.8	4.2	13.1	3.9

Table C.4 Comparison of Experimental and Theoretical Calculations

Rayleigh Number	Nu_{exp}	Nu_{th1}	Nu_{th2}	Nu_{th3}	Nu_{th4}
$2.092 \cdot 10^8$	66.568	76.006	62.394	70.960	61.714
$2.090 \cdot 10^8$	66.836	75.957	62.361	70.936	61.681
$2.082 \cdot 10^8$	67.356	75.854	62.292	70.867	61.612
$2.081 \cdot 10^8$	66.576	75.894	62.319	70.861	61.639
$2.071 \cdot 10^8$	67.408	75.728	62.207	70.782	61.527
$2.058 \cdot 10^8$	67.255	75.665	62.165	70.670	61.485
$2.058 \cdot 10^8$	64.629	75.679	62.174	70.669	61.494
$2.012 \cdot 10^8$	64.183	75.172	61.832	70.265	61.152
$1.933 \cdot 10^8$	63.969	74.290	61.237	69.571	60.557
$1.831 \cdot 10^8$	62.190	73.093	60.426	68.629	59.746
$1.679 \cdot 10^8$	60.954	71.228	59.157	67.161	58.477
$1.501 \cdot 10^8$	57.174	68.884	57.552	65.307	56.872
$1.213 \cdot 10^8$	53.683	64.630	54.606	61.914	53.926
$8.365 \cdot 10^7$	48.566	57.769	49.763	56.425	49.083
$8.332 \cdot 10^7$	48.433	57.669	49.691	56.368	49.011
$8.309 \cdot 10^7$	47.653	57.670	49.692	56.330	49.012
$8.306 \cdot 10^7$	48.443	57.601	49.642	56.324	48.962
$8.301 \cdot 10^7$	48.254	57.617	49.654	56.316	48.974
$8.233 \cdot 10^7$	48.725	57.436	49.524	56.201	48.844
$8.157 \cdot 10^7$	48.733	57.266	49.403	56.070	48.723
$8.115 \cdot 10^7$	47.780	57.281	49.414	55.998	48.734

Table C.4 (continued) Comparison of Experimental and Theoretical Calculations

$8.071 \cdot 10^7$	49.051	57.074	49.265	55.923	48.585
$7.804 \cdot 10^7$	46.034	56.631	48.947	55.454	48.267
$7.273 \cdot 10^7$	45.283	55.472	48.114	54.486	47.434
$6.549 \cdot 10^7$	44.170	53.789	46.896	53.076	46.216
$5.388 \cdot 10^7$	41.785	50.788	44.704	50.549	44.024

APPENDIX D

RADIATION ANALYSIS

The total heat transfer from a fin array involves two modes at steady-state. These are convection heat transfer and radiation heat transfer. In order to evaluate convection heat transfer rate, radiation contribution should be calculated and then, it should be subtracted from the total heat transfer rate to the surroundings. A channel of fin array may be enough for modeling the problem for radiation analysis. The basic fin model is given in Figure D.1. In the figure, the surfaces numbered as 1 and 3 are the fin surfaces; surface 5 is the fin base. All surfaces are assumed to be diffuse-gray. Remaining surfaces, 2, 4 and 6, are the openings to ambient air assumed to be blackbodies.

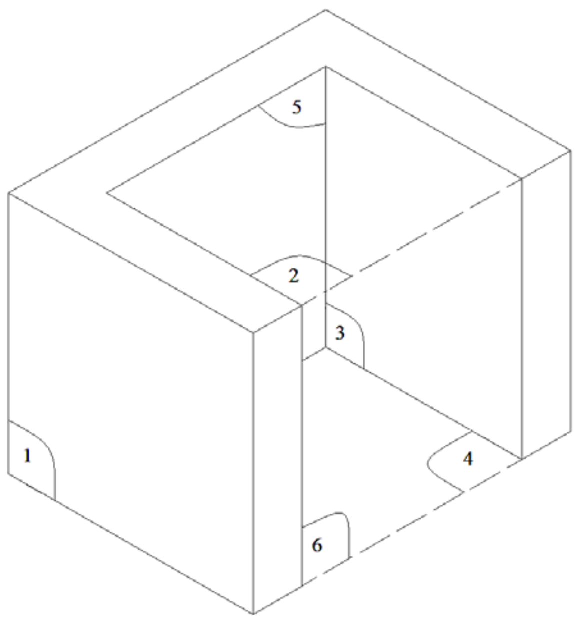

Figure D.1 Basic Fin Model for Radiation Analysis

In order to make the radiation analysis simpler, the following assumptions have to be made. These are:

- Fin surfaces and fin base are diffuse-gray bodies at base-plate temperature, T_w and openings are blackbodies at ambient temperature, T_a.
- Emissivity, ε and reflectivity, α do not depend on wavelength or direction, and therefore, they are temperature dependent only. ($\alpha(T) = \varepsilon(T) = 1 - \rho(T)$)
- Fin temperature and the base-plate temperature are considered as equal. Since the fin material has high conductivity (~130 W/(m·K)), the temperature variation within the material is quite low. Therefore, it does not affect the radiation analysis significantly.
- Properties of the surfaces are uniform.
- Air, which fills up the openings, is assumed to be non-absorbing and non-emitting.

The radiation heat transfer rate from a fin array may be expressed as:

$$\dot{Q}_r = n \cdot \left(\dot{Q}_{r,1} + \dot{Q}_{r,3}\right) + (n-1) \cdot \dot{Q}_{r,5} + \sigma \cdot n \cdot \varepsilon \cdot t \cdot (2 \cdot H + L)[T_w^4 - T_a^4] \qquad \text{(D.1)}$$

where $\dot{Q}_{r,1}$, $\dot{Q}_{r,3}$ and $\dot{Q}_{r,5}$, are the net radiative heat transfers from surfaces 1, 3 and 5, respectively; n, H, L and t are the geometric parameters of fin array, $\sigma = 5.67 \cdot 10^{-8}$ is the Stefan-Boltzmann constant and $\varepsilon = 0.20$ is the emissivity of the surfaces. Since surfaces 1 and 3 are identical, the net radiative heat transfers from surfaces 1 and 3 are equal. Therefore, equation becomes:

$$\dot{Q}_r = 2 \cdot n \cdot \dot{Q}_{r,1} + (n-1) \cdot \dot{Q}_{r,5} + \sigma \cdot n \cdot \varepsilon \cdot t \cdot (2 \cdot H + L)[T_w^4 - T_a^4] \qquad \text{(D.2)}$$

$\dot{Q}_{r,1}$ and $\dot{Q}_{r,5}$ are evaluated as:

$$\dot{Q}_{r,1} = \frac{E_{b1} - J_1}{\dfrac{(1-\varepsilon)}{\varepsilon \cdot A_1}} = \sum_{j=1}^{6} \frac{J_1 - J_j}{\left(A_1 \cdot F_{1j}\right)^{-1}} \tag{D.3}$$

$$\dot{Q}_{r,5} = \frac{E_{b5} - J_5}{\dfrac{(1-\varepsilon)}{\varepsilon \cdot A_5}} = \sum_{j=1}^{6} \frac{J_5 - J_j}{\left(A_5 \cdot F_{5j}\right)^{-1}} \tag{D.4}$$

where E_{b1} and E_{b5} are the blackbody radiosities, J_j are the radiosities, F_{1j} and F_{5j} are the view factors, A_1 and A_5 are the areas of the surfaces. The network representation of the radiative exchange between surfaces 1 and 5 and remaining surfaces are shown in Figures D.2 and D.3, respectively.

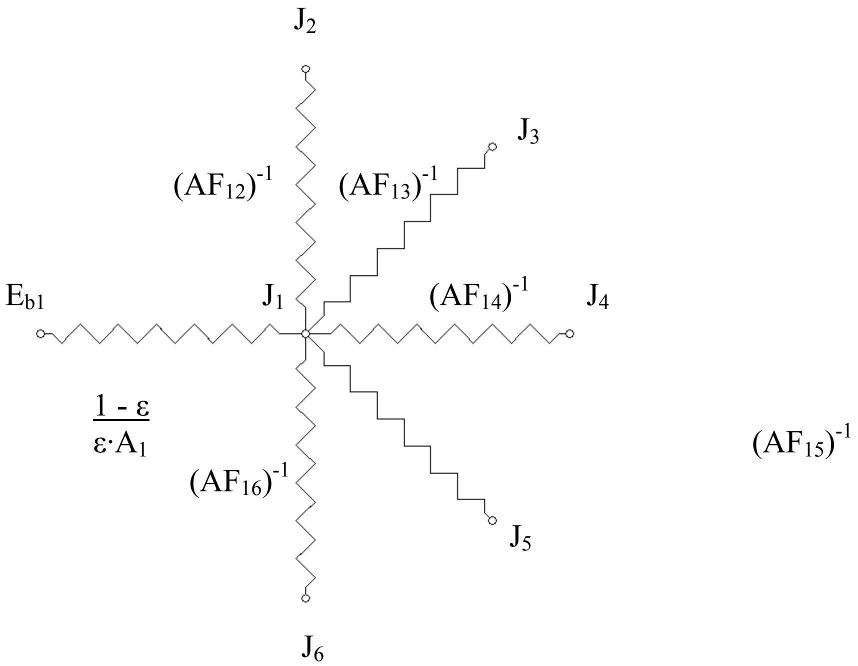

Figure D.2 Network Representation of the Radiative Exchange between Surface 1 and the Remaining Surfaces

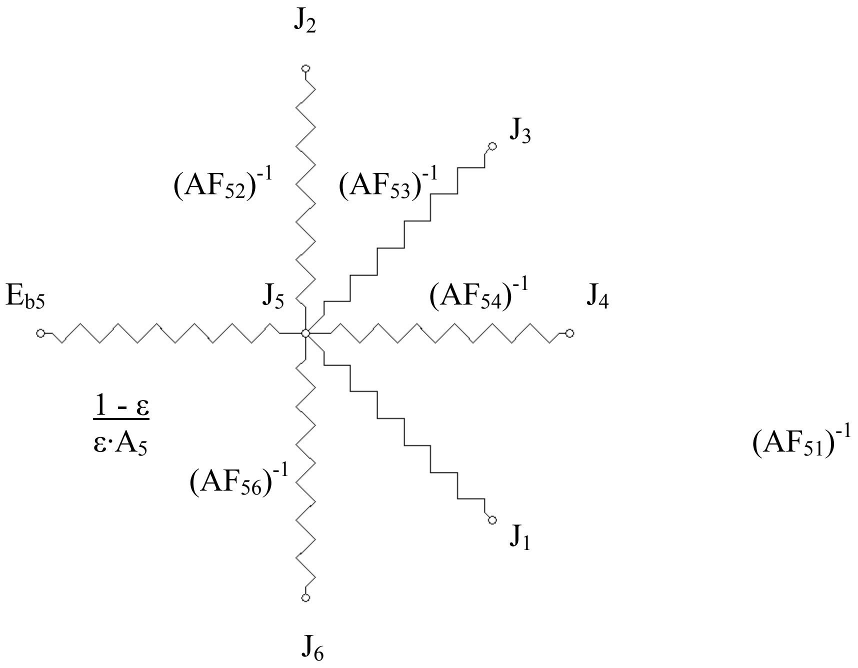

Figure D.3 Network Representation of the Radiative Exchange between Surface 5 and the Remaining Surfaces

The blackbody radiosities E_{b1} and E_{b5}, and the radiosities of the openings J_2, J_4 and J_6 may be determined from the measured base-plate and ambient temperatures.

$$E_{b1} = E_{b5} = \sigma \cdot (T_w)^4 \tag{D.5}$$

$$J_2 = J_4 = J_6 = \sigma \cdot (T_a)^4 \tag{D.6}$$

To determine the other radiosities (J_1 and J_5), Eqs. (D.3) and (D.4) must be solved simultaneously. However, the view factors that are used during the calculation must be determined in order to solve these equations. Two cases should be considered to evaluate the view factors. Figure D.4 shows the geometry of first case, perpendicular rectangles with a common edge. For this geometry, the view factors are expressed as [21]:

$$F_{AB} = \frac{1}{\pi X}\left\{ \begin{array}{l} X\tan^{-1}\dfrac{1}{X} + Y\tan^{-1}\dfrac{1}{Y} - \left(X^2 - Y^2\right)^{1/2}\tan^{-1}\dfrac{1}{\left(X^2+Y^2\right)^{1/2}} \\ + \dfrac{1}{4}\ln\left[\begin{array}{l} \dfrac{\left(1+X^2\right)\left(1+Y^2\right)}{1+X^2+Y^2}\left[\dfrac{X^2\left(1+X^2+Y^2\right)}{\left(1+X^2\right)\left(X^2+Y^2\right)}\right]^{X^2} \\ \times\left[\dfrac{Y^2\left(1+X^2+Y^2\right)}{\left(1+Y^2\right)\left(X^2+Y^2\right)}\right]^{Y^2} \end{array} \right] \end{array} \right\} \tag{D.7}$$

where X = (s / L) and Y = (H / L).

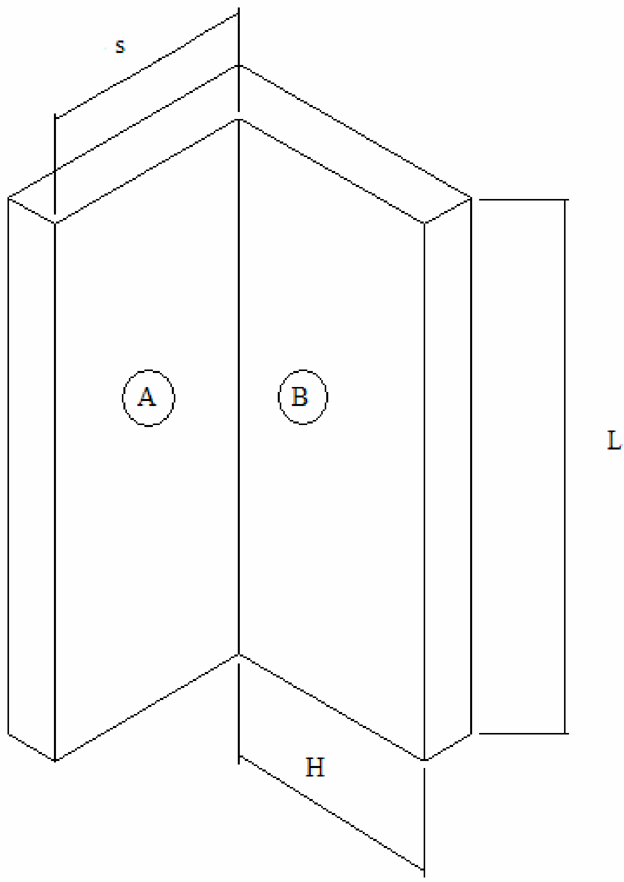

Figure D.4 Geometry for Perpendicular Rectangles with a Common Edge

Figure D.5 shows the geometry of other case, aligned parallel rectangles. For this geometry, the view factor relation is:

$$F_{AB} = \frac{2}{\pi PR}\left\{\begin{matrix} P\left(1+R^2\right)^{1/2}\tan^{-1}\dfrac{P}{\left(1+R^2\right)^{1/2}} + R\left(1+P^2\right)^{1/2}\tan^{-1}\dfrac{R}{\left(1+P^2\right)^{1/2}} \\ -P\tan^{-1}P - R\tan^{-1}R + \ln\left[\dfrac{\left(1+P^2\right)\left(1+R^2\right)}{1+P^2+R^2}\right]^{1/2} \end{matrix}\right\} \tag{D.8}$$

where P = (L / s) and R = (H / s)

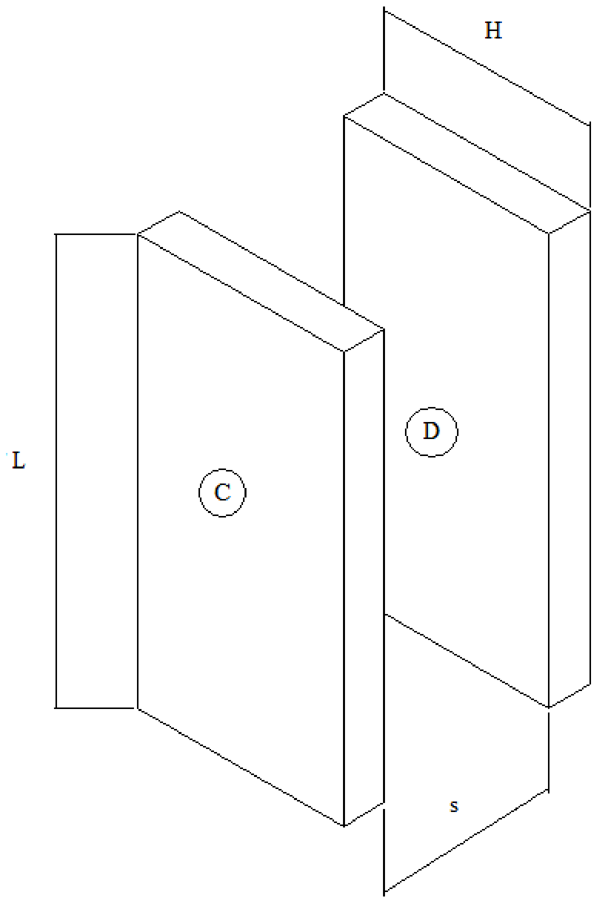

Figure D.5 Geometry for Aligned Parallel Rectangles

Using Eqs. (D.7) and (D.8) and the areas of the surfaces required to apply reciprocating rule, the view factors of all surfaces can be determined. The areas of the surfaces are given below. The ratios used for view factor calculations, X, Y, P and R, may change according to the position of analyzed surfaces. Table D.1 represents the relations used for all of the view factors.

$$A_1 = H \cdot L \quad A_2 = s \cdot H \quad A_3 = H \cdot L \tag{D.9}$$

$$A_4 = s \cdot H \quad A_5 = s \cdot L \quad A_6 = s \cdot L$$

The view factors and the radiosities for all surfaces and for all fin configurations were solved by a mathcad computer program. Then, using Eq. (D.2), the net radiative heat transfers from fin array were calculated.

Table D.1 View Factors

View Factor	Expression	Ratios	View Factor	Expression	Ratios
F_{11}	0	-	F_{41}	$(A_1/A_4)\cdot F_{14}$	-
F_{12}	D.7	X=L/H, Y=s/H	F_{42}	D.8	P=s/L, R=H/L
F_{13}	D.8	P=H/s, R=L/s	F_{43}	$(A_3/A_4)\cdot F_{34}$	-
F_{14}	D.7	X=L/H, Y=s/H	F_{44}	0	-
F_{15}	$(A_5/A_1)\cdot F_{51}$	-	F_{45}	$(A_5/A_4)\cdot F_{54}$	-
F_{16}	$(A_6/A_1)\cdot F_{61}$	-	F_{46}	$(A_6/A_4)\cdot F_{64}$	-
F_{21}	$(A_1/A_2)\cdot F_{12}$	-	F_{51}	D.7	X=s/L, Y=H/L
F_{22}	0	-	F_{52}	D.7	X=L/s, Y=H/s
F_{23}	$(A_3/A_2)\cdot F_{32}$	-	F_{53}	D.7	X=s/L, Y=H/L
F_{24}	D.8	P=s/L, R=H/L	F_{54}	D.7	X=L/s, Y=H/s
F_{25}	$(A_5/A_2)\cdot F_{52}$	-	F_{55}	0	-
F_{26}	$(A_6/A_2)\cdot F_{62}$	-	F_{56}	D.8	P=s/H, R=L/H
F_{31}	D.8	P=H/s, R=L/s	F_{61}	D.7	X=s/L, Y=H/L
F_{32}	D.7	X=L/H, Y=s/H	F_{62}	D.7	X=L/s, Y=H/s
F_{33}	0	-	F_{63}	D.7	X=s/L, Y=H/L
F_{34}	D.7	X=L/H, Y=s/H	F_{64}	D.7	X=L/s, Y=H/s
F_{35}	$(A_5/A_3)\cdot F_{53}$	-	F_{65}	D.8	P=s/H, R=L/H
F_{36}	$(A_6/A_3)\cdot F_{63}$	-	F_{66}	0	-

APPENDIX E

TABULATED DATA AND RESULTS

The data obtained during experiments with fin arrays for L=250 mm and L=340 mm are given in Table E.1 and Table E.2, respectively. Convection components of the total heat transfer rates from fin arrays and vertical plates for L=250 mm and L=340 mm are given in Table E.3 and Table E.4, respectively. Table E.1 and Table E.3 shows the data measured from fin arrays mounted onto Set-up 1. Table E.5 and Table E.6 represents the scale analysis data for L=250 mm and L=340 mm, respectively.

In the tables, $\dot{Q}$ is the power input in Watts, T_w is the wall temperature in ºC, which is measured in mV by means of six thermocouples and converted to ºC using Eq. (3.1), $(T_w - T_a)$ or ΔT is the base-to-ambient temperature difference, $\dot{Q}_c$ is the convection heat transfer rate from fin arrays in Watts, $\left(\dot{Q}_o\right)_c$ is the convection heat transfer rate from vertical plates in Watts.

Table E.1 Experimental Data for L=250 mm

H = 5 mm														
s=5.85 mm			s=8.8 mm			s=14.7 mm			s=32.4 mm			s=85.5 mm		
Q(W)	T_w (ºC)	T_w-T_a (ºC)	Q(W)	T_w (ºC)	T_w-T_a (ºC)	Q(W)	T_w (ºC)	T_w-T_a (ºC)	Q(W)	T_w (ºC)	T_w-T_a (ºC)	Q(W)	T_w (ºC)	T_w-T_a (ºC)
24.94	61.90	41.10	24.94	60.70	40.70	25.10	60.13	41.63	24.70	64.95	44.55	25.09	67.84	47.24
50.07	91.30	70.50	50.36	89.83	69.63	49.93	90.17	71.37	50.34	98.65	78.05	50.07	102.38	81.78
75.43	116.97	96.07	75.43	114.58	93.98	75.08	114.74	95.84	75.16	126.32	105.32	74.98	131.62	110.92
100.31	139.23	118.33	100.42	135.86	115.26	99.12	137.54	118.04	99.90	151.28	130.28	99.79	158.22	137.32
125.47	159.87	139.07	125.60	155.42	134.72	124.60	158.10	138.40	125.70	175.17	153.67	125.25	182.87	162.07

H = 15 mm														
s=5.85 mm			s=8.8 mm			s=14.7 mm			s=32.4 mm			s=85.5 mm		
Q(W)	T_w (ºC)	T_w-T_a (ºC)	Q(W)	T_w (ºC)	T_w-T_a (ºC)	Q(W)	T_w (ºC)	T_w-T_a (ºC)	Q(W)	T_w (ºC)	T_w-T_a (ºC)	Q(W)	T_w (ºC)	T_w-T_a (ºC)
24.90	50.02	30.72	24.85	49.41	30.41	25.04	50.58	30.83	25.14	57.82	36.32	25.25	60.55	41.55
50.13	71.90	52.40	49.94	69.58	50.33	49.86	72.45	52.35	50.63	84.60	63.20	50.63	91.44	72.54
74.73	90.12	70.42	75.78	87.31	67.81	75.43	90.01	69.76	74.90	105.97	84.67	75.76	117.60	98.60
100.91	106.19	86.39	100.42	103.05	83.30	100.60	106.74	86.24	99.81	125.50	104.20	99.50	140.45	121.05
125.37	120.89	100.89	125.05	117.92	98.12	124.82	120.61	99.91	126.50	144.88	123.48	125.25	162.36	142.96

Table E.1 (continued) Experimental Data for L=250 mm

H = 25 mm														
s=5.85 mm			s=8.8 mm			s=14.7 mm			s=32.4 mm			s=85.5 mm		
Q(W)	T_w (ºC)	T_w-T_a (ºC)	Q(W)	T_w (ºC)	T_w-T_a (ºC)	Q(W)	T_w (ºC)	T_w-T_a (ºC)	Q(W)	T_w (ºC)	T_w-T_a (ºC)	Q(W)	T_w (ºC)	T_w-T_a (ºC)
25.20	45.11	25.61	24.90	42.86	23.16	25.10	45.46	24.46	25.10	45.49	27.19	24.51	53.98	35.48
50.15	61.41	41.66	50.01	57.63	37.93	49.93	61.26	40.16	50.13	65.47	46.87	50.50	80.79	62.09
75.25	75.64	55.34	75.10	71.09	51.19	74.48	75.39	53.99	73.96	82.35	63.65	74.83	103.30	84.40
100.31	87.99	67.49	100.02	81.77	61.67	99.90	86.80	65.20	99.50	99.18	80.38	99.90	124.12	105.12
125.07	99.65	78.55	124.50	92.12	72.12	126.25	98.40	76.50	124.60	113.53	94.73	126.38	144.17	125.27

Table E.2 Experimental Data for L=340 mm

H = 5 mm														
s=5.85 mm			s=8.8 mm			s=14.7 mm			s=32.4 mm			s=85.5 mm		
Q(W)	T_w (ºC)	T_w-T_a (ºC)	Q(W)	T_w (ºC)	T_w-T_a (ºC)	Q(W)	T_w (ºC)	T_w-T_a (ºC)	Q(W)	T_w (ºC)	T_w-T_a (ºC)	Q(W)	T_w (ºC)	T_w-T_a (ºC)
25.16	56.54	35.74	24.97	55.45	35.45	25.22	54.32	35.82	24.97	58.64	38.24	25.12	60.33	39.73
50.17	81.84	61.04	50.66	80.42	60.22	50.45	80.42	61.62	50.66	87.67	67.07	50.09	88.75	68.15
75.51	104.00	83.10	75.25	101.59	80.99	75.16	102.30	83.40	75.15	111.09	90.09	75.58	113.88	93.18
99.93	123.16	102.26	101.13	121.85	101.25	100.23	121.50	102.00	100.94	133.14	112.14	100.03	135.86	114.96
125.76	141.68	120.88	124.96	138.90	118.20	124.41	139.24	119.54	125.64	152.53	131.03	125.74	156.58	135.78

Table E.2 (continued) Experimental Data for L=340 mm

H = 15 mm														
s=5.85 mm			s=8.8 mm			s=14.7 mm			s=32.4 mm			s=85.5 mm		
Q(W)	T_w (ºC)	T_w-T_a (ºC)	Q(W)	T_w (ºC)	T_w-T_a (ºC)	Q(W)	T_w (ºC)	T_w-T_a (ºC)	Q(W)	T_w (ºC)	T_w-T_a (ºC)	Q(W)	T_w (ºC)	T_w-T_a (ºC)
24.92	46.83	27.53	24.77	45.49	26.49	24.97	46.60	26.85	24.92	52.51	31.01	25.07	53.42	34.42
50.38	66.54	47.04	50.10	62.49	43.24	50.03	64.65	44.55	50.45	75.68	54.28	50.74	79.22	60.32
74.82	82.31	62.61	75.77	77.73	58.23	76.20	80.86	60.61	74.98	93.16	71.86	75.50	99.68	80.68
101.03	98.01	78.21	100.23	91.37	71.62	100.72	94.23	73.73	100.52	111.16	89.86	100.52	119.19	99.79
125.65	112.17	92.17	125.20	104.56	84.76	125.64	106.67	85.97	124.85	125.67	104.27	125.41	136.57	117.17

H = 25 mm														
s=5.85 mm			s=8.8 mm			s=14.7 mm			s=32.4 mm			s=85.5 mm		
Q(W)	T_w (ºC)	T_w-T_a (ºC)	Q(W)	T_w (ºC)	T_w-T_a (ºC)	Q(W)	T_w (ºC)	T_w-T_a (ºC)	Q(W)	T_w (ºC)	T_w-T_a (ºC)	Q(W)	T_w (ºC)	T_w-T_a (ºC)
25.17	42.90	23.40	25.07	40.75	21.05	25.02	42.78	21.78	25.17	42.55	24.25	24.72	49.18	30.68
50.10	58.27	38.52	50.24	53.95	34.25	50.31	56.24	35.14	50.10	60.40	41.80	50.03	71.75	53.05
75.42	69.80	49.50	74.99	64.09	44.19	75.25	67.76	46.36	74.04	73.51	54.81	75.42	91.05	72.15
101.33	80.93	60.43	100.23	73.07	52.97	99.93	78.38	56.78	101.03	88.85	70.05	100.13	108.85	89.85
124.96	91.08	69.98	125.86	81.70	61.70	125.53	88.63	66.73	125.08	100.95	82.15	125.76	125.63	106.73

Table E.3 Convection Heat Transfer Rates from Vertical Plate and Fin Arrays for L=250 mm

H=5 mm									
s=5.85 mm		s=8.8 mm		s=14.7 mm		s=32.4 mm		s=85.5 mm	
$T_w - T_a$ (°C)	Q_c(W)	$T_w - T_a$ (°C)	Q_c(W)	$T_w - T_a$ (°C)	Q_c(W)	$T_w - T_a$ (°C)	Q_c(W)	$T_w - T_a$ (°C)	Q_c(W)
41.10	9.30	40.70	9.70	41.63	10.14	44.55	10.02	47.24	10.33
70.50	18.82	69.63	19.80	71.37	20.20	78.05	20.39	81.78	20.49
96.07	28.08	93.98	29.49	95.84	30.36	105.32	30.13	110.92	30.30
118.33	36.85	115.26	39.02	118.04	39.51	130.28	39.41	137.32	39.59
139.07	45.39	134.72	48.37	138.40	49.20	153.67	48.70	162.07	48.74

H=15 mm									
s=5.85 mm		s=8.8 mm		s=14.7 mm		s=32.4 mm		s=85.5 mm	
$T_w - T_a$ (°C)	Q_c(W)	$T_w - T_a$ (°C)	Q_c(W)	$T_w - T_a$ (°C)	Q_c(W)	$T_w - T_a$ (°C)	Q_c(W)	$T_w - T_a$ (°C)	Q_c(W)
30.72	9.16	30.41	9.47	30.83	9.96	36.32	10.01	41.55	10.31
52.40	18.99	50.33	19.85	52.35	20.26	63.20	20.31	72.54	20.62
70.42	28.54	67.81	30.50	69.76	31.12	84.67	30.06	98.60	30.56
86.39	38.88	83.30	40.65	86.24	41.45	104.20	39.89	121.05	39.54
100.89	48.14	98.12	50.07	99.91	51.49	123.48	50.13	142.96	49.08

Vertical plate	
$T_w - T_a$ (°C)	$(Q_o)_c$(W)
46.98	9.66
65.14	14.51
81.97	19.15
97.9	23.73
111.99	28.70
125.91	32.76
140.38	37.94
155.33	42.59
166.41	46.38
179.96	50.98
192.48	55.68
202.53	59.31
213.85	63.86

Table E.3 (continued) Convection Heat Transfer Rates from Vertical Plate and Fin Arrays for L=250 mm

H=25 mm									
s=5.85 mm		s=8.8 mm		s=14.7 mm		s=32.4 mm		s=85.5 mm	
$T_w - T_a$ (ºC)	Q_c(W)	$T_w - T_a$ (ºC)	Q_c(W)	$T_w - T_a$ (ºC)	Q_c(W)	$T_w - T_a$ (ºC)	Q_c(W)	$T_w - T_a$ (ºC)	Q_c(W)
25.61	9.45	23.16	9.90	24.46	10.13	27.19	10.57	35.48	10.01
41.66	19.85	37.93	20.93	40.16	21.00	46.87	21.45	62.09	20.89
55.34	30.36	51.19	31.82	53.99	31.68	63.65	31.67	84.40	30.72
67.49	40.93	61.67	43.04	65.20	43.15	80.38	42.39	105.12	40.61
78.55	51.25	72.12	53.78	76.50	54.81	94.73	52.96	125.27	50.75

Table E.4 Convection Heat Transfer Rates from Vertical Plate and Fin Arrays for L=340 mm

H=5 mm									
s=5.85 mm		s=8.8 mm		s=14.7 mm		s=32.4 mm		s=85.5 mm	
$T_w - T_a$ (ºC)	Q_c(W)	$T_w - T_a$ (ºC)	Q_c(W)	$T_w - T_a$ (ºC)	Q_c(W)	$T_w - T_a$ (ºC)	Q_c(W)	$T_w - T_a$ (ºC)	Q_c(W)
35.74	10.13	35.45	10.45	35.82	11.09	38.24	11.04	39.73	11.31
61.04	20.73	60.22	21.99	61.62	22.57	67.07	22.65	68.15	22.89
83.10	31.29	80.99	32.76	83.40	33.67	90.09	33.62	93.18	34.49
102.26	41.21	101.25	43.77	102.00	44.99	112.14	44.88	114.96	45.29
120.88	51.40	118.20	53.72	119.54	55.43	131.03	55.45	135.78	56.46

Table E.4 (continued) Convection Heat Transfer Rates from Vertical Plate and Fin Arrays for L=340 mm

H=15 mm									
s=5.85 mm		s=8.8 mm		s=14.7 mm		s=32.4 mm		s=85.5 mm	
$T_w - T_a$ (ºC)	Q_c(W)	$T_w - T_a$ (ºC)	Q_c(W)	$T_w - T_a$ (ºC)	Q_c(W)	$T_w - T_a$ (ºC)	Q_c(W)	$T_w - T_a$ (ºC)	Q_c(W)
27.53	9.84	26.49	10.29	26.85	10.84	31.01	10.85	34.42	11.31
47.04	20.79	43.24	22.26	44.55	22.79	54.28	22.43	60.32	23.23
62.61	31.52	58.23	34.35	60.61	35.25	71.86	33.91	80.68	34.85
78.21	42.76	71.62	45.64	73.73	47.03	89.86	45.32	99.79	46.23
92.17	52.89	84.76	56.90	85.97	58.91	104.27	56.44	117.17	57.42

H=25 mm									
s=5.85 mm		s=8.8 mm		s=14.7 mm		s=32.4 mm		s=85.5 mm	
$T_w - T_a$ (ºC)	Q_c(W)	$T_w - T_a$ (ºC)	Q_c(W)	$T_w - T_a$ (ºC)	Q_c(W)	$T_w - T_a$ (ºC)	Q_c(W)	$T_w - T_a$ (ºC)	Q_c(W)
23.40	10.12	21.05	10.88	21.78	11.04	24.25	11.59	30.68	11.06
38.52	21.46	34.25	23.22	35.14	23.64	41.80	23.60	53.05	22.94
49.50	33.90	44.19	35.88	46.36	36.26	54.81	35.63	72.15	34.84
60.43	46.35	52.97	49.00	56.78	48.67	70.05	48.56	89.85	46.04
69.98	57.51	61.70	62.22	66.73	61.49	82.15	60.14	106.73	57.48

Vertical plate	
$T_w - T_a$ (ºC)	$(Q_o)_c$(W)
39.81	10.42
55.25	15.72
68.48	21.16
82.11	26.36
94.89	31.87
107.07	36.64
119.73	41.97
128.23	47.38
139.98	51.95
151.5	57.01
162.64	62.32
171.84	67.12
182.35	72.19

Table E.5 Scale Analysis Data for L=250 mm

H=5 mm									
$s < s_{opt}$				$s > s_{opt}$					
s=5.85 mm		s=8.8 mm		s=14.7 mm		s=32.4 mm		s=85.5 mm	
$Q_c^{(1)}/(n \cdot H \cdot k \cdot \Delta T)$	Ra_s	$Q_c^{(1)}/(n \cdot H \cdot k \cdot \Delta T)$	Ra_s	$Q_c^{(2)}/(n \cdot H \cdot k \cdot \Delta T)$	$Ra_L^{0.25}$	$Q_c^{(2)}/(n \cdot H \cdot k \cdot \Delta T)$	$Ra_L^{0.25}$	$Q_c^{(2)}/(n \cdot H \cdot k \cdot \Delta T)$	$Ra_L^{0.25}$
6.605	$6.016\cdot10^{2}$	14.496	$2.059\cdot10^{3}$	26.789	$8.368\cdot10^{1}$	29.696	$8.405\cdot10^{1}$	46.372	$8.480\cdot10^{1}$
9.547	$9.682\cdot10^{2}$	20.761	$3.290\cdot10^{3}$	33.113	$9.372\cdot10^{1}$	37.543	$9.437\cdot10^{1}$	53.733	$9.484\cdot10^{1}$
10.929	$1.100\cdot10^{3}$	24.325	$3.723\cdot10^{3}$	41.665	$9.656\cdot10^{1}$	45.214	$9.694\cdot10^{1}$	66.102	$9.733\cdot10^{1}$
12.038	$1.167\cdot10^{3}$	27.780	$3.956\cdot10^{3}$	43.341	$9.790\cdot10^{1}$	47.568	$9.815\cdot10^{1}$	68.947	$9.831\cdot10^{1}$
12.724	$1.199\cdot10^{3}$	30.538	$4.074\cdot10^{3}$	47.994	$9.852\cdot10^{1}$	50.317	$9.830\cdot10^{1}$	71.299	$9.839\cdot10^{1}$

H=15 mm									
$s < s_{opt}$				$s > s_{opt}$					
s=5.85 mm		s=8.8 mm		s=14.7 mm		s=32.4 mm		s=85.5 mm	
$Q_c^{(1)}/(n \cdot H \cdot k \cdot \Delta T)$	Ra_s	$Q_c^{(1)}/(n \cdot H \cdot k \cdot \Delta T)$	Ra_s	$Q_c^{(2)}/(n \cdot H \cdot k \cdot \Delta T)$	$Ra_L^{0.25}$	$Q_c^{(2)}/(n \cdot H \cdot k \cdot \Delta T)$	$Ra_L^{0.25}$	$Q_c^{(2)}/(n \cdot H \cdot k \cdot \Delta T)$	$Ra_L^{0.25}$
9.142	$4.980\cdot10^{2}$	15.424	$1.690\cdot10^{3}$	27.975	$7.888\cdot10^{1}$	36.653	$8.077\cdot10^{1}$	57.223	$8.350\cdot10^{1}$
12.203	$8.327\cdot10^{2}$	22.549	$2.772\cdot10^{3}$	35.622	$8.967\cdot10^{1}$	44.191	$9.185\cdot10^{1}$	64.440	$9.388\cdot10^{1}$
14.039	$9.755\cdot10^{2}$	26.700	$3.265\cdot10^{3}$	43.407	$9.321\cdot10^{1}$	50.276	$9.506\cdot10^{1}$	71.021	$9.677\cdot10^{1}$
16.286	$1.066\cdot10^{3}$	29.247	$3.577\cdot10^{3}$	46.801	$9.537\cdot10^{1}$	55.459	$9.681\cdot10^{1}$	73.380	$9.805\cdot10^{1}$
17.321	$1.124\cdot10^{3}$	30.125	$3.798\cdot10^{3}$	50.901	$9.660\cdot10^{1}$	59.230	$9.784\cdot10^{1}$	77.568	$9.861\cdot10^{1}$

Table E.5 (continued) Scale Analysis Data for L=250 mm

H=25 mm									
$s < s_{opt}$				$s > s_{opt}$					
s=5.85 mm		s=8.8 mm		s=14.7 mm		s=32.4 mm		s=85.5 mm	
$Q_c^{(1)}/(n \cdot H \cdot k \cdot \Delta T)$	Ra_s	$Q_c^{(1)}/(n \cdot H \cdot k \cdot \Delta T)$	Ra_s	$Q_c^{(2)}/(n \cdot H \cdot k \cdot \Delta T)$	$Ra_L^{0.25}$	$Q_c^{(2)}/(n \cdot H \cdot k \cdot \Delta T)$	$Ra_L^{0.25}$	$Q_c^{(2)}/(n \cdot H \cdot k \cdot \Delta T)$	$Ra_L^{0.25}$
9.362	$4.308 \cdot 10^2$	18.739	$1.348 \cdot 10^3$	29.214	$7.500 \cdot 10^1$	56.520	$7.742 \cdot 10^1$	63.901	$8.136 \cdot 10^1$
13.566	$7.187 \cdot 10^2$	26.427	$2.296 \cdot 10^3$	40.024	$8.578 \cdot 10^1$	68.136	$8.842 \cdot 10^1$	81.435	$9.210 \cdot 10^1$
16.084	$8.546 \cdot 10^2$	29.933	$2.786 \cdot 10^3$	45.193	$8.986 \cdot 10^1$	72.862	$9.240 \cdot 10^1$	86.131	$9.544 \cdot 10^1$
18.043	$9.498 \cdot 10^2$	34.268	$3.094 \cdot 10^3$	52.209	$9.219 \cdot 10^1$	75.572	$9.498 \cdot 10^1$	89.917	$9.725 \cdot 10^1$
19.507	$1.015 \cdot 10^3$	36.558	$3.351 \cdot 10^3$	56.758	$9.394 \cdot 10^1$	79.774	$9.648 \cdot 10^1$	92.734	$9.830 \cdot 10^1$

Table E.6 Scale Analysis Data for L=340 mm

H=5 mm									
$s < s_{opt}$				$s > s_{opt}$					
s=5.85 mm		s=8.8 mm		s=14.7 mm		s=32.4 mm		s=85.5 mm	
$Q_c^{(1)}/(n \cdot H \cdot k \cdot \Delta T)$	Ra_s	$Q_c^{(1)}/(n \cdot H \cdot k \cdot \Delta T)$	Ra_s	$Q_c^{(2)}/(n \cdot H \cdot k \cdot \Delta T)$	$Ra_L^{0.25}$	$Q_c^{(2)}/(n \cdot H \cdot k \cdot \Delta T)$	$Ra_L^{0.25}$	$Q_c^{(2)}/(n \cdot H \cdot k \cdot \Delta T)$	$Ra_L^{0.25}$
6.739	$5.448 \cdot 10^2$	14.389	$1.866 \cdot 10^3$	32.706	$1.026 \cdot 10^2$	37.768	$1.031 \cdot 10^2$	76.677	$1.037 \cdot 10^2$
10.544	$8.993 \cdot 10^2$	25.433	$3.052 \cdot 10^3$	41.999	$1.159 \cdot 10^2$	45.462	$1.167 \cdot 10^2$	108.675	$1.170 \cdot 10^2$
12.784	$1.041 \cdot 10^3$	29.813	$3.515 \cdot 10^3$	47.836	$1.200 \cdot 10^2$	56.926	$1.205 \cdot 10^2$	129.287	$1.209 \cdot 10^2$
14.242	$1.122 \cdot 10^3$	31.691	$3.816 \cdot 10^3$	57.548	$1.221 \cdot 10^2$	63.733	$1.226 \cdot 10^2$	140.006	$1.228 \cdot 10^2$
15.312	$1.173 \cdot 10^3$	33.563	$3.977 \cdot 10^3$	60.528	$1.233 \cdot 10^2$	71.736	$1.235 \cdot 10^2$	154.069	$1.238 \cdot 10^2$

Table E.6 (continued) Scale Analysis Data for L=340 mm

H=15 mm									
$s < s_{opt}$				$s > s_{opt}$					
s=5.85 mm		s=8.8 mm		s=14.7 mm		s=32.4 mm		s=85.5 mm	
$Q_c^{(1)}/(n·H·k·\Delta T)$	Ra_s	$Q_c^{(1)}/(n·H·k·\Delta T)$	Ra_s	$Q_c^{(2)}/(n·H·k·\Delta T)$	$Ra_L^{0.25}$	$Q_c^{(2)}/(n·H·k·\Delta T)$	$Ra_L^{0.25}$	$Q_c^{(2)}/(n·H·k·\Delta T)$	$Ra_L^{0.25}$
9.697	$4.576·10^2$	18.701	$1.518·10^3$	34.099	$9.671·10^1$	46.223	$9.878·10^1$	89.083	$1.017·10^2$
13.495	$7.794·10^2$	30.112	$2.518·10^3$	49.043	$1.101·10^2$	56.272	$1.133·10^2$	105.406	$1.155·10^2$
16.328	$9.192·10^2$	35.792	$3.012·10^3$	57.231	$1.153·10^2$	70.575	$1.176·10^2$	128.186	$1.196·10^2$
17.904	$1.023·10^3$	38.714	$3.346·10^3$	64.068	$1.181·10^2$	74.447	$1.204·10^2$	138.641	$1.219·10^2$
18.542	$1.091·10^3$	40.314	$3.601·10^3$	69.583	$1.200·10^2$	82.770	$1.219·10^2$	148.290	$1.233·10^2$

H=25 mm									
$s < s_{opt}$				$s > s_{opt}$					
s=5.85 mm		s=8.8 mm		s=14.7 mm		s=32.4 mm		s=85.5 mm	
$Q_c^{(1)}/(n·H·k·\Delta T)$	Ra_s	$Q_c^{(1)}/(n·H·k·\Delta T)$	Ra_s	$Q_c^{(2)}/(n·H·k·\Delta T)$	$Ra_L^{0.25}$	$Q_c^{(2)}/(n·H·k·\Delta T)$	$Ra_L^{0.25}$	$Q_c^{(2)}/(n·H·k·\Delta T)$	$Ra_L^{0.25}$
10.015	$4.005·10^2$	21.798	$1.246·10^3$	34.723	$9.225·10^1$	67.215	$9.531·10^1$	81.936	$9.973·10^1$
14.571	$6.814·10^2$	31.643	$2.135·10^3$	51.809	$1.055·10^2$	80.888	$1.093·10^2$	104.384	$1.135·10^2$
19.634	$7.995·10^2$	39.700	$2.541·10^3$	61.891	$1.106·10^2$	96.770	$1.140·10^2$	119.399	$1.182·10^2$
22.502	$8.964·10^2$	46.396	$2.840·10^3$	68.153	$1.139·10^2$	100.902	$1.178·10^2$	123.630	$1.209·10^2$
24.209	$9.626·10^2$	50.973	$3.097·10^3$	73.298	$1.164·10^2$	105.797	$1.199·10^2$	127.795	$1.226·10^2$

APPENDIX F

UNCERTAINTY ANALYSIS

This analysis is applied for indicating the uncertainties in the experimental measurements. The uncertainties in the calculations are estimated by using the following procedure.

Let the result R is a function of the independent variables $x_1, x_2, \ldots\ldots, x_n$ as:

$$R = R(x_1, x_2, \ldots\ldots, x_n) \tag{F.1}$$

If the uncertainty in the result and the uncertainties in the independent variables are denoted as w_R and $w_1, w_2, \ldots\ldots, w_n$, respectively, the uncertainty in the result may be expressed as:

$$w_R = \left[\left(\frac{\partial R}{\partial x_1}\cdot w_1\right)^2 + \left(\frac{\partial R}{\partial x_2}\cdot w_2\right)^2 + \ldots + \left(\frac{\partial R}{\partial x_n}\cdot w_n\right)^2\right]^{1/2} \tag{F.2}$$

For a sample calculation, the uncertainties of the power input can be estimated. The power input to the heater is:

$$P = V \cdot I \tag{F.3}$$

where V and I are the independent variables and measured as:

$V = 105.2\ V \pm 1\%$

$I = 1.189$ A ± 0.1%

The nominal value of the power input is:

$P = 105.2 \cdot 1.189 = 125.08$ W

Then the uncertainty of the power input is calculated as:

$$w_P = \left[(1.189 \cdot 0.01 \cdot 105.2)^2 + (105.2 \cdot 0.001 \cdot 1.189)^2\right]^{1/2} \cong 1.257 \text{ W}$$

or

$$w_p(\%) = \frac{w_p}{P} \cong 1 \%$$

Using this method, the uncertainty of the power input is estimated as 1 percent.

As discussed in Appendix D, the radiation heat transfer rate from the fin array may be expressed as:

$$\dot{Q}_r = 2 \cdot n \cdot \dot{Q}_{r,1} + (n-1) \cdot \dot{Q}_{r,5} + \sigma \cdot n \cdot \varepsilon \cdot t \cdot (2 \cdot H + L)[T_w^4 - T_a^4] \quad \text{(D.2)}$$

The necessary data required to make a sample uncertainty analysis in the total radiation heat transfer are:

$\sigma = 5.67 \cdot 10^{-8}$ W/(m^2/K^4)

$\varepsilon = 0.20$

$n = 6$

$H = 0.025$ m ± 0.001 m

$L = 0.34$ m ± 0.001 m

$t = 0.003$ m ± 0.0001 m

T_a (K) = 291.8 K ± 1 %

T_w (mV) = 4.32 mV ± 1 %

The uncertainty of the base-plate temperature evaluated by Eq. (3.1) as:

$$w_{T_w(K)} = \left[\left(\left(0.020 \cdot T_w^2(\mathrm{mV}) - 0.766 \cdot T_w(\mathrm{mV}) + 24.186 \right) \cdot 0.01 \cdot 4.32 \right)^2 \right]^{1/2} \cong 0.92 \text{ K}$$

or

$$w_{T_w(K)}(\%) = \frac{w_{T_w(K)}}{T_w(K)} \cong 0.31 \ \%$$

where $T_w(K)$ is the nominal value of the base-plate temperature in K.

$$T_w(K) = 0.0067 \cdot 4.32^3 - 0.383 \cdot 4.32^2 + 24.186 \cdot 4.32 + 3.0861 = 373.95 \text{ K}$$

The uncertainty of the radiation heat transfer rate may be calculated as:

$$w_r = \begin{bmatrix} \left(4 \cdot \sigma \cdot n \cdot \varepsilon \cdot t \cdot (2 \cdot H + L) \cdot T_w^3(K) \cdot 0.92 \right)^2 \\ + \left(4 \cdot \sigma \cdot n \cdot \varepsilon \cdot t \cdot (2 \cdot H + L) \cdot T_a^3 \cdot 0.01 \cdot T_a \right)^2 \\ + \left(\sigma \cdot n \cdot \varepsilon \cdot (2 \cdot H + L) \cdot \left(T_w^4(K) - T_a^4 \right) \cdot 0.0001 \right)^2 \\ + \left(2 \cdot \sigma \cdot n \cdot \varepsilon \cdot t \cdot \left(T_w^4(K) - T_a^4 \right) \cdot 0.001 \right)^2 \\ + \left(\sigma \cdot n \cdot \varepsilon \cdot t \cdot \left(T_w^4(K) - T_a^4 \right) \cdot 0.001 \right)^2 \end{bmatrix}^{1/2}$$

$w_r = 0.043$ W

or

$$w_{\dot{Q}_r}(\%) = \frac{w_{\dot{Q}_r}}{\dot{Q}_r} \cong 0.24 \ \%$$

The uncertainty of the total heat transfer from the fin arrays may be evaluated using the calibration equation of Set-up 2, Eq. (4.18) as:

$$w_{\dot{Q}_{out}} = \left[\left(0.6396 \cdot 1.257 \right)^2 + \left(-0.0222 \cdot 0.92 \right)^2 + \left(-0.0222 \cdot 0.001 \cdot T_a \right)^2 \right]^{1/2} \cong 0.804 \text{ W}$$

or

$$w_{\dot{Q}_{out}}(\%) = \frac{w_{\dot{Q}_{out}}}{\dot{Q}_{out}} \cong 1.03\ \%$$

The convection heat transfer rate is obtained as:

$$\dot{Q}_c = \dot{Q}_{out} - \dot{Q}_r$$

The uncertainty of the convection heat transfer rate from the fin arrays is:

$$w_{\dot{Q}_c} = \left[(0.804)^2 + (-0.043)^2\right]^{1/2} \cong 0.805\ \text{W}$$

The nominal value of the convection heat transfer rate is:

$$\dot{Q}_c = 78.18 - 18.04 = 60.14\ \text{W}$$

$$w_{\dot{Q}_c}(\%) = \frac{w_{\dot{Q}_c}}{\dot{Q}_c} \cong 1.3\ \%$$

This procedure is repeated for all voltmeter-ammeter readings taken throughout the experiments and it is seen that the uncertainty of the convection heat transfer rate varies between 1 percent and 2.5 percent. The average uncertainty is estimated as 1.6 percent.

APPENDIX G

A SAMPLE CALCULATION FOR FIN ARRAYS

In order to examine the steady-state heat transfer performances of fin arrays, the radiation and convection heat transfer rates should be determined. A sample calculation given below represents the solution procedure.

The required data for calculation are:

$L = 0.25$ m

$W = 0.18$ m

$H = 0.015$ m

$s = 0.0324$ m

$t = 0.003$ m

$n = 6$ fins

$\dot{Q} = 77.3\text{V} \cdot 0.969\text{A} = 74.904$ W

$T_a = 21.3$ ºC

The steady-state temperature of fin array is measured by taking the average of six thermocouple readings in mV. Then, mV value is converted to ºC using the calibration equation, Eq. (3.1):

$T_w(\text{mV}) = (4.70 + 4.63 + 4.60 + 4.55 + 4.49 + 4.37)/6 = 4.56$ mV

$$T_w(°\text{C}) = 0.0067 \cdot (T_w(\text{mV}))^3 - 0.383 \cdot (T_w(\text{mV}))^2 + 24.186 \cdot T_w(\text{mV}) + 3.0861 \quad (3.1)$$

$T_w(°\text{C}) = 105.97$ °C

Base-to-ambient temperature difference is calculated as:

$\Delta T = T_w - T_a = 84.67\ °C$

The total heat transfer rate from the fin array is obtained by using Eq. (4.2) as:

$\dot{Q}_{out} = 0.5601 \cdot \dot{Q} - 0.0043 \cdot (T_w - T_a) = 41.59\ W$

To determine the convection heat transfer rate from the fin array, first the radiation heat transfer rate should be calculated. The radiation heat transfer rate from the fin array is:

$$\dot{Q}_r = 2 \cdot n \cdot \dot{Q}_{r,1} + (n-1) \cdot \dot{Q}_{r,5} + \sigma \cdot n \cdot \varepsilon \cdot t \cdot (2 \cdot H + L)[T_w^4 - T_a^4] \quad \text{(D.2)}$$

The radiation heat transfer rates from surface 1 and 5 are calculated as:

$$\dot{Q}_{r,1} = \frac{E_{b1} - J_1}{\frac{(1-\varepsilon)}{\varepsilon \cdot A_1}} = \sum_{j=1}^{6} \frac{J_1 - J_j}{\left(A_1 \cdot F_{1j}\right)^{-1}} \quad \text{(D.3)}$$

$$\dot{Q}_{r,5} = \frac{E_{b5} - J_5}{\frac{(1-\varepsilon)}{\varepsilon \cdot A_5}} = \sum_{j=1}^{6} \frac{J_5 - J_j}{\left(A_5 \cdot F_{5j}\right)^{-1}} \quad \text{(D.4)}$$

The blackbody radiosities of surfaces 1 and 5 and the radiosities of surfaces 2,4 and 6 are calculated as:

$E_{b1} = E_{b5} = \sigma \cdot (T_w)^4 = 1169.506\ W/m^2$

$J_2 = J_4 = J_6 = \sigma \cdot (T_a)^4 = 425.348\ W/m^2$

The surface areas of the six faces are:

$A_1 = A_3 = H \cdot L = 0.00375 \text{ m}^2$

$A_2 = A_4 = s \cdot H = 0.00081 \text{ m}^2$

$A_5 = A_6 = s \cdot L = 0.0081 \text{ m}^2$

Using Eqs. (D.7) and (D.8), and Table D.1, view factors are calculated, and the results are presented in Table F.1. After calculating the view factors, these values are substituted into Eqs. (D.3) and (D.4) to determine the radiation heat transfer rates from the surfaces 1 and 5. A mathcad computer program was prepared for the calculation of the view factors and radiation heat transfer rates. The results are:

$\dot{Q}_{r,1} = 0.457 \text{ W}$

$\dot{Q}_{r,5} = 1.061 \text{ W}$

Substituting the values into Eq. (D.2), the total radiation heat transfer rate from the fin array is calculated as:

$$\dot{Q}_r = 2 \cdot 6 \cdot 0.457 + (6-1) \cdot 1.061$$
$$+ 5.67 \cdot 10^{-8} \cdot 6 \cdot 0.20 \cdot 0.003 \cdot (2 \cdot 0.015 + 0.250)[378.97^4 - 294.3^4]$$

$\dot{Q}_r = 11.53 \text{ W}$

The convection heat transfer rate is obtained by subtracting the radiation heat transfer rate from total heat transfer rate from fin arrays as:

$\dot{Q}_c = \dot{Q}_{out} - \dot{Q}_r = 41.59 - 11.53 = 30.06 \text{ W}$

In order to utilize the experimental data in scale analysis, the convection heat transfer from fins should be calculated. Referring to Table D.3, the convection heat transfer rate from vertical plate at ΔT=84.67 °C can be found as a result of interpolation, and hence, the convection heat transfer rate from fins on the base-plate is evaluated as:

$$\dot{Q}_c^{(2)} = \dot{Q}_c - \left(\dot{Q}_o\right)_c = 30.06 - 20.04 = 10.02 \text{ W}$$

Table G.1 View Factors for Sample Calculation

View Factor	Results	View Factor	Results
F_{11}	0	F_{41}	0.201
F_{12}	0.026	F_{42}	0.002
F_{13}	0.202	F_{43}	0.201
F_{14}	0.026	F_{44}	0
F_{15}	0.385	F_{45}	0.394
F_{16}	0.385	F_{46}	0.394
F_{21}	0.201	F_{51}	0.178
F_{22}	0	F_{52}	0.024
F_{23}	0.201	F_{53}	0.178
F_{24}	0.002	F_{54}	0.024
F_{25}	0.394	F_{55}	0
F_{26}	0.394	F_{56}	0.611
F_{31}	0.202	F_{61}	0.178
F_{32}	0.026	F_{62}	0.024
F_{33}	0	F_{63}	0.178
F_{34}	0.026	F_{64}	0.024
F_{35}	0.385	F_{65}	0.611
F_{36}	0.385	F_{66}	0

Since the separation between adjacent fins is larger than optimum fin spacing value, the following dimensionless equation derived for the case of large-s limit should be used.

$$\frac{\dot{Q}_c^{(2)}}{n \cdot k \cdot H \cdot \Delta T} \approx 2 \cdot Ra_L^{0.25} \tag{6.16}$$

Thermophysical properties of air are evaluated at film temperature, T_f.

$$T_f = \frac{T_w + T_a}{2} = 52.99\ °C \qquad \beta = \frac{1}{T_f + 273} = 3.07 \cdot 10^{-3}$$

$$k = 0.0282\ W/(m \cdot K) \qquad \alpha = 2.63 \cdot 10^{-5}\ m^2/s \qquad \nu = 1.85 \cdot 10^{-5}\ m^2/s$$

Substituting geometric parameters and thermophysical properties into Eq. (6.16), the dimensionless terms are evaluated as:

$$\frac{\dot{Q}_c^{(2)}}{n \cdot k \cdot H \cdot \Delta T} = 50.276$$

$$Ra_L^{0.25} = \left(\frac{g \cdot \beta \cdot L^3 \cdot (T_w - T_a)}{\nu \cdot \alpha} \right)^{0.25} = 9.506 \cdot 10^1$$

APPENDIX H

METHOD OF SCALE ANALYSIS

The purpose of this application is to estimate a correlation which determines the optimum fin spacing that maximizes the heat transfer rate from rectangular fins extending perpendicularly out of vertical rectangular fins. The problem, natural convection along vertically-based rectangular fins, is modeled as discussed in Chapter 6 to apply the method of scale analysis.

In order to determine an optimum fin spacing for which the convection heat transfer rate from the fins is maximized, the following two extreme conditions should be considered:

1. In the limiting cases of very small value of s (small-s limit), the flow is fully developed channel flow.
2. When fin spacing s, is much greater than the boundary layer thickness (large-s limit), the flow is boundary layer flow.

In the small-s limit, the total heat transfer rate from single channel can be written as:

$$\dot{Q}^{(1)}_{c_{\substack{single\\channel}}} = \dot{m} \cdot C_p \cdot \Delta T \tag{H.1}$$

where $\dot{m}$ is the mass flow rate through a single channel, C_p is the specific heat of air at constant pressure and ΔT is order-of-magnitude of the temperature difference.

In Eq. (H.1), the mass flow rate may be written as:

$$\dot{m} = \rho \cdot V \cdot A \tag{H.2}$$

The velocity term in the mass flow rate expression for the case of fully developed flow can be obtained by performing a scale analysis. Using Navier-Stokes equations with the steady, constant property, one-dimensional flow ($x \ll y$ and $u=0$) assumptions, the continuity equation becomes:

$$\frac{\partial v}{\partial y} = 0 \tag{H.3}$$

Assuming the density variations are negligible except in the buoyancy term (Boussinesq approximation), the momentum equation in y-direction becomes:

$$\nu \cdot \frac{\partial^2 v}{\partial x^2} + g \cdot \beta \cdot \Delta T = 0 \tag{H.4}$$

For the velocity term in Eq. (H.4), a balance equation can be obtained for the case of fully developed flow ($v \sim V$, $x \sim s$, $y \sim L$), as:

$$V \approx \frac{g \cdot \beta \cdot \Delta T \cdot s^2}{\nu} \tag{H.5}$$

Introducing Eq. (H.5) into Eq. (H.2), a balance between mass flow rate and other parameters is given by:

$$\dot{m} \approx \frac{\rho \cdot g \cdot \beta \cdot s^3 \cdot \Delta T}{\nu} \cdot H \tag{H.6}$$

In the large-s limit, under the boundary layer flow conditions, the total convection heat transfer rate from a single fin can be expressed as:

$$\dot{Q}^{(2)}_{c_{\substack{\text{single}\\ \text{fin}}}} = 2 \cdot h \cdot A \cdot \Delta T \tag{H.7}$$

where h is the heat transfer coefficient over single fin, A is the area of single fin and ΔT is order-of-magnitude of the temperature difference.

In order to perform the scale analysis for boundary layer flow, Navier-Stokes equations with the assumptions of steady, constant property and two-dimensional flow can be employed. In the presence of these assumptions, the continuity equation becomes:

$$\frac{\partial u}{\partial x}+\frac{\partial v}{\partial y}=0 \tag{H.8}$$

Using Boussinesq approximation, the momentum equation in y-direction can be written as:

$$u\cdot\frac{\partial v}{\partial x}+v\cdot\frac{\partial v}{\partial y}=\nu\cdot\frac{\partial^2 v}{\partial x^2}+g\cdot\beta\cdot\Delta T \tag{H.9}$$

And the energy equation is:

$$g\cdot C_p\cdot\left(u\cdot\frac{\partial T}{\partial x}+v\cdot\frac{\partial T}{\partial y}\right)=k\cdot\frac{\partial^2 T}{\partial x^2} \tag{H.10}$$

A balance equation for the velocity in x-direction can be obtained by using the continuity equation with velocity boundary layer consideration (v~V, x~δ, y~L) as:

$$u\approx V\cdot\frac{\delta}{L} \tag{H.11}$$

As a result of scale analysis applied to momentum equation in y-direction, two balance equations are obtained.

$$V\approx\nu\cdot\frac{L}{\delta^2} \tag{H.12}$$

$$\left(\frac{L}{\delta}\right)^4 \approx \frac{g \cdot \beta \cdot L^3 \cdot \Delta T}{\nu^2} \tag{H.13}$$

From the scale analysis of energy equation, a balance equation can be written by using thermal boundary layer consideration and Eqs. (H.11) and (H.12) (v~V, x~δ_t, y~L) as:

$$\nu \cdot \frac{\Delta T}{\delta^2}\left(\frac{\delta}{\delta_t} + 1\right) \approx \alpha \cdot \frac{\Delta T}{\delta_t^2} \tag{H.14}$$

Since Prandtl number for air is close to unity (Pr ≈ 1), the velocity and thermal boundary layers thicknesses may be accepted as equal ($\delta = \delta_t$). Also, considering the definition of Prandtl number, the kinematic viscosity and the thermal diffusivity of air can be assumed as equal ($\nu = \alpha$). This approach satisfies the balance between two sides of Eq. (H.14). Using these assumptions, Eq. (H.13) can be rearranged as:

$$\frac{L}{\delta} \approx \left(\frac{g \cdot \beta \cdot L^3 \cdot \Delta T}{\nu \cdot \alpha}\right)^{0.25} \tag{H.15}$$

The heat flux can be defined as:

$$\dot{q}'' = k \cdot \left(\frac{\partial T}{\partial x}\right)_{x=0} \tag{H.16}$$

A balance for the heat flux may be written as:

$$\dot{q}'' \approx k \cdot \frac{\Delta T}{L} \cdot \frac{L}{\delta} \tag{H.17}$$

The convection heat transfer rate can be expressed as:

$$h = \frac{\dot{q}''}{\Delta T} \tag{H.18}$$

A balance for convection heat transfer may be obtained as:

$$h \approx \frac{k}{L} \cdot \frac{L}{\delta} \tag{H.19}$$

Substitution of Eq. (H.15) into Eq. (H.19), a balance equation for heat transfer coefficient is estimated as:

$$h \approx \left(\frac{g \cdot \beta \cdot L^3 \cdot \Delta T}{\nu \cdot \alpha} \right)^{0.25} \cdot \frac{k}{L} \tag{H.20}$$

APPENDIX I

EXPERIMENTAL DATA OBTAINED FROM AVAILABLE LITERATURE

In order to extend the present experimental results, the experimental data in available literature were obtained. In these studies [2,3,9,10,11,12,14], heat transfer performances of vertically-based rectangular fins were investigated experimentally. The results of experiments were displayed in graphs. The graphs utilized to obtain experimental data are presented in Figures I.1 through I.11. In these figures, $\dot{Q}$ denotes total heat transfer rate from the fin array, $\dot{Q}_c$ shows convection heat transfer rate from the fin array and s is the separation between adjacent fins. Summary of the values of experimental and geometric parameters used in available literature are given in Table I.1.

Table I.1 Summary of the Values of Experimental and Geometric Parameters Used in Available Literature

Reference Number	Number of Fin Arrays Tested	Fin Length L(mm)	Fin Width W(mm)	Fin Thickness t(mm)	Fin Height H(mm)	Fin Spacing s(mm)	Base-to-Ambient Temperature Difference ΔT(ºC)	Optimum Fin Spacing s_{opt}(mm)	Fin Material
2	16	150	190	3	10-17	3-45	20-40	9-9.5	Duralumin
3	11	250	190	3	60	2.85-33.2	20-80	10	Light Aluminum Alloy
9	36	250	190	3	32-90	3-77	20-60	10.5	Duralumin
10	22	250-375	190	3	60	5-77	40	10-11	Duralumin
11	40	500	190	1-19	65	3-54	20-40	11-19	Duralumin
12	14	500	190	3	60	5-77	20-40	12	Stainless Steel
14	15	100	250	3	5-25	4.5-58.75	14-106	7	Aluminum

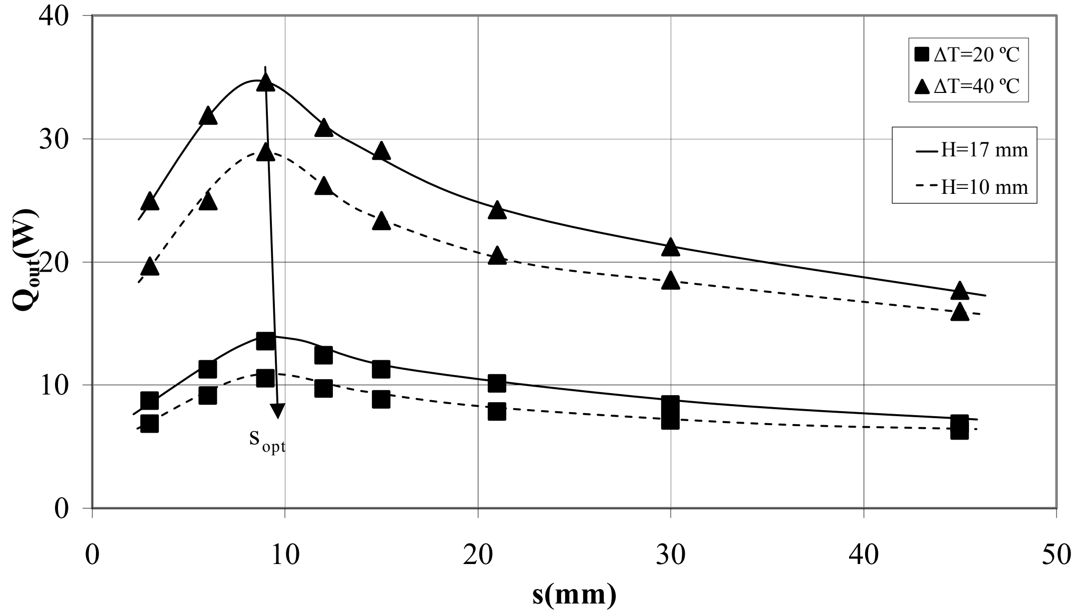

Figure I.1 Variation of Total Heat Transfer Rate with Base-to-Ambient Temperature Difference for Fin Heights of H=10 mm and H=17 mm Presented in Ref. [2]

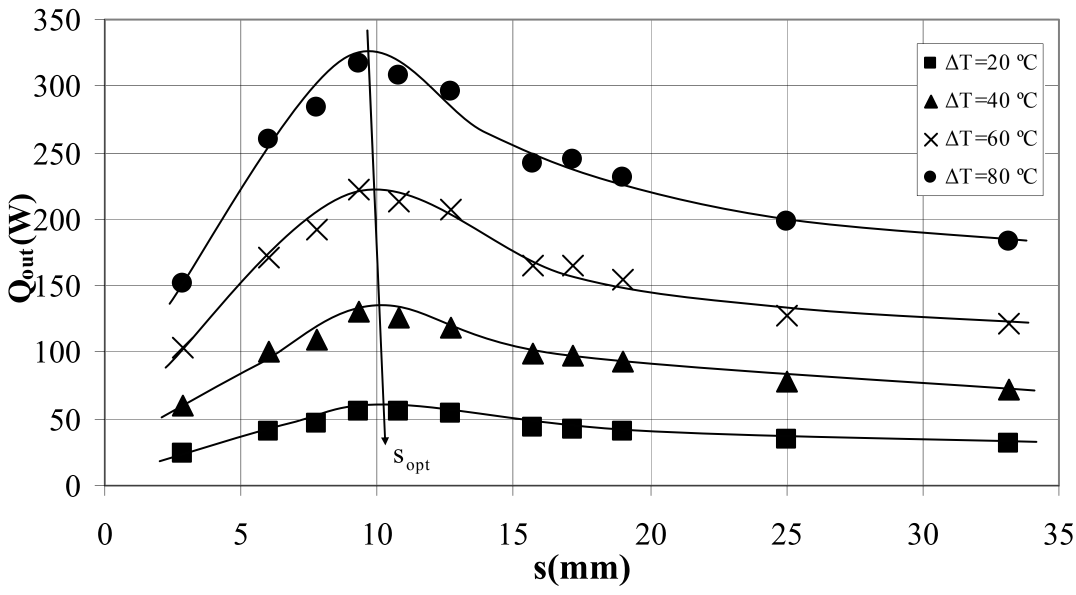

Figure I.2 Variation of Total Heat Transfer Rate with Base-to-Ambient Temperature Difference Presented in Ref. [3]

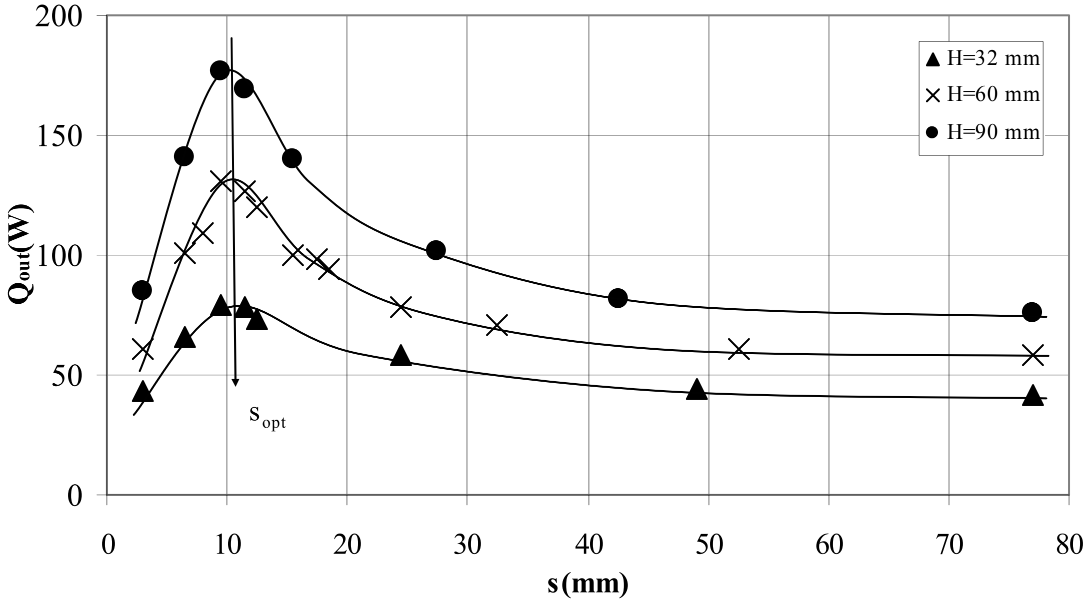

Figure I.3 Variation of Total Heat Transfer Rate with Fin Height at a Base-to-Ambient Temperature Difference of ΔT=40 ºC Presented in Ref. [9]

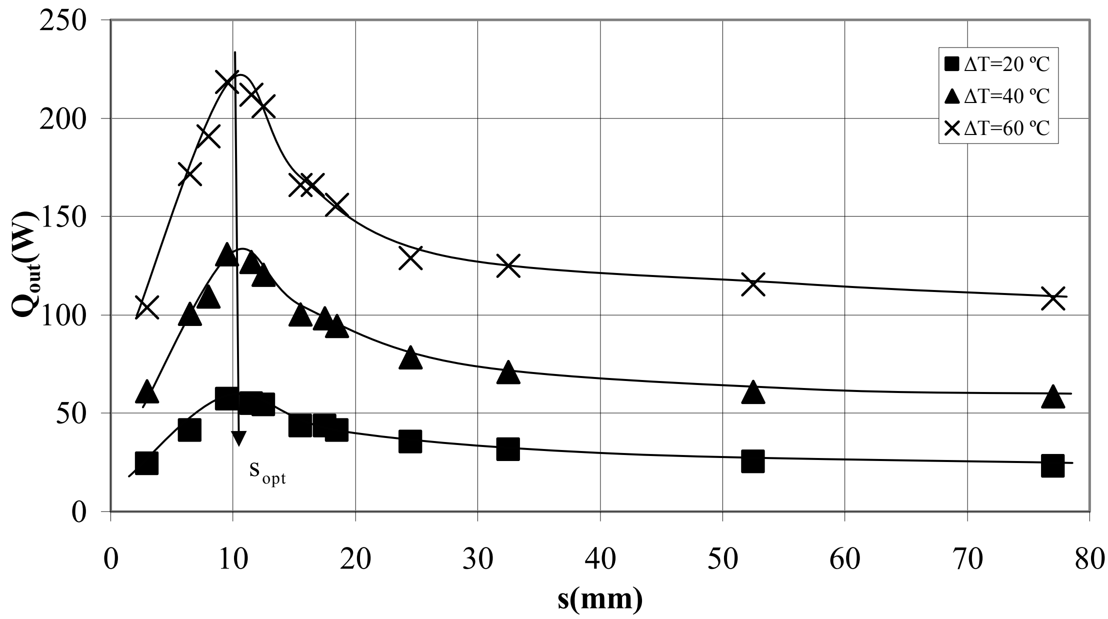

Figure I.4 Variation of Total Heat Transfer Rate with Base-to-Ambient Temperature Difference Presented in Ref. [9]

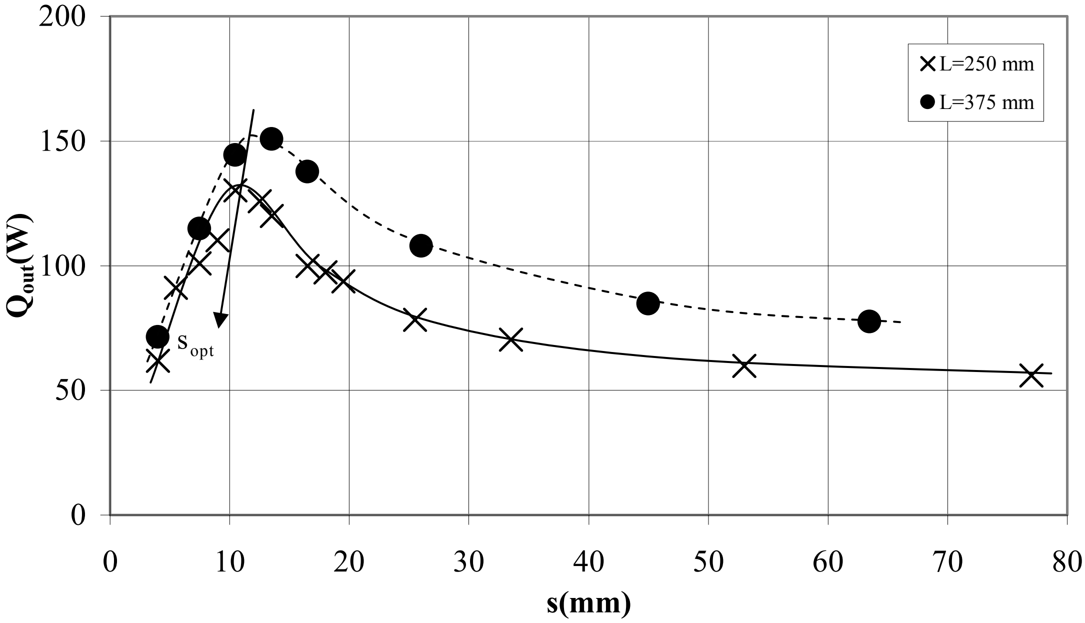

Figure I.5 Variation of Total Heat Transfer Rate with Fin Length at a Base-to-Ambient Temperature Difference of ΔT=40 ºC Presented in Ref. [10]

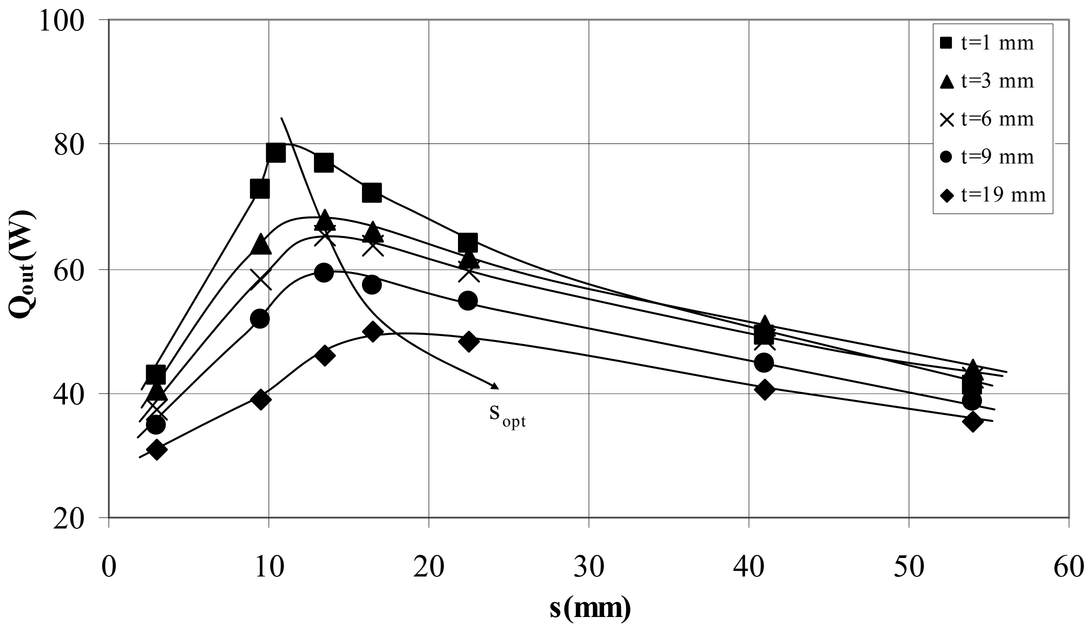

Figure I.6 Variation of Total Heat Transfer Rate with Fin Thickness at a Base-to-Ambient Temperature Difference of ΔT=20 ºC Presented in Ref. [11]

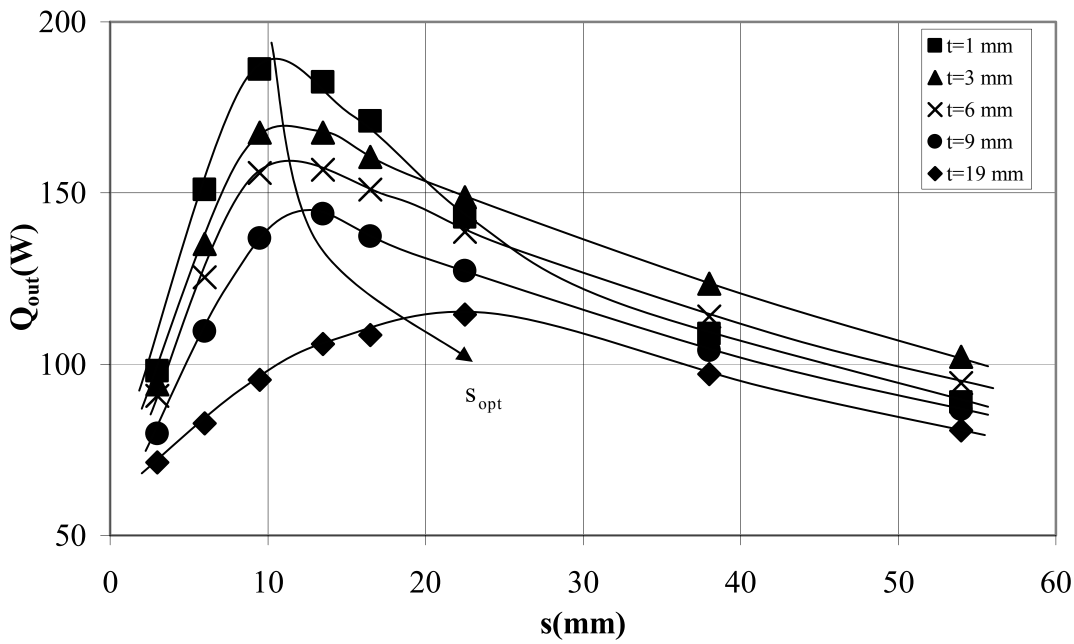

Figure I.7 Variation of Total Heat Transfer Rate with Fin Thickness at a Base-to-Ambient Temperature Difference of ΔT=40 ºC Presented in Ref. [11]

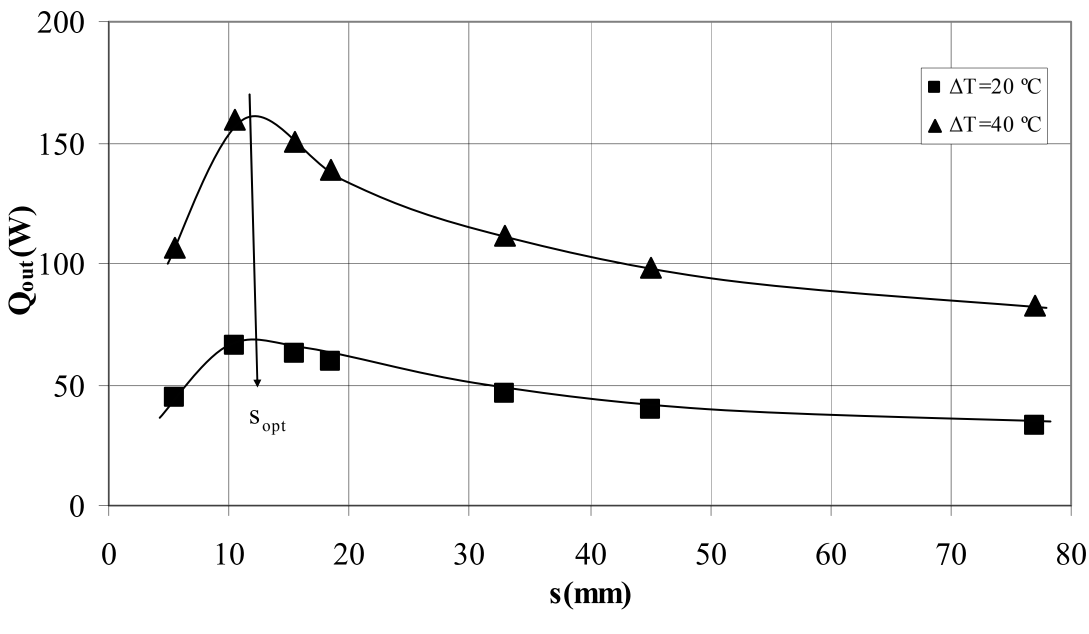

Figure I.8 Variation of Total Heat Transfer Rate with Base-to-Ambient Temperature Difference Presented in Ref. [12]

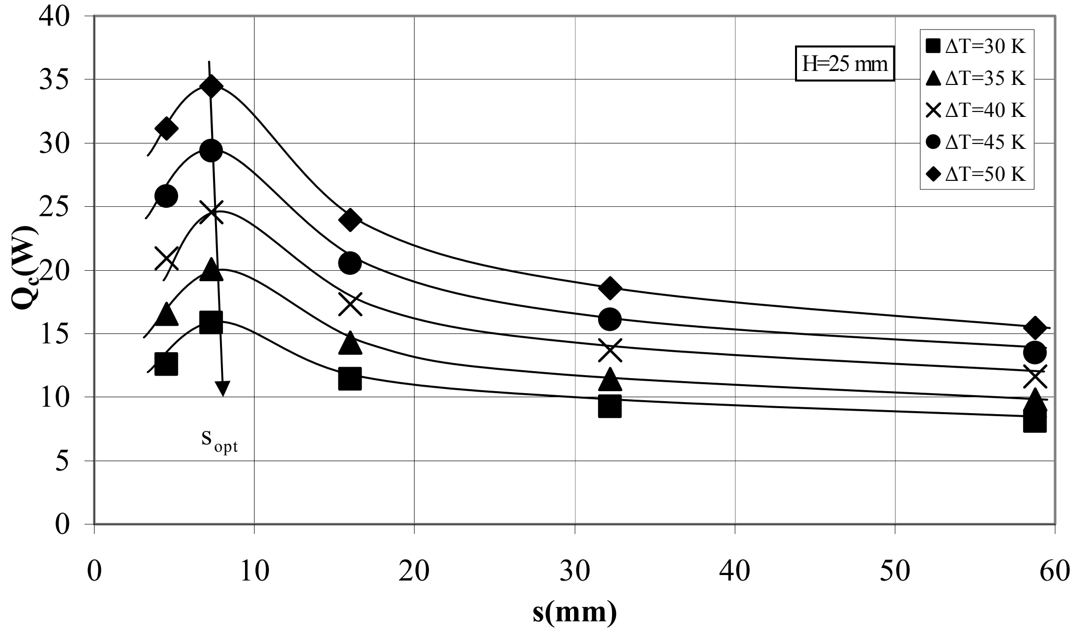

Figure I.9 Variation of Convection Heat Transfer Rate with Base-to-Ambient Temperature Difference for Fin Heights of H=25 mm Presented in Ref. [14]

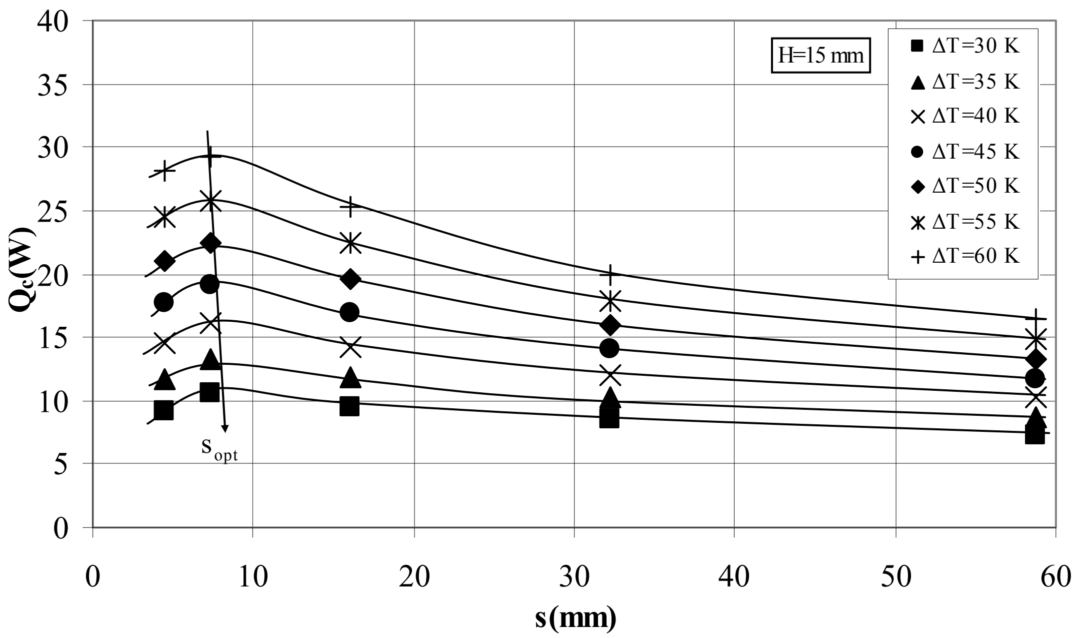

Figure I.10 Variation of Convection Heat Transfer Rate with Base-to-Ambient Temperature Difference for Fin Heights of H=15 mm Presented in Ref. [14]

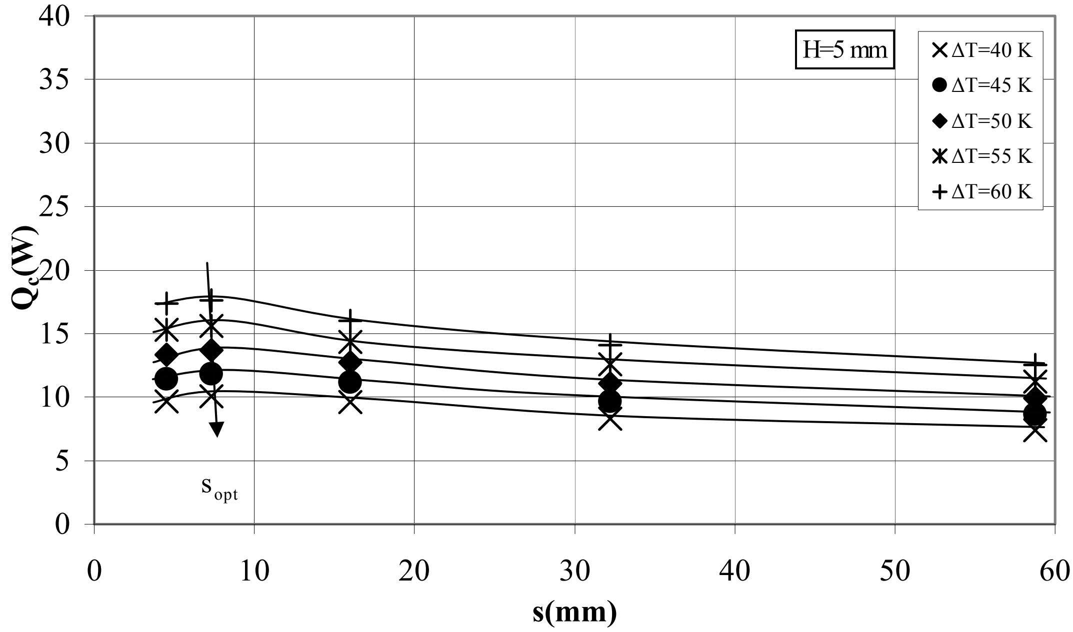

Figure I.11 Variation of Convection Heat Transfer Rate with Base-to-Ambient Temperature Difference for Fin Heights of H=5 mm Presented in Ref. [14]

In Refs. [2,3,9,10,11,12], the experimental data were reported in graphs which display total heat transfer rate from fin array, $\dot{Q}_{out}$ versus fin spacing, s. The data of heat transfer rates and fin spacing values were directly read from these graphs. However, the data of the convection heat transfer rates from fins were required to be substituted into Eqs. (6.8) or (6.16). Thus, for each total heat transfer rate data, the following procedure was applied:

Radiation contribution, $\dot{Q}_r$ were evaluated by using the radiation analysis proposed in Appendix D, and the convection heat transfer rate from the fin array, $\dot{Q}_c$ was obtained as:

$$\dot{Q}_c = \dot{Q}_{out} - \dot{Q}_r \tag{I.1}$$

Then, Churchill and Chu's second relation, the most recent relation among the vertical plate correlations in literature, were used to evaluate Nusselt number as:

$$\mathrm{Nu_L} = 0.68 + \frac{0.67 \cdot \left(\mathrm{Ra_L}\right)^{1/4}}{\left[1 + \left(\frac{0.492}{\mathrm{Pr}}\right)^{9/16}\right]^{4/9}} \tag{I.2}$$

From the definition of Nusselt number, heat transfer coefficient was evaluated as:

$$\mathrm{h} = \frac{\mathrm{Nu_L} \cdot \mathrm{k}}{\mathrm{L}} \tag{I.3}$$

where k is the conductivity of the ambient air and L is the characteristic length of the vertical plate.

Using the general convection heat transfer equation, the convection heat transfer rate from the base-plate, $\left(\dot{\mathrm{Q}}_{\mathrm{o}}\right)_{\mathrm{c}}$ was obtained as:

$$\left(\dot{\mathrm{Q}}_{\mathrm{o}}\right)_{\mathrm{c}} = \mathrm{h} \cdot \mathrm{A} \cdot \Delta \mathrm{T} \tag{I.4}$$

Finally, the convection heat transfer rate from fins was calculated as:

$$\dot{\mathrm{Q}}_{\mathrm{c}}^{(1)\text{ or }(2)} = \dot{\mathrm{Q}}_{\mathrm{c}} - \left(\dot{\mathrm{Q}}_{\mathrm{o}}\right)_{\mathrm{c}} \tag{I.5}$$